Coded modulations for the multiple-antenna and cooperative fading channels.

Ghassan M. Kraidy, ENST, Paris, France

Contents

List of Figures

List of Tables

Chapter 1

Introduction

Over the past few years, wireless networks applications have gained ever-increasing popularity. They provide novel opportunities for increased reliability that are non-existent in point to point communications. However, due to the nature of the wireless channel, effects such as fading, shadowing, and interference from other transmitters can cause the channel quality to fluctuate during transmission. One approach to combat such channel fluctuations is to design a communication system that provides some sort of diversity, i.e. provides many replicas of the signal to the receiver. Diversity can be temporal, spatial, or frequential [2]. Multiple-antenna systems (also called Multiple-Input Multiple-Ouput (MIMO) systems)have been shown to provide spatial diversity that boosts the performance in fading environments. In addition, the need to transmit at high data rates is fulfilled with such systems as they allow the simultaneous transmission of multiple streams (spatial multiplexing). However, in some cases, due to space or cost limitations, the implementation of more than one antenna on the same terminal is impossible. For this reason, the concept of cooperative communications was proposed, which means that terminals can cooperate between each others to provide spatial diversity in a distributed configuration, thus forming a virtual antenna array.
In this report, we study the design of space-time bit-interleaved coded modulations (ST-BICM) suited for frequency non-selective single-user block-fading channels. The outline of the manuscript is as follows:

- In Chapter 2, we first introduce the fundamental information theoretical limits of block-fading channels in general (namely the outage probability), limits that are used throughout the report for the analysis of coded modulations. We then describe the ST-BICM transmitter model, before describing the iterative receiver that can lead to quasi-maximum likelihood (ML) performance with reasonably low complexity. We end up this chapter by recalling the Singleton bound on the diversity order of coded systems for a given coding rate.

- In Chapter 3, we propose ST-BICM schemes suited for the multiple-input multiple-output (MIMO) channel with iterative decoding. First, we design space-time pre-

coding matrices that minimize the discrete input outage probability, and we show the good performance of these precoders since the first iteration of an iterative receiver. Second, we investigate a low-complexity coded scheme for a four-transmit antenna configuration based on the Alamouti scheme. Finally, we propose the design of turbo codes for MIMO channels, and we will show that this scheme dramatically approaches the outage probability limit with relatively low decoding complexity using intelligent switches (called "code multiplexers") at the output of the turbo encoder.

- In Chapter 4, the design of ST-BICM for the amplify-and-forward cooperative protocol with multiple relays is considered. We derive bounds on the diversity order for this protocol, and we show that precoders that do not entail an increase in the detection complexity are optimal diversity-wise. We next discuss coding gain issues for this protocol, and show simulation results for various coding rates and network configurations. We finally show the performance of code multiplexers with turbo codes over this protocol.

- In Chapter 5, in a goal to achieve optimal coding gain over block-fading channels, a new method for the design of irregular turbo codes is proposed. We first show that irregular turbo codes outperform LDPC codes for the AWGN channel, and then we show they outperform the regular turbo codes on block-fading channels using density evolution methods.

We end up this manuscript by the concluding remarks and some future perspectives.

Chapter 2

Generalities

2.1 Introduction

In this manuscript, we deal with wireless block-fading channels, that were introduced in [3] to model slowly varying fading channels. In this model, a frame (or a codeword) sent over the wireless channel sees a fixed number of fading coefficients. Standards such as Global System for Mobile Communications (GSM) or the promising Orthogonal Frequency Division Multiplexing (OFDM) that involve slow time-frequency hopping are well represented by this channel model. The block-fading channel model leads to a null capacity, as the capacity depends on the instantaneous channel instance. In this chapter, we will start by introducing the information theoretical limit of block-fading channels, that is outage probability. We will then present the general communication system we will use throughout this report; a transmitter consisting of a space-time precoded coded modulation, and a receiver consisting of an iterative detection and decoding blocks. The last part of this chapter presents the bound on the diversity order of coded systems on block-fading channels.

2.2 Information theory of fading channels

Back in 1948, Claude E. Shannon established the definition of channel capacity through the noisy-channel coding theorem [4] as the maximum theoretical rate at which we can reliably transmit data (i.e. with a vanishing error rate) over a channel with a specified bandwidth and at a particular noise level. Channel capacity is a deterministic bound that takes different expressions depending on the channel type. Now suppose that the input and the output of the channel are given by the two random variables X and Y respectively. The channel capacity is by definition given by:

$$C = \max_{p(x)} \mathcal{I}(X;Y) \tag{2.1}$$

where $p(x)$ is the input distribution and the mutual information $\mathcal{I}(X;Y)$ between X and Y is given by:

$$\mathcal{I}(X;Y) = H(X) + H(Y) - H(Y,X) = H(Y) - H(Y/X) = H(X) - H(X/Y) \quad (2.2)$$

and the entropy function H gives the average amount of bits one needs to represent a random process. For the additive white Gaussian noise (AWGN) channel for instance, the channel capacity for a Gaussian input is given by:

$$C_{AWGN} = \log_2\left(1 + R\frac{E_b}{N_0}\right) \text{ bits/s/Hz} \quad (2.3)$$

It is thus possible to reliably transmit information on an AWGN channel at a rate $R < C_{AWGN}$ through an infinite length codeword. Now for wireless channels, the channel input-output model is given by:

$$\mathbf{y} = \mathbf{xH} + \mathbf{w} \quad (2.4)$$

where $\mathbf{x}$ is the input vector, $\mathbf{y}$ is the output vector, $\mathbf{H}$ is the channel matrix with complex Gaussian fading coefficients, and $\mathbf{w}$ is the AWGN vector. In the presence of ergodic Rayleigh fading, it was shown in [5] [6] that the channel capacity for a Gaussian input without side information at the transmitter is given by:

$$C = \mathbb{E}_H\left[C_H\right] = \mathbb{E}_H\left[\log_2 \det\left(I + \mathcal{P}\mathbf{H}^\dagger\mathbf{H}\right)\right] \quad (2.5)$$

where $\mathcal{P}$ is a function of the signal-to-noise ratio. For single-antenna quasi-static fading channels, $\mathbf{H} = h$ has a single entry. For multiple-antenna and amplify-and-forward cooperative channels, the complex channel matrix $\mathbf{H}$ takes different forms that will be discussed in the next chapters. Now as the channel gain process is ergodic, i.e. the time average is equal to the ensemble average, the channel changes at each realization. In other words, the randomness of the channel coefficients can be averaged out (removed) over time as shown in (2.5). This results in the fact that the capacity of an ergodic channel is information stable as it tends to a deterministic value and long-term constant bit rates can be supported.

Now for non-ergodic fading channels, the channel gain is a random variable and does not change with time (at least for the duration of a codeword). The channel gain process is stationary but not ergodic, i.e. the time average is not equal to the ensemble average. This means that certain "weak" realizations of the channel coefficients can cause the capacity of the channel to fall below the transmission rate we want to maintain. Non-ergodic channels are information unstable [7] as channel capacity is not deterministic. The expression for the channel capacity is a random variable with probability density function $p_{C_H}(i)$ that defines the "outage" probability [3][8]:

$$P_o = P\left(C_H < R\right) = \int_0^R p_{C_H}(i)di \quad (2.6)$$

For block-fading channels, we suppose that a codeword sees n_c different realizations of the channel matrix, and this gives the following expression for the Gaussian input outage probability:

$$P_{o,n_c} = P\left(\frac{1}{n_c}\sum_{j=1}^{n_c}\log_2\det\left(I+\mathcal{P}\mathbf{H}_j^{\dagger}\mathbf{H}_j\right) < \ R\right) \tag{2.7}$$

Note that when $D \to \infty$, the averaging over the channel realizations leads to the ergodic channel capacity as in (2.5). It is clear that area under the tail of the capacity given the channel distribution $p_{C_H}(i)$ in (2.6) is a cumulative distribution function $F_I(R)$. The outage capacity can be seen as the ϵ-capacity [7] [9] [10] of the channel as:

$$C_\epsilon = \sup_{p(x)} \ \sup \ \{R : F_I(R) \leq \epsilon\} \ \ 0 \leq \epsilon \leq 1 \tag{2.8}$$

The ϵ-capacity C_ϵ is the optimum asymptotic rate at which information can be encoded over the channel via a sequence of channel codes that yield a maximal probability of decoding error of ϵ. Note that:

$$C_{\epsilon\downarrow 0} = C \tag{2.9}$$

which gives the Shannon capacity. The ϵ-capacity approach for outage capacity suits the convention of "x percent outage" followed by certain papers (see [11] for example). However, in this report, we will use the outage measure as a probability as in (2.6) to be able to compare it with word error rate performance of coded modulations.
As proved in [5], maximum capacity over ergodic fading channels (consequently minimum outage probability over block-fading channels) is achieved with Gaussian inputs, i.e. when $p(x)$ follows the normal distribution. However, with practical communication systems, we always deal with discrete input constellations. For this reason, the expression in (2.5) for Gaussian inputs does not hold anymore. From (2.2), we have:

$$\mathcal{I}(X;Y) = H(Y) - H(Y/X) \tag{2.10}$$

Now let $X \in \Omega$, a discrete alphabet of 2^n vectors. The entropies from (2.10) can be expressed as [12]:

$$\begin{aligned} H(Y) &= -\int_y p(y)log_2(p(y))dy \\ &= -\int_y \sum_x p(y/x)p(x)log_2\left(\sum_{x'} p(y/x')p(x')\right)dy \qquad (2.11) \\ H(Y/X) &= -\sum_x p(x)\int_y p(y/x)log_2(p(y/x))dy \qquad (2.12) \end{aligned}$$

This gives the expression of the mutual information as:

$$\mathcal{I}_H = n - \frac{1}{2^n}\sum_x \int_y p(y/x) log_2(\frac{\sum_{x'} p(y/x')}{p(y/x)}) dy \tag{2.13}$$

$$= n - \frac{1}{n_c}\sum_{j=1}^{n_c} \mathbb{E}_{\mathbf{x},\mathbf{y}|\mathbf{H}_j}\left[\log_2\left(\frac{\sum_{\mathbf{x}'} p(\mathbf{y}|\mathbf{x}',\mathbf{H}_j)}{p(\mathbf{y}|\mathbf{x},\mathbf{H}_j)}\right)\right] \tag{2.14}$$

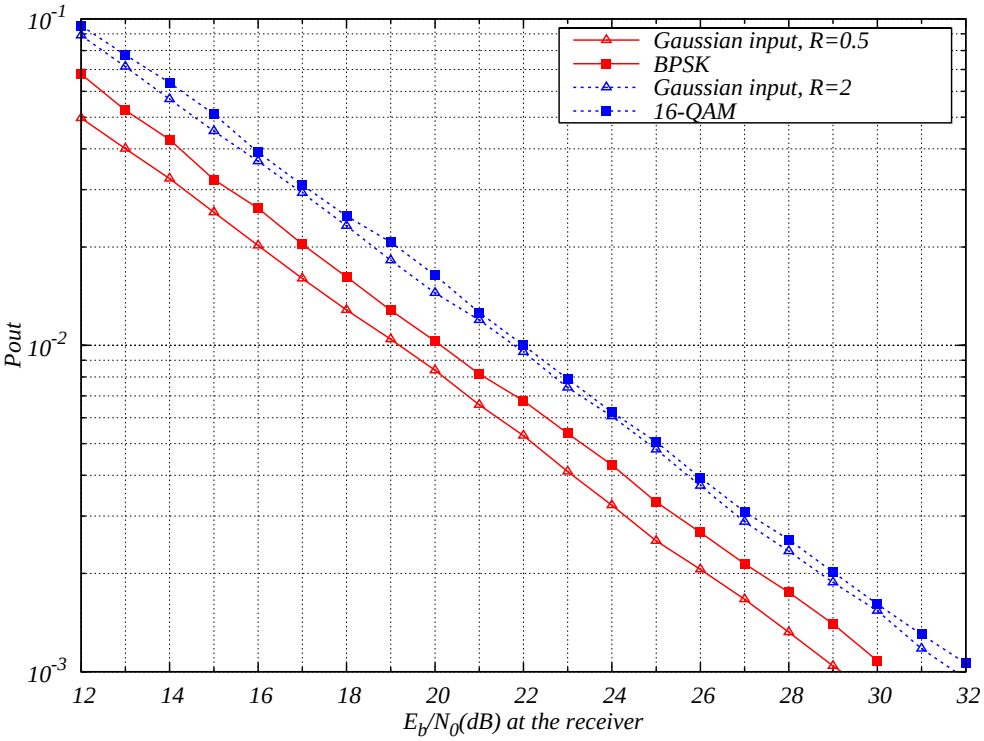

Figure 2.1: Outage limits for quasi-static channel, BPSK, 16QAM, and Gaussian input, half-rate channel coding.

Fig. 2.1 shows the outage probabilities of a quasi-static fading channel for different inputs and half-rate channel coding. As mentioned earlier, Gaussian inputs outperform all other distributions at the same spectral efficiency. We also notice that with half-rate coding, the 16-QAM constellation outage probability is closer to the Gaussian input outage probability than the BPSK modulation. As the outage probability reflects the variations of the mutual information function depending on the channel realizations, this behavior is explained by the fact that the mutual information curve of the 16-QAM constellation at half-rate coding is closer to the Gaussian mutual information line than the BPSK constellation at the same coding rate (see [13, Fig. 2]). Fig. 2.2 shows the outage probabilities for different MIMO channel antenna configurations, half-rate channel coding and Gaussian input. The diversity order is given by $n_t \times n_r$, but the coding gain differs for the same diversity order depending on the configuration.

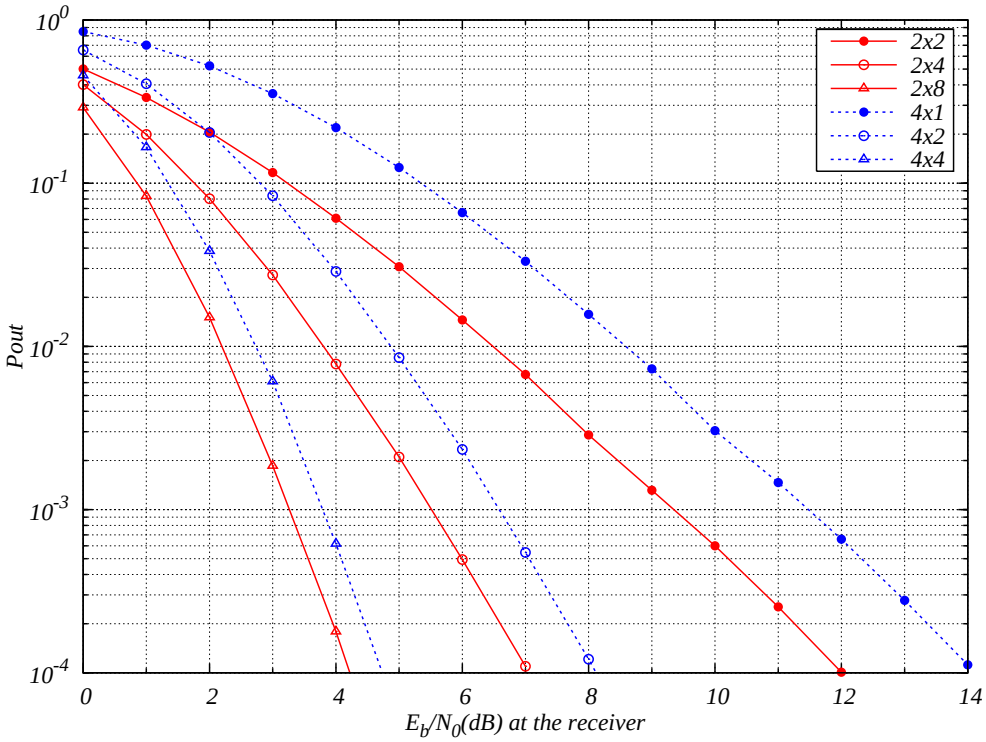

Figure 2.2: Outage limits for different MIMO configurations, Gaussian input, half-rate channel coding.

2.3 Bit-interleaved coded modulation (BICM) with iterative decoding

In 1992, it was shown in [14] that by cascading an error correcting code, a random interleaver and a modulator, a communication system achieves very high gains. Later, the authors in [15] established a framework for the analysis and design of the so-called "Bit-interleaved coded modulation" (BICM), and showed that this structure allows to approach the information theoretical limits of the channel, for the AWGN case as well as for the ergodic fading case. Since then, this structure has been widely studied for different scenarios. In [16] [17] [18] among others, the authors studied BICM for non-ergodic fading channels, and it was proved that this scheme can also approach the outage limit of the channel. In this report, the BICM model for block-fading channels (i.e. non-ergodic channels) will be considered.

2.3.1 Structure of the BICM transmitter

The general structure of a BICM is shown in Fig. 2.3. It consists of an error correcting code $\mathcal{C}$ of rate R_c, a deterministic interleaver Π, a symbol mapper, and a space-time precoder. We will now describe each block and give historical notes and classifications that justify our choices.

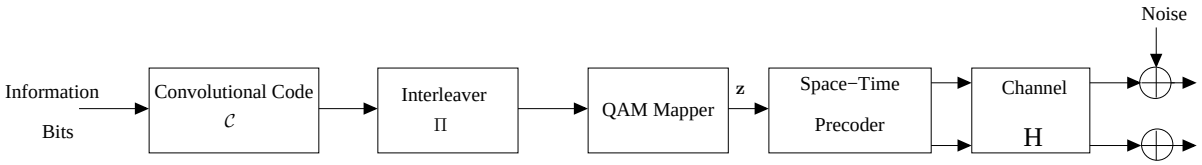

Figure 2.3: ST-BICM transmitter scheme.

The error correcting code

The field of channel coding started with Shannon's landmark paper in 1948 [4]. The idea is to protect data sent through a channel by adding some redundancy to the transmitted signal in way to ensure reliable communication. The encoder is a bijection between the information sequence $\mathbf{b}$ of length K and the coded sequence $\mathbf{c}$ of length N. The coding rate is $R_c = K/N$. There are different types of error correcting codes, and they can be classified into two major categories [19]:

- Algebraic linear block codes: Hamming, Golay, Reed-Muller, BCH, and Reed-Solomon codes among others. Algebraic coding theory dominated the first decades of channel coding history. The main objective of this design theory is to maximize the minimum distance d (also called Hamming distance (d_{min})) between any two distinct codewords, that is the minimum number of bits in which they differ. They are mostly used for high data rates, but fail to approach fundamental limits. In particular, Reed-Solomon codes are efficient in applications that suffer from bursty errors, such as magnetic tape and disk storage for instance. They can provide high error-correction power with relatively small redundancy at very high data rates.

- Probabilistic codes: in [19], it is stated that "*probabilistic coding is more concerned with finding classes of codes that optimize average performance as a function of coding and decoding complexity*". This class includes convolutional codes, product codes, concatenated codes, and trellis decoding of block codes. Convolutional codes were invented in [20]. They can be grouped into two major categories: non-recursive non-systematic convolutional (NRNSC) codes, where all information bits are encoded through shift registers, and recursive systematic convolutional (RSC) where the uncoded information sequence is sent through the channel and at the same time is encoded through a feedback register. As a result, the code can be represented by a trellis, which allows for low complexity decoders. Although they have infinite length, convolutional codewords can be made finite by proper trellis termination. In this report, we will mainly use NRNSC codes with BICM due to their flexibility. Product codes and compound codes were proposed in [21] and [22] respectively. They consist of a serial concatenation of two or more codes at the transmitter, and by individual decoding of every code at the receiver. Their concept lead to the invention of "Turbo-codes" that will be discussed in chapter 5. Another example of concatenated codes are "low-density parity-check" (LDPC) codes [23]. They are based on sparse generator matrices that allow for probabilistic iterative

decoding under the message-passing algorithm. Both LDPC and turbo codes have been proved to be capacity approaching codes for the AWGN channel. However, in this report, we will only deal with trellis codes (NRNSC convolutional and turbo codes).

The interleaver

The role of an interleaver is to scramble the bits of a codeword. It is a very important block in a BICM under iterative decoding, as it ensures independance between the extrinsic probabilities and the *a priori* probabilities exchanged by the nodes in a graph. In addition, if maximum-likelihood (ML) decoding is possible, an interleaver spreads the consecutive bits of an error events thus it limits their interference. There are different types of interleavers: pseudo-random, S-random [24], where two consecutive bits at the input of the interleaver will be placed a distance S away from each other at the output. In [18], a class of optimized interleavers for block-fading channels was proposed, class that respects the "ideal interleaving" conditions. These conditions are summarized as (see proposition 5, chapter 3 in [18]), : "*...the interleaver should uniformly place consecutive bits on all the channel time realizations, transmit antennas, and bit positions of the mapping and prohibit the interference of these consecutive bits in the mapping*". This class of interleavers will be frequently employed throughout this report.

The modulator

This block converts m coded bits into a constellation symbol at each channel use. The bijection from bits to symbols is called mapping (or labeling) The cardinality of the constellation Ω is given by $|\Omega| = M = 2^m$. Now in the case of MIMO systems with $n_t \geq 2$ transmit antennas for instance, the mapper takes $m \times n_t$ bits at each channel use and converts them into a vector of n_t modulation symbols. There exist different types of mappings, each suited for certain applications or specific channel types. Gray mapping, the most widely used, allows for only one bit to change between any two neighbors of the constellation, but it only exists for square constellations (i.e. $|\Omega| = 2^{2u}$). The mapping presented in [13] known as "Ungerboeck mapping" maximizes the Euclidean distance between neighbor constellation symbols and is suited for trellis-coded modulations. Mapping issues will not be treated in this report, and only Quadrature Amplitude Modulations (QAM) will be considered. The energy per M-QAM symbol is given by:

$$E_s = \frac{2(M-1)}{3} \tag{2.15}$$

The space-time precoder

The precoder **S** spreads the QAM symbols over s time periods. In most cases, the precoder is linear, i.e. it maps the QAM vector onto a linear combination of the constellation symbols. However, in some cases, the space-time precoder is not linear, as is the case for orthogonal designs [25] [26] and the scheme presented in section 3.7.

2.3.2 The BICM iterative receiver

The codewords at the output of the concatenation of a space-time precoder and a BICM can be seen as global Euclidean codes [18]. Ideally, such codes should be decoded with a maximum-likelihood (ML) decoding algorithm, but an exhaustive search over all the codewords is unfeasible in practice as the codeword size increases. For this reason, the receiver for such systems is at the image of the transmitter, whereas corresponding blocks iteratively exchange soft information. Thus the receiver of a space-time (ST) BICM consists of two main nodes: a soft-input soft-output (SISO) *a posteriori* probability (APP) QAM detector, that converts the information carried by the constellation mapper and the space-time precoder as soft information on the coded bits, and a SISO decoder that takes the information from the detector as *a priori* and generates more reliable soft information (extrinsic probabilities) on coded bits. The final decision is made on the APP on information bits at the output of the SISO decoder.
Ideally, the optimal SISO detector computes the channel realizations over all possible "space-time codewords". This operation might be too complex for high data rates (large constellation size, large number of antennas, large number of relays...). A complexity reduction method called "List sphere decoding" [27] reduces the exhaustive list of candidates to a smaller list without degrading the overall system performance. There also exist sub-optimal detectors such as SISO Minimum Mean-Square Error (MMSE) detectors or Serial/Parallel Interference Cancellation (SIC/PIC) detectors developed in multi-user detection theory (see [28] and references therein).
As for the channel decoders, there exist hard output decoders and soft output decoders. For algebraic codes, there only exist hard output decoders [29] [30]. For convolutional codes, the most famous hard output decoder is the "Viterbi algorithm" [31] (also known as Maximum-Likelihood Sequence Estimator (MLSE)), that is optimal in the ML sense. The first soft-output decoding algorithm was proposed back in the 1950s [32]. In 1963, Gallager proposed what is known as the "sum-product algorithm" (or also "belief propagation") for the iterative decoding of LDPC codes. Later, in the 1970s, the "forward-backward algorithm" (or BCJR, following the initials of the authors) was proposed as a SISO trellis decoder that gives the APP on information bits. Due to its additional complexity and to its sub-optimality codeword-wise, this algorithm did not replace the Viterbi algorithm until the invention of turbo codes, where the exchange of soft information was

mandatory (see chapter 5). In the late 1980s, the "soft-output Viterbi algorithm" was proposed in [33] as a Viterbi algorithm that gives soft information on coded bits, but this algorithm is sub-optimal compared to the BCJR for iterative processing. Throughout this report, the BCJR algorithm will be used for the decoding of error correcting codes, due to its optimality in generating soft information on messages.

As mentioned previously, the optimum decoding of a ST-BICM is to compute a ML decoding algorithm over the global code. This means that the separation between detection and decoding is largely sub-optimal; an exhaustive ML search of the transmitted vector at the detector level can provide information that can mislead the decoder in choosing the probable codeword. For this reason, in a way to approach the optimality of the global ML detection, we will use an iterative detection and decoding receiver throughout this manuscript.

Fig. 2.4 shows the general structure of an iterative receiver suited for fading channels. The two major blocks represent the SISO detector and the SISO decoder, that are separated by interleaving blocks (the block Π^{-1} is a de-interleaver). The iterative process consists of exchanging soft information between the two blocks.

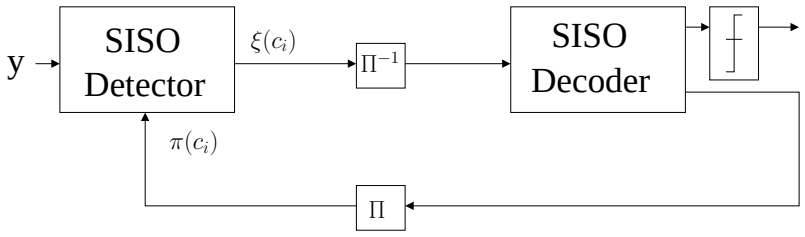

Figure 2.4: ST-BICM iterative receiver.

The SISO detector receives a complex vector $\mathbf{y} \in \mathbb{C}^{N_r}$ given by:

$$\mathbf{y} = \mathbf{zSH} + \mathbf{w} = \mathbf{xH} + \mathbf{w} \tag{2.16}$$

where $\mathbf{z} \in \mathbb{C}^{N_t}$ is the vector of QAM symbols, $\mathbf{S}$ is a $N_t \times N_t$ space-time precoder, $\mathbf{H}$ is the complex channel matrix, and $\mathbf{w}$ is a circularly symmetric zero-mean complex Gaussian noise vector with variance N_0. For a MIMO system with n_r receive antennas, $N_r = s.n_r$, while for a cooperative system with β single-antenna relays, $N_r = \beta + 1$. In addition, $N_t = s.n_t$ for a MIMO system with n_t transmit antennas, and $N_t = \beta + 1$ for a cooperative system, all employing $2^m - QAM$ modulations. The detector first computes the channel likelihoods $p(\mathbf{y}/\mathbf{x})$ over $\mathbb{C}^{N_r}$, then it generates the extrinsic probabilities on coded bits $\xi(c_i)$ based on the channel likelihoods and the *a priori* probabilities $\pi(c_i)$ fed from the SISO decoder. At the first iteration, all the *a priori* probabilities are unbiased. Throughout the iterative process, the exchange of probabilities on coded bits between the

two blocks should give more reliable soft information on the information bits. An ideal convergence of the process would lead to near-ML performance.
In the following we will describe the optimal APP detector based on a marginalization over an exhaustive list. Note that complexity reduction for such detectors was proposed in [27]. By definition, the APP of a coded bit c_i is the probability to detect c_i when $\mathbf{y}$ is received:

$$APP(c_i) = p(c_i/\mathbf{y}) = \frac{p(\mathbf{y}/c_i)p(c_i)}{p(\mathbf{y})} \qquad i = 1, ..., mN_t \tag{2.17}$$

where $N_t = s.n_t$ for a MIMO system with n_t transmit antennas, and $N_t = \beta + 1$ for a cooperative system, all employing $2^m - QAM$ modulations. In this expression of the APP on coded bits at the detector, it is obvious that the probability on coded bits $p(c_i)$ is nothing but the *a priori* probability fed from the SISO decoder, thus $p(c_i) = \pi(c_i)$. Now the conditional probability density function $p(\mathbf{y}/c_i)p(c_i)$ is obtained by the marginalization of the joint probability density function of the channel likelihood and the coded bits as follows:

$$p(\mathbf{y}/c_i) = \sum_{j \neq i,\ j \leq mN_t} p(\mathbf{y}, c_j/c_i) \tag{2.18}$$

$$= \sum_{j \neq i,\ j \leq mN_t} p(\mathbf{y}/c_j) \prod_{u \neq i} \pi(c_u) \tag{2.19}$$

Here we suppose that the coded bits transmitted during the same time period are independent. Now as the noise is AWGN and by supposing that the receive antennas are independent we can write:

$$p(\mathbf{y}/c_1, ..., c_{mN_t}) = \frac{1}{2\pi N_0} e^{-\|\mathbf{y}-\mathbf{xH}\|^2/2N_0} \tag{2.20}$$

Now in an iterative process in general, a block (i.e. a detector or a decoder) should not give information on a bit to the other block that is known to this block. The APP on a coded bit computed by the detector can be written as the product of two independent probabilities:

$$APP(c_i) = \xi(c_i)\pi(c_i) \tag{2.21}$$

As $\pi(c_i)$ is computed by the SISO decoder, giving back $APP(c_i)$ to the SISO decoder is not appropriate. For this reason, the extrinsic probability $\xi(c_i)$ is given to the SISO decoder. Now let us define $c_1, ..., c_i, ..., c_{mN_t} \in \Omega(c_i)$ as the set of the mN_t bits in $\mathbf{y}$ having the i^{th} bit equal to c_i, we can write the following normalized expression for the extrinsic probabilities [18]:

$$\xi(c_i) = \frac{p(\mathbf{y}/c_i = 1)}{p(\mathbf{y}/c_i = 0) + p(\mathbf{y}/c_i = 1)} \tag{2.22}$$

$$= \frac{\sum_{x' \in \Omega(c_i=1)} \left[\left(e^{-\|\mathbf{y}-\mathbf{x}'\mathbf{H}\|^2/2N_0} \right) \prod_{u \neq i} \pi(c_u) \right]}{\sum_{x \in \Omega(c_i=1)} \left[\left(e^{-\|\mathbf{y}-\mathbf{xH}\|^2/2N_0} \right) \prod_{u \neq i} \pi(c_u) \right]} \tag{2.23}$$

Note that, luckily enough, the expression for $p(\mathbf{y})$ from (2.17) is cancelled through the normalization. Indeed, the computation of this quantity that depends on the transmitted signal and the noise is tedious.

2.4 Bounds on diversity for coded systems on non-ergodic channels

On a single-antenna ergodic fading channel, a frame sees different channel realizations at each time epoch. This gives a Nakagami distribution of high order (represented by the sum of the $\|h_j\|^2$) at the output of the detector and thus gives a high order of diversity. The diversity order that can be achieved by a ST-BICM on such channels is thus mainly limited by the minimum Hamming distance d_{min} of the channel code. Over block-fading channels with a limited number of states, the situation is different. In the sequel, we will call *BO-channel* the binary-oriented channel with input c_i and output $\xi(c_i)$ as observed by the channel encoder and the channel decoder.

Definition 1 *Under the genie condition (i.e. perfect* a priori *information) in the BO-channel, the number of independent binary-input non-ergodic fading sub-channels is denoted by D_{st} and called the* state diversity.

As an example, in the single-input single-output block-fading channel where a codeword spans n_c channel realizations, we have that $D_{st} = n_c$. Now let $\omega_H(c)$ denote the Hamming weight of a codeword c of length L_c generated by a linear binary code. We write $\omega_H(c) = \sum_{i=1}^{D_{st}} \omega_i$, where ω_i is the partial Hamming weight transmitted on the binary-input sub-channel i within the BO-channel. The state diversity $d_{st}(c)$ achieved by the codeword c is the number of non-zero partial weights. For a given transmitter structure, the achievable state diversity is $d_{st} = \min_{c \neq 0} d_{st}(c)$. Now suppose that each L_c/D_{st} bits are transmitted over one channel state. By grouping all the bits transmitted over one channel state into one symbol, we get a non-binary code of length $N_s = D_{st}$ built on an alphabet of size $2^{L_c/D_{st}}$. The Singleton bound on the Hamming distance of the non-binary code (K_s, N_s) is thus given by:

$$d_{st} \leq N_s - K_s + 1 = N_s - N_s.R_c + 1 \tag{2.24}$$

Finally, state diversity is upper-bounded by [34][35]

$$d_{st} \leq \lfloor D_{st}(1 - R_c) + 1 \rfloor \leq D_{st} \tag{2.25}$$

Note that the maximal diversity given by the outage limit under a finite size QAM alphabet also achieves the above Singleton bound [10]. We can notice from (2.25) that full diversity is attained only if $R_c \leq 1/D_{st}$. As D_{st} grows to infinity (i.e. tends to an ergodic fading channel), the diversity order of a coded system is limited by $\omega_H(c)$.

2.5 Conclusions

We discussed the outage probability for block-fading channels, that represents the fundamental lower-bound on the performance of coded modulations for long enough codewords on this type of channels. We then presented our system model, that will be used throughout this manuscript to design schemes that approach the outage probability limit. We finally explained the bounds on the diversity order of a binary code over block-fading channels, bound that will be elaborated further to fit to specific types of block-fading channels, namely the multiple-input multiple-output (MIMO) channel and amplify-and-forward cooperative fading channel.

Chapter 3

Coded modulations for the multiple-antenna channel

3.1 Introduction

Since the late nineties, employing multiple-antennas on a communicating terminal has been of great interest as a result of the dramatic increase in capacity these systems can provide [5][6]. Moreover, for block-fading channels, multiple-antennas are a mean to provide spatial diversity that allows to combat the fluctuations of the quality of the channel. Since then, researchers in the wireless communication community studied and designed efficient schemes for such systems that allow for maximal diversity orders and high performance. With the exception of few works that will be mentioned in this chapter, most designs only considered the protection of constellation symbols under ML decoding, without taking into account the presence of an error correcting code. In this chapter, we will propose coded modulation schemes for the multiple-antenna channel that perform close to channel limits. We will start by a state-of-the-art of coding schemes for the MIMO channel in section 3.2. We will then show the frame error rate of uncoded space-time rotations as a function of the frame length (that constitutes the motivation behind our work), the general system model, and the bounds on the diversity order achieved by multiple-antenna systems. Next we will discuss our three proposed schemes; the first one consists of designing space-time precoders that minimize the discrete-input outage probability (section 3.6), the second consists of the extension of the Alamouti scheme to a system with $n_t = 4$ transmit antennas (section 3.7), and the third considers code multiplexer design for turbo codes (section 3.8).

3.2 A brief historical note

After the pioneering works in [5][6] on multiple-antenna channels, the author in [36] proposed the Bell-Labs Layered Space Time codes (BLAST), that demultiplex the symbol

stream over n_t transmit antennas, while the receiver recovers the transmitted symbols through n_r receive antennas. This scheme was capable of achieving high data rates through spatial multiplexing, but it was not capable of recovering the diversity provided by the transmit antennas as no "smart" processing was performed at the transmitter level. For that reason, the authors in [26][37] proposed design criteria for "space-time codes", in a goal to make benefit from the transmit diversity at the receiver. These criteria consisted of minimizing the pairwise error probability of a pair of space-time codewords by maximizing both the determinant and the rank of the codeword matrix. The codes proposed at first were constructed following orthogonal designs, from the famous Alamouti code for $n_t = 2$ [25] to the generalization for any number of transmit antennas in [26]. In the same paper [26], the authors proposed the "space-time trellis codes"; these codes follow the concept of convolutional codes as they are encoded via a trellis. They have better error rate performance than orthogonal space-time block codes, but they require a viterbi decoder thus an increase in decoding complexity. The problem with these codes is that they severely degrade the information rate by introducing redundancy, and this degradation is proportional to the number of transmit antennas. Indeed, for an orthogonal complex space-time block code employing n_t antennas, the maximal achievable rate is:

$$R_p = \frac{1 + \log_2 n_t}{2.\log_2 n_t} \tag{3.1}$$

As a nresult of this limitation of orthogonal designs, the use of algebraic tools to build space-time rotations that attain full diversity and full spatial multiplexing was considered. Indeed, precoding signals for fading channels, which is well-known in single antenna transmissions, has been rediscovered for multiple-antenna channels. In fact, Battail was the first to suggest rotations to combat channel fluctuations in [38]. The pioneering work on multi-dimensional rotated modulations achieved in the nineties, such as [39][40][41], opened the way for the study of multi-dimensional rotations (i.e. linear unitary precoders) in MIMO channels. Rotations in single antenna systems have been designed by classical algebraic criteria, except for orthogonal transforms proposed by Rainish which are based on the minimization of the cut-off rate [42]. Also, it has been shown in [43] that random rotations perform as good as algebraic rotations in a high-diversity high-dimensional environment. In [44] [45] [46] among others, the authors proposed then algebraic constructions of space-time codes for uncoded multiple-antenna systems, and they outperformed orthogonal designs as they were full-rate, i.e. one symbol is sent per transmit antenna per symbol time. However, new problems have arisen with these designs, as the determinant of the codeword matrix vanishes with an increase in the constellation size. The race to the optimal space-time code for uncoded systems was ended by the works in [47] [48] [49] for $n_t = 2$ and by [50] for $n_t = 3, 4, 6$. Indeed, these works provide space-time codes that have non-vanishing determinants, thus they yield optimal performance with uncoded systems under maximum-likelihood detection. As an example, the Golden code [47] is an

algebraic precoder optimized for $n_t = n_r = 2$, its precoding matrix is:

$$\mathbf{S_{GC}} = \begin{bmatrix} 0.52e^{-j0.55} & 0 & 0 & 0.85e^{+j1.01} \\ 0.85e^{-j0.55} & 0 & 0 & 0.52e^{-j2.12} \\ 0 & 0.85e^{+j2.58} & 0.52e^{-j0.55} & 0 \\ 0 & 0.52e^{-j0.55} & 0.85e^{-j0.55} & 0 \end{bmatrix} \tag{3.2}$$

As an alternative to the design criteria proposed in [26][37], linear dispersion (LD) codes [51] were designed for multiple antenna channels by a search that maximizes the ergodic capacity of the channel under a Gaussian channel input. Such a design is not necessarily suitable for a non-ergodic channel with a finite number of states, as these channels are information unstable [7]. Also, the type of input alphabet is not considered in the search for linear dispersion codes.

The major drawback of the aforementioned design criteria is that they do not take into account the concatenation with an error correcting code in the system. Furthermore, space-time signal modulations must be combined to error-correcting codes in order to achieve optimal performance in the information theoretical sense.

For this reason, the authors in [17][18] considered bit-interleaved coded modulations for space-time coding (ST-BICM). They showed that quasi-optimal global ML performance of the coded modulation is achieved by imposing specific constraints (called *genie conditions*) on the structure of the space-time precoder under ideal interleaving. In fact, in order to guarantee maximum diversity order and maximum coding gain at the output of the detector, the design must guarantee two conditions:

- Orthogonal sub-rows in the linear precoding matrix.
- Equal norm sub-rows in the linear precoding matrix.

If these conditions are met, perfect *a priori* probability feedback will be assumed in the iterative joint detection and decoding of ST-BICM, hence quasi-ML performance will be attained in practice after some iterations at a high signal-to-noise ratio. As an example, the cyclotomic rotation given below is an algebraic precoder satisfying the genie conditions for ST-BICM with $n_t = 2$:

$$\mathbf{S_{Cyclo}} = [\phi_{ij}] = \frac{1}{2}\begin{bmatrix} 1 & 1 & e^{j6\pi/15} & -e^{j6\pi/15} \\ e^{j2\pi/15} & je^{j2\pi/15} & -e^{j8\pi/15} & je^{j8\pi/15} \\ e^{j4\pi/15} & -e^{j4\pi/15} & e^{j10\pi/15} & e^{j10\pi/15} \\ e^{j6\pi/15} & -je^{j6\pi/15} & -e^{j12\pi/15} & -je^{j12\pi/15} \end{bmatrix} \tag{3.3}$$

where we have the following:

- Vector $(\phi_{i,1}, \phi_{i,2})$ is orthogonal to vector $(\phi_{i,3}, \phi_{i,4})$ on any row i, $i = 1 \ldots 4$.
- Vectors $(\phi_{i,1}, \phi_{i,2})$ and $(\phi_{i,3}, \phi_{i,4})$ have equal norms.

Note that most of the algebraic space-time rotations designed for uncoded systems guarantee at least one of the above conditions. The precoding matrix $\mathbf{S_{GC}}$ of the Golden code from (3.2) for instance guarantees the first genie condition, and the second condition can be compensated by an error correcting code with high coding gain [18].
In this chapter, we will propose space-time precoders suited for the ST-BICM scheme whose design is mostly based on the conditions established in [17][18] for optimal performance. Before doing so, we will show the behavior of the frame error rate performance of uncoded space-time rotations and recall the bounds on the diversity orders that can be attained by a ST-BICM on MIMO block-fading channels under ideal interleaving.

3.3 Upper bound on the frame error rate for uncoded space-time signaling

Suppose that we concatenate N_f space-time precoded blocks forming a frame to be transmitted on a block-fading channel with a probability of error $P_f(N_f)$. Suppose now that each block has diversity order d, so the probability of error P_c of each independent code is a function of the signal-to-noise ratio γ and a chi-square random variable y given by:

$$y = \sum_{i=1}^{2d} y_i^2 \quad y_i \sim \mathcal{N}_f\left(0, \sigma^2\right) \tag{3.4}$$

$$p(y) = \frac{y^{d-1} e^{-y/2\sigma^2}}{(d-1)!} \tag{3.5}$$

Now let $P_f(N_f)$ denote the frame error rate as a function of N_f:

$$P_f(N_f) = \int_0^{+\infty} \left[1 - (1 - P_c(\gamma, y))^{N_f}\right] p(y) dy \tag{3.6}$$

We can write that [34]:

$$P_f(N_f) \leq 1 - (1 - P_c(\gamma, y))^{N_f} \leq N_f . P_c(\gamma, y) \tag{3.7}$$

which gives the upper bound on $P_f(N_f)$ as N_f goes to infinity as [18, Appendix A]:

$$P_f(N_f) \leq \int_0^{+\infty} min\left[1, N_f . P_c(\gamma, y)\right] p(y) dy \tag{3.8}$$

$$= \int_0^{\alpha} p(y) dy + \int_{\alpha}^{+\infty} N_f . P_c(\gamma, y) p(y) dy \tag{3.9}$$

where α is given by:

$$P_c(\gamma, \alpha) = \frac{1}{N_f} \tag{3.10}$$

Now let us suppose that when γ goes to infinity we get:

$$P_c(\gamma, y) \cong e^{-y\gamma/2} \tag{3.11}$$

which gives the value for α as:

$$\alpha = \frac{2}{\gamma}\log(\frac{N_f}{2}) \tag{3.12}$$

Now we can write the first term of (3.9) as:

$$P_{f1}(N_f) = \int_0^{\alpha} p(y)dy = 1 - e^{-\alpha}\sum_{k=0}^{d-1}\frac{\alpha^k}{k!} = e^{-\alpha}\sum_{k=d}^{+\infty}\frac{\alpha^k}{k!} \tag{3.13}$$

Then we can write:

$$\lim_{\gamma\to+\infty, N_f\to+\infty,} P_{f1}(N_f) = \frac{\left[\frac{2}{\gamma}\log(\frac{N_f}{2})\right]^d}{d!} \tag{3.14}$$

Finally we can write the second term of (3.9) as:

$$P_{f2}(N_f) = \int_{\alpha}^{+\infty} N_f.P_c(\gamma, y)p(y)dy \tag{3.15}$$

and:

$$\lim_{\gamma\to+\infty} P_{f2}(N_f) = \lim_{\gamma\to+\infty}\int_{\alpha}^{+\infty} N\frac{y^{m-1}e^{-(1+\frac{\gamma}{2})y}}{(m-1)!}dy \tag{3.16}$$

$$= \lim_{\gamma\to+\infty} N\frac{e^{-\gamma(1+\frac{\gamma}{2})}}{(1+\frac{\gamma}{2})^d}\sum_{k=0}^{d-1}\frac{\left[\gamma(1+\frac{\gamma}{2})\right]^k}{k!} \tag{3.17}$$

$$= \lim_{\gamma\to+\infty}\frac{1}{(1+\frac{\gamma}{2})^d} \tag{3.18}$$

We can notice from equation (3.14) that the frame error rate of an uncoded system degrades as $\log(N_f)^d$ where d is the diversity order. Hence, it is impossible to approach outage probability with uncoded systems, as a coding scheme that approaches outage probability has to be insensitive (or slightly sensitive) to block length. For the Alamouti scheme for instance, the frame error rate is upper-bounded by:

$$P_f(N_f) \leq \frac{2\log^2(\frac{N_f}{2}) + 4\log(\frac{N_f}{2}) + 4}{\gamma^2} \tag{3.19}$$

In a similar way, it was found in [52] that the frame error rate obtained by concatenating N_f $(8, 4, 4)$ block codes is upper-bounded by:

$$P_f(N_f) \leq \frac{2\log^2(2N_f) + 3/7\log(7N_f) + 2\log(2N_f) + 24/7}{(2R_c\gamma)^2} \tag{3.20}$$

In addition, it was observed in [53] that the frame error rate of convolutional codes varies logarithmically with N_f on block-fading channels.

3.4 System model and notations

In this chapter, we consider the BICM scheme as presented in section 2.3 concatenated with a space-time precoder as shown in Fig. 2.3.

The channel model for a precoded ST-BICM is given by:

$$\mathbf{y} = \mathbf{zSH} + \mathbf{w} = \mathbf{xH} + \mathbf{w} \tag{3.21}$$

where $\mathbf{z} \in \Omega = (M\text{-QAM})^{N_t}$ and $N_t = R_p \cdot s \cdot n_t$, the parameter s being the time spreading of a precoding matrix $\mathbf{S}$ of dimensions $N_t \times N_t/R_p$, where R_p is the rate of the precoder. In general, $\mathbf{S}$ is a full-rate unitary matrix (i.e. $R_p = 1$) whose structure is matched to iterative detection as the class of cyclotomic rotations proposed in [17][18]. The MIMO channel matrix has dimensions $N_t/R_p \times N_r/R_p$, and assuming that the number of independent channel realizations observed during one codeword transmission is n_c, we get:

$$\mathbf{H} = diag\left(\overbrace{\underbrace{\mathbf{H}_1,\ldots,\mathbf{H}_1}_{s.R_p/n_c},\ldots,\mathbf{H}_{n_c},\ldots,\mathbf{H}_{n_c},\ldots,\underbrace{\mathbf{H}_1,\ldots,\mathbf{H}_1}_{s.R_p/n_c},\ldots,\mathbf{H}_{n_c},\ldots,\mathbf{H}_{n_c}}^{1/R_p}\right) \tag{3.22}$$

the additive white Gaussian noise vector $\mathbf{w}$ of dimension N_r/R_p is assumed to be circularly symmetric with zero mean and mean N_0. The Rayleigh fading channel is quasi-static frequency non-selective, i.e. the whole transmitted frame undergoes one channel realization. The channel coefficients are supposed to be perfectly known (perfect CSI) to the receiver, but not to the transmitter. We make the assumption of perfect channel estimation and perfect synchronization. Digital transmission is made as follows: uniformly distributed information bits are fed to a binary convolutional encoder $\mathcal{C}$. Coded bits $\{c_i\}$ are then interleaved through Π, Gray mapped into QAM symbols, precoded through $\mathbf{S}$ and transmitted on the MIMO channel given by (3.22). The coherent MIMO detector computes an extrinsic information $\xi(c_i)$ based on the knowledge of $\mathbf{H}$, the received vector $\mathbf{y}$, and independent *a priori* information $\pi(c_j)$ for all coded bits. The coding rate is $R_c \in [0, 1]$. The transmitted information rate is equal to $R = R_p R_c n_t \log_2 M$ bits per channel use, where M is the cardinality of the bi-dimensional QAM constellation. An interleaver $\mathbf{\Pi}$ enables iterative probabilistic MIMO detection [54][55] of the binary-oriented channel.

3.5 Diversity bounds for coded multiple-antenna systems

In ST-BICM, there exists a strong interaction between the error correcting code with interleaving and the linear precoder, both in terms of diversity and coding gain maximization [18]. Complexity can be controlled by the choice of a space-time rotation $\mathbf{S}$ with minimal time spreading factor s that guarantees full diversity [56]. In other terms, the lowest complexity solution would be to first let the channel decoder recover the highest

amount of diversity possible, then the detector recovers the remaining diversity through time spreading. For a MIMO channel, the *channel diversity* is defined as $D_{ch} = n_t n_c n_r$, which is equal to the intrinsic diversity order of the physical channel. For a given transmitter structure, the achievable channel diversity is $d_{ch} = \lim_{SNR\to+\infty} -\log(P_e)/\log(SNR)$, where SNR is the signal-to-noise ratio and P_e is the error probability.

When $\mathbf{S}$ is the identity matrix, the ST-BICM diversity order is upper-bounded by [35]:

$$d_{ch} \leq \min\left(n_r \left\lfloor n_t n_c (1 - R_c) + 1 \right\rfloor,\ D_{ch}\right) \tag{3.23}$$

With a vanishing coding rate, i.e. $R_c \to 0$, it is possible to attain the overall system diversity order $n_r n_c n_t$ produced by the receive antennas, the transmit antennas and the distinct channel states. Unfortunately, this is unacceptable due to the vanishing transmitted information rate. Precoding is one means to achieve maximum diversity with a non-vanishing coding rate. Under linear precoding that spreads QAM symbols over s time periods, the Singleton bound becomes [56]:

$$d_{ch} \leq \min\left(s n_r \left\lfloor \lfloor \frac{n_t n_c}{s} \rfloor (1 - R_c) + 1 \right\rfloor,\ D_{ch}\right) \tag{3.24}$$

Now if $s = n_t.n_c$, from the above inequality, we observe that precoding may achieve maximal diversity $n_t n_c$ without the use of error-correcting codes. Unfortunately, near-outage performance is impossible in this case due to the weak coding gain of all kinds of space-time precoders, as was discussed in section 3.3. The near-outage performance of ST-BICM is a judicious trade-off between error-control coding and linear QAM precoding. The genie conditions are optimal, in terms of ML performance, when all diversity given by the transmit antennas is collected at the detector (i.e. $s = n_t$). A supplementary condition (that will be discussed later) called "Dispersive Nucleo Algebraic" (DNA) has been proposed in [18] to keep optimality when $s < n_t$ while having the genie conditions on sub-groups of transmit antennas.

With a judicious choice of an error-correcting code and a linear precoder, maximum diversity is easily attained ($d_{ch} = D_{ch}$). In general, a Nakagami distribution of order D_{ch}/D_{st} is associated to each binary-input sub-channel embedded within the BO-channel. Recall that D_{st} is the state diversity seen by the binary code. To illustrate the above definitions, we list the following examples:

- For $n_t = 2$, $n_r = 1$, $D_{ch} = 2$, and without rotation ($s = 1$). We get $D_{st} = 2$.
- For $n_t = 2$, $n_r = 2$, $D_{ch} = 4$. Without rotation ($s = 1$), we have $D_{st} = 2$. With a cyclotomic rotation ($s = 2$), we get $D_{st} = 1$.
- For $n_t = 4$, $n_r = 2$, $D_{ch} = 8$. Without rotation ($s = 1$), we have $D_{st} = 4$. With a cyclotomic DNA rotation ($s = 2$), we get $D_{st} = 2$.

3.6 Space-time precoders based on information outage minimization

3.6.1 Introduction

At that stage, in the existing works, the authors achieved optimal (quasi-ML) performance with a space-time precoded BICM under iterative detection and decoding. The genie conditions ensure that *a priori* information fed back from the decoder becomes perfect after a certain number of iterations. However, in some practical receivers, an iterative algorithm might not be possible due to resource limitations. The high data rates and the high processing speed required in a communication system can put strict constraints on the number of iterations. For this reason, we will present full-rate space-time precoders that lead the ST-BICM to perform well since the first iteration. Hence, we propose a simple information theoretical design of multi-dimensional rotations that take into account the interaction between channel coding and symbol space-time spreading.

3.6.2 Linear precoding designs

For a fixed rotation $\mathbf{S}$ and n_c fixed MIMO channel matrices $\mathbf{H}_i$, $i = 1 \dots n_c$, defined by the n_c fading blocks, let $\mathcal{I}_{SH} = \mathcal{I}(\mathbf{z};\mathbf{y})$ denote the average mutual information of the equivalent channel with QAM input $\mathbf{z}$ and complex output $\mathbf{y}$ as in (3.21). The expression of $\mathcal{I}_{SH}$ is a slight modification of (2.14) that gives:

$$\mathcal{I}_{SH} = s.m.n_t - \frac{1}{n_c}\sum_{i=1}^{n_c} E_{\mathbf{z},\mathbf{y}|\mathbf{SH}_i}\left[\log_2\left(\frac{\sum_{\mathbf{z}'} p(\mathbf{y}|\mathbf{z}',\mathbf{SH}_i)}{p(\mathbf{y}|\mathbf{z},\mathbf{SH}_i)}\right)\right] \tag{3.25}$$

where $E_{\mathbf{z},\mathbf{y}|\mathbf{SH}_i}$ is the conditional mathematical expectation over $\mathbf{z}$ and $\mathbf{y}$. The channel likelihood is written in its classical form

$$p(\mathbf{y}|\mathbf{z},\mathbf{SH}) \propto \exp\left(-\frac{\|\mathbf{y}-\mathbf{zSH}\|^2}{2\sigma^2}\right) \tag{3.26}$$

Expression (3.25) assumes that the precoder $\mathbf{S}$ does space-time spreading within the same fading block $\mathbf{H}_i$. Its main role is to collect transmit diversity. Time diversity n_c is collected by the convolutional code whereas receive diversity is naturally collected by the detector. The information rate transmitted by the space-time BICM is $R = s.m.n_t.R_c$ bits per s time periods (with $R_p = 1$ for full-rate precoders). An outage occurs if the instantaneous capacity, i.e. $\mathcal{I}_{SH}$ in our case, is less than R (see section 2.2). The outage probability associated to the rotation $\mathbf{S}$ at a given signal-to-noise ratio is

$$P_{out}(\mathbf{S}) = P\left(\mathcal{I}_{SH} < s.m.n_t.R_c\right) \tag{3.27}$$

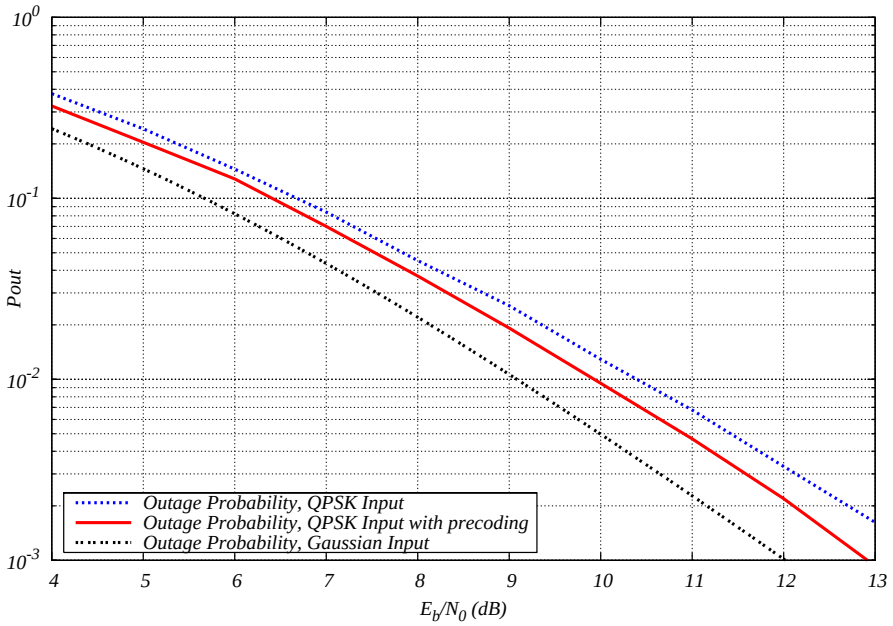

Figure 3.1: Outage limits for $n_t = n_c = s = 2$, $n_r = 1$, and $R_c = 1/2$.

The new design, called IOM (Information Outage Minimization), selects a matrix $\mathbf{S_{IOM}}$ within the ensemble $\aleph$ of random unitary matrices such that

$$\mathbf{S_{IOM}} = \arg \min_{\mathbf{S}\in\aleph} P_{out}(\mathbf{S}) \tag{3.28}$$

As an example, choosing the best rotation within an ensemble $\aleph$ limited to 2000 matrices yields the matrix written below, for QPSK alphabet with $n_t = s = 2$ and coding rate $R_c = 1/2$

$$\mathbf{S_{IOM}} = \begin{bmatrix} 0.57e^{+j1.71} & 0.64e^{+j1.55} & 0.14e^{-j1.89} & 0.49e^{+j1.22} \\ 0.34e^{-j0.94} & 0.51e^{+j2.82} & 0.57e^{+j1.26} & 0.54e^{+j0.27} \\ 0.59e^{-j1.38} & 0.04e^{-j0.04} & 0.61e^{-j1.46} & 0.52e^{+j1.25} \\ 0.46e^{-j0.84} & 0.57e^{+j1.74} & 0.53e^{+j3.05} & 0.43e^{-j2.66} \end{bmatrix}$$

By minimizing the discrete-input outage probability, the random rotation makes the distribution of the input vector $\mathbf{x} = \mathbf{zS}$ to the channel look like a Gaussian distribution. Fig. 3.2 shows the distribution of the vector $\mathbf{zS_{IOM}}$ for a BPSK modulation, the bell shape of the curve is flagrant. The problem with the matrix $\mathbf{S_{IOM}}$ is that it does not satisfy the genie conditions. Although it boosts the performance after a "one-shot" detection and decoding process, it does not guarantee optimal convergence of the iterative process. To make our design suited for both "one-shot" detection and iterative decoding, a smaller set $\aleph_G$ of random unitary matrices is obtained by adding to $\aleph$ the first genie constraint, i.e. orthogonal sub-rows in $\mathbf{S}$. This condition is much more important than the second genie constraint (i.e. equal-norm sub-rows) as it gives independent extrinsic probabilities at the output of the SISO detector. This second design, called G-IOM, selects a matrix

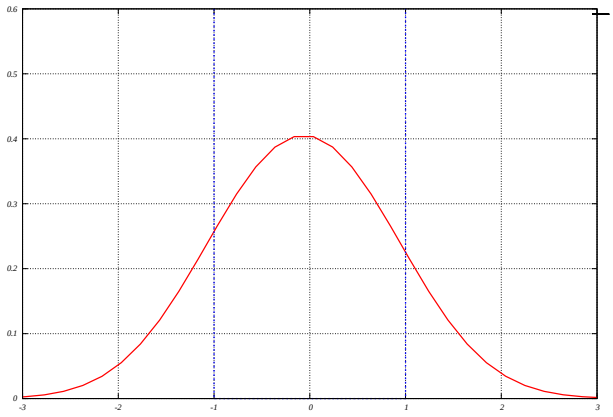

Figure 3.2: Distribution of $\mathbf{zS_{IOM}}$ for a BPSK modulation.

$\mathbf{S_{G-IOM}}$ satisfying

$$\mathbf{S_{G-IOM}} = \arg \min_{S \in \aleph_G} P_{out}(\mathbf{S}) \tag{3.29}$$

As an example, choosing the best rotation within an ensemble $\aleph_G$ limited to 2000 matrices yields the matrix written below, for QPSK alphabet with $n_t = s = 2$ and coding rate $R_c = 1/2$

$$\mathbf{S_{G-IOM}} = \begin{bmatrix} 0.88e^{-j0.30} & 0 & 0 & 0.48e^{-j0.55} \\ 0.48e^{-j0.33} & 0 & 0 & 0.88e^{+j2.57} \\ 0 & 0.47e^{-j2.12} & 0.88e^{+j2.85} & 0 \\ 0 & 0.88e^{+j2.96} & 0.47e^{-j1.49} & 0 \end{bmatrix}$$

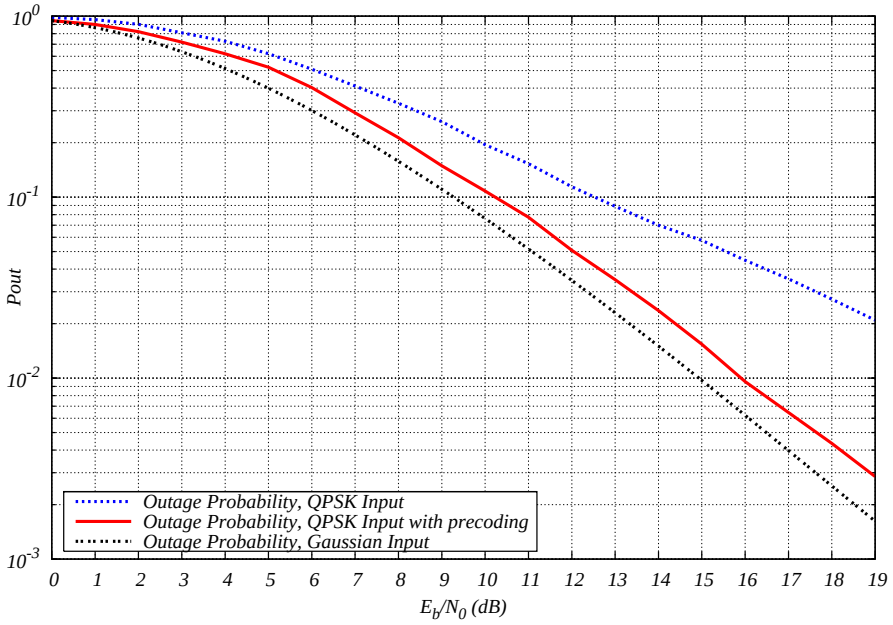

Figure 3.3: Outage limits for $n_t = n_c = s = 2$, $n_r = 1$, and $R_c = 3/4$.

Now for the case of $n_t = 4$, using a half-rate convolutional code allows us to employ a

DNA precoder with $s = 2$ as it ensures maximal diversity through (3.24). We thus design a DNA-IOM precoder that minimizes and satisfies DNA constraints [18]; the first step is to pick a 4×4 rotation from the ensemble $\aleph_{DNA}$ of random rotation, and the second step is to place the orthogonal nucleotides inside an 8×8 matrix and separate them with null nucleotides. We obtain the following rotation for $n_t = 4$ and $s = 2$ (see proposition (2), page 54, in [18]):

$$\mathbf{S_{DNA}} = \begin{bmatrix} \phi_{11} & \phi_{12} & 0 & 0 & \phi_{13} & \phi_{14} & 0 & 0 \\ 0 & 0 & \phi_{11} & \phi_{12} & 0 & 0 & \phi_{13} & \phi_{14} \\ \phi_{21} & \phi_{22} & 0 & 0 & \phi_{23} & \phi_{24} & 0 & 0 \\ 0 & 0 & \phi_{21} & \phi_{22} & 0 & 0 & \phi_{23} & \phi_{24} \\ \phi_{31} & \phi_{32} & 0 & 0 & \phi_{33} & \phi_{34} & 0 & 0 \\ 0 & 0 & \phi_{31} & \phi_{32} & 0 & 0 & \phi_{33} & \phi_{34} \\ \phi_{41} & \phi_{42} & 0 & 0 & \phi_{43} & \phi_{44} & 0 & 0 \\ 0 & 0 & \phi_{41} & \phi_{42} & 0 & 0 & \phi_{43} & \phi_{44} \end{bmatrix} \tag{3.30}$$

with:

$$\mathbf{\Phi_{DNA-IOM}} = \begin{bmatrix} 0.73e^{-j0.81} & 0.22e^{+j4.62} & 0.15e^{+j0.60} & 0.61e^{+j2.59} \\ 0.21e^{+j3.99} & 0.56e^{+j4.44} & 0.62e^{+j0.25} & 0.50e^{-j1.29} \\ 0.57e^{+j0.79} & 0.13e^{-j1.28} & 0.57e^{-j0.63} & 0.57e^{+j0.90} \\ 0.29e^{+j1.01} & 0.78e^{+j3.49} & 0.51e^{+j2.27} & 0.20e^{+j0.91} \end{bmatrix}$$

The DNA-IOM precoder is thus obtained by combining $\mathbf{S_{DNA}}$ with $\mathbf{\Phi_{DNA-IOM}}$. Also, the DNA-cyclotomic precoder is constructed by combining $\mathbf{S_{DNA}}$ to $\mathbf{\Phi_{DNA-Cyclo}} = \mathbf{S_{Cyclo}}$ given previously in (3.3).

Fig. 3.1 and 3.3 show the outage limit for different type of precoders in terms of Word Error Rate versus signal-to-noise ratio. The outage probability has been also evaluated for other system parameters. In fig. 3.1, the precoding matrix enhances the coding gain of the discrete-input outage curve. In fig. 3.3, following the expression in (3.24), a precoding matrix with $s = 2$ is mandatory to recover the diversity at the receiver, as illustrated by the discrete-input outage curves of the unrotated case (that does not achieve diversity), and the rotated case. All outage evaluations have been made by (3.25) and (4.13), without Gaussian and analytical approximations when the channel input is a Gaussian alphabet as in [57][11].

3.6.3 Simulation results

In order to emphasize the diversity order created by coding at the transmitter side, all computer simulations have been conducted with the number of receive antennas $n_r = 1$. Fig. 3.4 and 3.5 illustrate the word error rate performance of a space-time BICM for $n_t = 2$ transmit antennas, $n_c = 2$ channel states, $s = 2$ time period spreading and a coding rate $R_c = 1/2$. Fig. 3.6 illustrates the case with $n_t = 4$ transmit antennas and a precoding

spread factor $s = 2$. At the first iteration, for $n_t = 2$, IOM precoding slightly outperforms other rotations. After 10 detection/decoding iterations, IOM is outperformed by G-IOM and other algebraic rotations. The slight difference in performance is still apparent for $n_t = 4$.

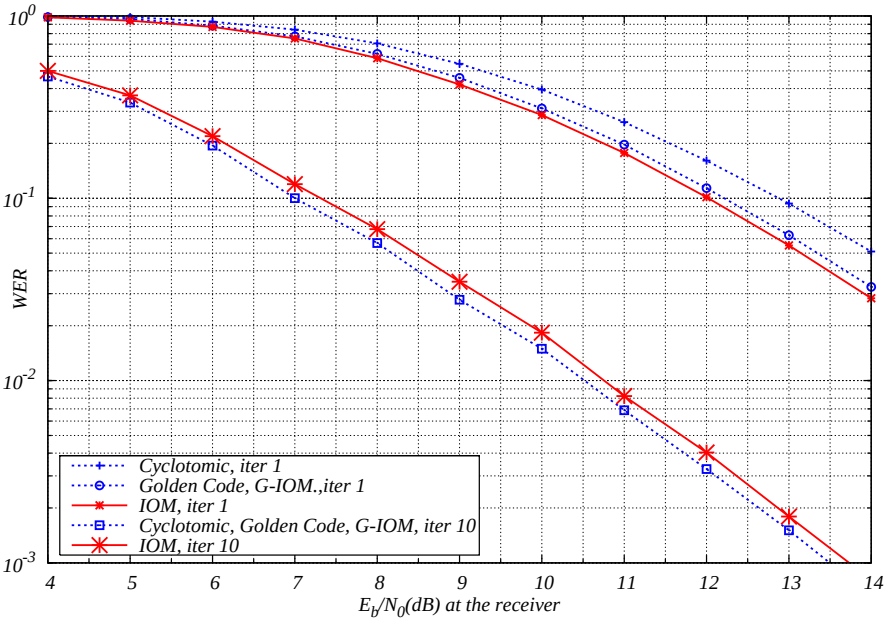

Figure 3.4: QPSK modulation, $n_t = s = n_c = 2$, $n_r = 1$, rate 1/2 16-state $(23, 35)$ convolutional code, interleaver size $N = 2048$ bits, 1 and 10 iterations.

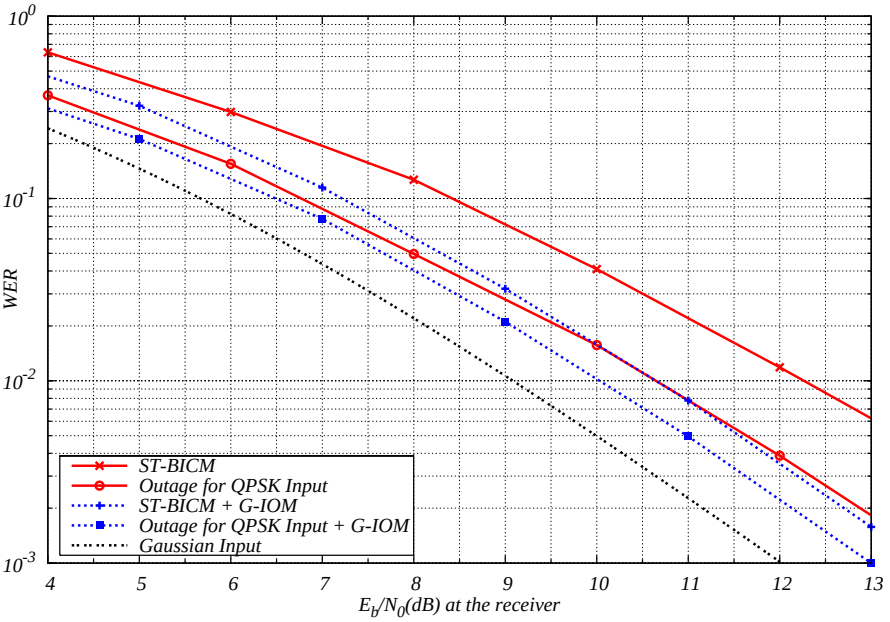

Figure 3.5: QPSK modulation, $n_t = s = n_c = 2$, $n_r = 1$, rate 1/2 16-state $(23, 35)$ convolutional code, interleaver size $N = 2048$ bits.

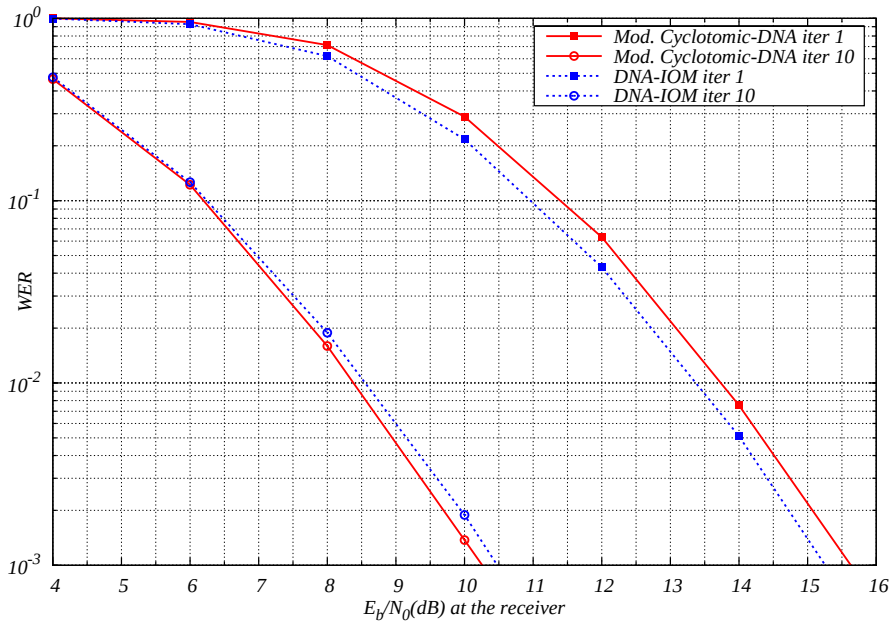

Figure 3.6: BPSK modulation, $n_t = 4$, $s = n_c = 2$, $n_r = 1$, rate 1/2 16-state $(23, 35)$ convolutional code, interleaver size $N = 2048$ bits.

3.7 Space-time precoders based on the Alamouti scheme

3.7.1 Introduction

One orthogonal design that highly caught the attention of the wireless communications community is the Alamouti code [25] with $R_p = 1/2$ for $n_t = 2$. This pragmatic orthogonal scheme allows to convert a 2×1 $(n_t \times n_r)$ antenna configuration onto a 1×2 configuration, by creating two independent parallel channels. Many attempts have tried to generalize the Alamouti scheme to systems with larger antenna configurations, among them the ABBA code [58], but in all cases the optimization was done by trading one parameter (diversity order, rate of the precoder $R_p < 1/2$...). In this section, we present a ST-BICM design suited for a MIMO system with $n_t = 4$, design that uses the Alamouti structure to separate blocks of space-time rotated symbols. In our case, the rate of the precoder is still $R_p = 1/2$ even though we have more than two transmit antennas. However, the difference with the $n_t = 2$ case is that interference among blocks is introduced. For this reason, we look at the problem as if we had a Code-Division Multiple Access (CDMA) system with two users (represented by the two blocks), and inter-block interference becomes similar to inter-user interference in CDMA. There exists several methods to remove the inter-user interference in a CDMA system, and the most efficient algorithms are those that use soft information from a channel decoder [28][59]. In our case, we chose to remove the inter-block interference using the parallel interference cancellation (PIC) algorithm, that proves to be optimal in computer simulations in our context. The performance of this system under quasi-static fading and iterative detection and decoding proved to be close

to system limits. All these points will be clarified in the sequel.

3.7.2 Matrix-Alamouti scheme

In a ST-BICM, the cardinality of the generated set of vectors is given by $|\Omega| = 2^{mN_t}$, m being the number of bits per bi-dimensional QAM constellation symbol. The cardinality increases exponentially with n_t thus leading to a high decoding complexity at the receiver. If $n_t = 4$, $m = 2$, and $R_p \cdot s = 2$ for instance, $|\Omega| = 2^{16} = 65536$, which is intractable for practical applications. In the sequel, we investigate a non-linear space-time precoding scheme that combines the symbols in a matrix-Alamouti form [25]. Let us first define the operators $mat(.)$ and $vec(.)$: $mat(.)$ transforms a vector into a matrix by putting its last sub-part beneath its first sub-part, while $vec(.)$ performs exactly the inverse task. Let us also define the operator ‡ where:

$$\mathbf{u}^{\ddagger} = vec(\mathbf{U}^{\dagger}) \tag{3.31}$$

where $\mathbf{u}$ is a complex vector and $\mathbf{U}$ is any complex matrix. In the new model, $\mathbf{x}$ is rewritten as a 1×16 row vector:

$$\mathbf{x} = \begin{bmatrix} \mathbf{x}_1 & \mathbf{x}_2 & -\mathbf{x}_2^{\ddagger} & \mathbf{x}_1^{\ddagger} \end{bmatrix} \tag{3.32}$$

where $\mathbf{x}_1 = \mathbf{z}_1\mathbf{S}$ and $\mathbf{x}_2 = \mathbf{z}_2\mathbf{S}$ are space-time vectors in $\mathbb{C}^4$, obtained by multiplying a QAM symbol vector $\mathbf{z}_i \in (\text{M-QAM})^4$ with a 4×4 space-time rotation $\mathbf{S}$. Many design criteria for $n_t = 2$ antennas lead to different classes of rotations $\mathbf{S}$ as found in [17][44][47], or IOM and G-IOM rotations presented in section 3.6. Although the rate of the precoder in (3.32) is $R_p = \frac{1}{2}$, it is capable of converting the set of cardinality $|\Omega| = 2^{mN_t}$ onto a smaller set Ω_c of cardinality $|\Omega_c| = 2^{\frac{mN_t}{2}}$, and this is due to the orthogonality inherent to the Alamouti structure. In addition, the bound on the diversity of this scheme is exactly that of a system with $n_t = 2$, as it creates two "parallel" streams via $\mathbf{x}_1$ and $\mathbf{x}_2$ that have a diversity order of $2 \times n_r$ each, independently from the coding rate R_c in (3.24). With a conventional $4 \times n_r$ system, when $R_c \to 1$, full spreading with $s = 4$ is mandatory to recover full channel diversity, yielding an exponential increase in detection complexity. With the scheme proposed in this section, full spreading means $s = 2$. The purpose is then to drastically reduce the complexity at the detector while recovering maximum diversity with high coding rates.

By replacing $\mathbf{x}$ in (3.21) by its form in (3.32), we get a slightly different channel model than the one of (3.21) and (3.22) as follows:

$$\begin{bmatrix} \mathbf{y}_1 & \mathbf{y}_2 \end{bmatrix} = \begin{bmatrix} \mathbf{x}_1 & \mathbf{x}_2 & -\mathbf{x}_2^{\ddagger} & \mathbf{x}_1^{\ddagger} \end{bmatrix} \begin{bmatrix} \mathbf{H}_{b1} & 0 \\ \mathbf{H}_{b2} & 0 \\ 0 & \mathbf{H}_{b1} \\ 0 & \mathbf{H}_{b2} \end{bmatrix} + \begin{bmatrix} \mathbf{w}_1 & \mathbf{w}_2 \end{bmatrix} \tag{3.33}$$

where all vectors $\mathbf{y}_1$, $\mathbf{y}_2$, $\mathbf{w}_1$ and $\mathbf{w}_2$ are in $\mathbb{C}^{2n_r}$, and:

$$\mathbf{H}_{b1} = \begin{bmatrix} \mathbf{H}_1 & 0 \\ 0 & \mathbf{H}_1 \end{bmatrix} \; ; \; \mathbf{H}_{b2} = \begin{bmatrix} \mathbf{H}_2 & 0 \\ 0 & \mathbf{H}_2 \end{bmatrix}$$

where $\mathbf{H}_1$ and $\mathbf{H}_2$ are $2 \times n_r$ channel coefficients matrices. We can write the received signal vectors from (3.33) as follows:

$$\begin{aligned} \mathbf{y}_1 &= \mathbf{x}_1\mathbf{H}_{b1} + \mathbf{x}_2\mathbf{H}_{b2} + \mathbf{w}_1 && (3.34) \\ \mathbf{y}_2 &= -\mathbf{x}_2^{\ddagger}\mathbf{H}_{b1} + \mathbf{x}_1^{\ddagger}\mathbf{H}_{b2} + \mathbf{w}_2 && (3.35) \end{aligned}$$

The new expressions for $\mathbf{y}_1$ and $\mathbf{y}_2$ from (3.34) and (3.35) become:

$$\begin{aligned} \mathbf{Y}_1 = mat(\mathbf{y}_1) &= mat(\mathbf{x}_1)\mathbf{H}_1 + mat(\mathbf{x}_2)\mathbf{H}_2 + mat(\mathbf{w}_1) \\ &= \mathbf{G}_1\mathbf{H}_1 + \mathbf{G}_2\mathbf{H}_2 + \mathbf{W}_1 && (3.36) \end{aligned}$$

$$\begin{aligned} \mathbf{Y}_2 = mat(\mathbf{y}_2) &= mat\left(-\mathbf{x}_2^{\ddagger}\right)\mathbf{H}_1 + mat\left(\mathbf{x}_1^{\ddagger}\right)\mathbf{H}_2 + mat(\mathbf{w}_2) \\ &= -\mathbf{G}_2^{\dagger}\mathbf{H}_1 + \mathbf{G}_1^{\dagger}\mathbf{H}_1 + \mathbf{W}_2 && (3.37) \end{aligned}$$

where $\mathbf{G}_1$ and $\mathbf{G}_1$ are 2×2 matrices, and $\mathbf{W}_1$ and $\mathbf{W}_2$ are $2 \times n_r$ matrices.
In order to recover the transmit diversity, the combining scheme in [25] has to be performed on (3.36) and (3.37). However, as matrix multiplication is not commutative, two combining schemes can be implemented.

First combining scheme - FCS

We can write the combined versions of $\mathbf{G}_1$ and $\mathbf{G}_2$ as follows:

$$\begin{aligned} \mathbf{\Gamma}_1 &= \mathbf{H}_1^{\dagger}\mathbf{Y}_1 + \mathbf{Y}_2^{\dagger}\mathbf{H}_2 \\ &= \mathbf{H}_1^{\dagger}\mathbf{G}_1\mathbf{H}_1 + \mathbf{H}_2^{\dagger}\mathbf{G}_1\mathbf{H}_2 + \mathbf{H}_1^{\dagger}\mathbf{W}_1 + \mathbf{W}_2^{\dagger}\mathbf{H}_2 && (3.38) \end{aligned}$$

$$\begin{aligned} \mathbf{\Gamma}_2 &= \mathbf{H}_2^{\dagger}\mathbf{Y}_1 - \mathbf{Y}_2^{\dagger}\mathbf{H}_1 \\ &= \mathbf{H}_1^{\dagger}\mathbf{G}_2\mathbf{H}_1 + \mathbf{H}_2^{\dagger}\mathbf{G}_2\mathbf{H}_2 + \mathbf{H}_2^{\dagger}\mathbf{W}_1 - \mathbf{W}_2^{\dagger}\mathbf{H}_1 && (3.39) \end{aligned}$$

Although this combining scheme introduces colored noise, it is capable of totally removing the inter-block interference. However, it gives an estimate of the signal as $\mathbf{H}_i^{\dagger}\mathbf{G}_j\mathbf{H}_i$ that is not of the form of the matched filter (i.e. $\mathbf{H}_i^{\dagger}\mathbf{H}_i$), thus it does not recover all the

transmit diversity. Indeed, for $n_r = 2$ for instance, the equivalent channel matrix after combining is given by:

$$vec(\mathbf{H}_1^\dagger \mathbf{G}_1 \mathbf{H}_1 + \mathbf{H}_2^\dagger \mathbf{G}_1 \mathbf{H}_2) \triangleq$$

$$\mathbf{z}_1\mathbf{S} \begin{bmatrix} |h_{11}|^2 + |h_{31}|^2 & h_{12}^* h_{11} + h_{32}^* h_{31} & h_{11}^* h_{12} + h_{31}^* h_{32} & |h_{12}|^2 + |h_{32}|^2 \\ h_{21}^* h_{11} + h_{41}^* h_{31} & h_{22}^* h_{11} + h_{42}^* h_{31} & h_{21}^* h_{12} + h_{41}^* h_{32} & h_{22}^* h_{12} + h_{42}^* h_{32} \\ h_{11}^* h_{21} + h_{31}^* h_{41} & h_{12}^* h_{21} + h_{32}^* h_{41} & h_{11}^* h_{22} + h_{31}^* h_{42} & h_{12}^* h_{22} + h_{32}^* h_{42} \\ |h_{21}|^2 + |h_{41}|^2 & h_{22}^* h_{21} + h_{42}^* h_{41} & h_{21}^* h_{22} + h_{41}^* h_{42} & |h_{22}|^2 + |h_{42}|^2 \end{bmatrix} \tag{3.40}$$

We observe from (3.40) that only 2 of the 4 symbols of $\mathbf{z}_1\mathbf{S}$ are multiplied by Nakagami distributed random variables of order 4, thus the overall system diversity is limited to 4. The same reasoning applies to $\mathbf{\Gamma}_2$.

Second combining scheme - SCS

By permuting the matrix product of the first combining scheme, we get other versions of $\mathbf{\Gamma}_1$ and $\mathbf{\Gamma}_2$ denoted by $\mathbf{G}_{c1}$ and $\mathbf{G}_{c2}$ in the sequel:

$$\begin{aligned} \mathbf{G}_{c1} &= \mathbf{Y}_1\mathbf{H}_1^\dagger + \mathbf{H}_2\mathbf{Y}_2^\dagger \\ &= \mathbf{G}_1\mathbf{H}_1\mathbf{H}_1^\dagger + \mathbf{H}_2^\dagger\mathbf{H}_2\mathbf{G}_1 + \mathbf{G}_2\mathbf{H}_2\mathbf{H}_1^\dagger - \mathbf{H}_2\mathbf{H}_1^\dagger\mathbf{G}_2 + \mathbf{W}_1\mathbf{H}_1^\dagger + \mathbf{H}_2\mathbf{W}_2^\dagger \end{aligned} \tag{3.41}$$

$$\begin{aligned} \mathbf{G}_{c2} &= \mathbf{Y}_1\mathbf{H}_2^\dagger - \mathbf{H}_1\mathbf{Y}_2^\dagger \\ &= \mathbf{H}_1\mathbf{H}_1^\dagger\mathbf{G}_2 + \mathbf{G}_2\mathbf{H}_2\mathbf{H}_2^\dagger + \mathbf{G}_1\mathbf{H}_1\mathbf{H}_2^\dagger - \mathbf{H}_1\mathbf{H}_2^\dagger\mathbf{G}_1 + \mathbf{W}_1\mathbf{H}_2^\dagger - \mathbf{H}_1\mathbf{W}_2^\dagger \end{aligned} \tag{3.42}$$

The first two terms of (3.41) and (3.42) are the desired signal estimates. The second two terms are the interference introduced by the combining scheme, and the last two terms are the colored noise components. In this scheme we are able to recover the transmit diversity via the first two terms of (3.41) and (3.42), as shown in the following equation for $n_r = 2$:

$$vec(\mathbf{G}_1\mathbf{H}_1\mathbf{H}_1^\dagger + \mathbf{H}_2\mathbf{H}_2^\dagger\mathbf{G}_1) \triangleq \mathbf{z}_1\mathbf{S}\mathbf{H}_{S_1} \tag{3.43}$$

where

$$\mathbf{H}_{S_1} = \begin{bmatrix} A_1 + A_3 & h_{31}^* h_{41} + h_{32}^* h_{42} & h_{11}h_{21}^* + h_{12}h_{22}^* & 0 \\ h_{31}h_{41}^* + h_{32}h_{42}^* & A_1 + A_4 & 0 & h_{11}h_{21}^* + h_{12}h_{22}^* \\ h_{11}^* h_{21} + h_{12}^* h_{22} & 0 & A_2 + A_3 & h_{31}^* h_{41} + h_{32}^* h_{42} \\ 0 & h_{11}^* h_{21} + h_{12}^* h_{22} & h_{31}h_{41}^* + h_{32}h_{42}^* & A_2 + A_4 \end{bmatrix} \tag{3.44}$$

and

$$A_1 = |h_{11}|^2 + |h_{12}|^2, \quad A_2 = |h_{21}|^2 + |h_{22}|^2, \quad A_3 = |h_{31}|^2 + |h_{32}|^2, \quad A_4 = |h_{41}|^2 + |h_{42}|^2$$

By symmetry, we get:

$$\mathbf{H}_{S_2} = \mathbf{H}_{S_1}^{\dagger} = \begin{bmatrix} A_1 + A_3 & h_{31}h_{41}^* + h_{32}h_{42}^* & h_{11}^*h_{21} + h_{12}^*h_{22} & 0 \\ h_{31}^*h_{41} + h_{32}^*h_{42} & A_1 + A_4 & 0 & h_{11}^*h_{21} + h_{12}^*h_{22} \\ h_{11}h_{21}^* + h_{12}h_{22}^* & 0 & A_2 + A_3 & h_{31}h_{41}^* + h_{32}h_{42}^* \\ 0 & h_{11}h_{21}^* + h_{12}h_{22}^* & h_{31}^*h_{41} + h_{32}^*h_{42} & A_2 + A_4 \end{bmatrix} \tag{3.45}$$

As shown in (3.43), every symbol in $\mathbf{z}_1\mathbf{S}$ and $\mathbf{z}_2\mathbf{S}$ undergoes Nakagami distributed random variables of order 4, which leads to an overall system diversity of 8.

However, this combining scheme introduces considerable interference along with colored noise. In an uncoded system, this combining scheme does not converge as the received signal constellation is not clearly delimited within distinct Voronoï regions, even for significantly high signal-to-noise ratios. This scenario is similar to that of multi-user detection (MUD) in heavily loaded CDMA systems, where users introduce interference to each others. Hence, we can use detection techniques known for coded MUD-CDMA as in [28][59] and their references to get reliable estimates of the signals. Therefore, we choose to map one interleaved codeword through $\mathbf{z}_1$, and another interleaved codeword using $\mathbf{z}_2$, as if we had two "virtual" users. This results in sending a frame that has the length of two codewords. The transmitter for the proposed system is shown in Fig. 3.7.

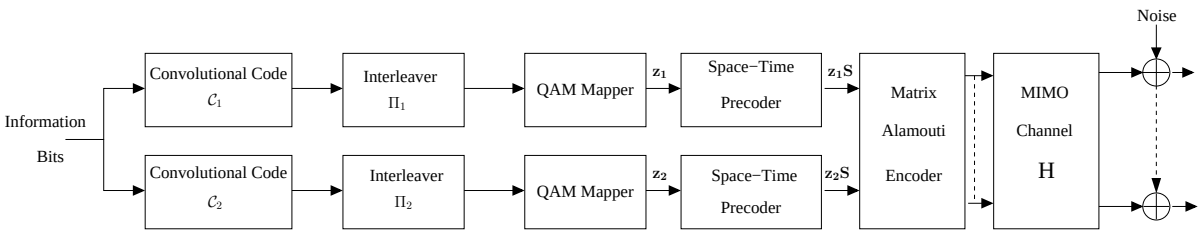

Figure 3.7: Transmitter model for matrix-Alamouti encoded ST-BICM.

In our case, as convolutional codes are employed, one can send a unique codeword instead of two. However, we have to make sure that the coded bits that are mapped onto $\mathbf{z}_1$ are far from the coded bits that are mapped onto $\mathbf{z}_2$ in the trellis of the code, and the two parts of the code should be interleaved separately. In this way we avoid introducing inter-block interference at the transmitter.

3.7.3 Iterative joint detection and decoding

Let us write (3.41) and (3.42) as:

$$\mathbf{g}_{c1} = vec(\mathbf{G}_{c1}) = \mathbf{z}_1\mathbf{S}\mathbf{H}_{S_1} + \mathbf{z}_2\mathbf{S}\mathbf{H}_{I_1} + vec(\mathbf{W}_1\mathbf{H}_1^{\dagger} + \mathbf{H}_2\mathbf{W}_2^{\dagger}) \tag{3.46}$$

$$\mathbf{g}_{c2} = vec(\mathbf{G}_{c2}) = \mathbf{z}_2\mathbf{S}\mathbf{H}_{S_2} + \mathbf{z}_1\mathbf{S}\mathbf{H}_{I_2} + vec(\mathbf{W}_1\mathbf{H}_2^{\dagger} - \mathbf{H}_1\mathbf{W}_2^{\dagger}) \tag{3.47}$$

where $\mathbf{H}_{S_1}$ and $\mathbf{H}_{S_2}$ are taken from (3.44) and (3.45). In addition, we have:

$$\mathbf{H}_{I_1} = \begin{bmatrix} 0 & -h_{41}h_{11}^* - h_{42}h_{22}^* & h_{31}h_{21}^* + h_{32}h_{22}^* & 0 \\ -h_{31}h_{21}^* - h_{32}h_{22}^* & B & 0 & h_{31}h_{21}^* + h_{32}h_{22}^* \\ h_{41}h_{11}^* + h_{42}h_{22}^* & 0 & -B & -h_{41}h_{11}^* - h_{42}h_{22}^* \\ 0 & h_{41}h_{11}^* + h_{42}h_{22}^* & -h_{31}h_{21}^* - h_{32}h_{22}^* & 0 \end{bmatrix}$$

where

$$B = h_{31}h_{11}^* + h_{32}h_{12}^* - h_{41}h_{21}^* - h_{42}h_{22}^*$$

and $\mathbf{H}_{I_2} = \mathbf{H}_{I_1}^\dagger$ by symmetry.

Now let N denote the number of M-QAM symbols in one convolutional codeword (i.e. there are $2N$ M-QAM symbols in a frame for both convolutional codes). In order to get reliable estimates of the combined signals, one has to efficiently remove interference from (3.46) and (3.47). This gives us:

$$\begin{aligned} \widetilde{\mathbf{g}_{c1}} &= \mathbf{g}_{c1} - \widetilde{\mathbf{z}_2}\mathbf{S}\mathbf{H}_{I_1} \\ &= \mathbf{z}_1\mathbf{S}\mathbf{H}_{S_1} + (\mathbf{z}_2 - \widetilde{\mathbf{z}_2})\mathbf{S}\mathbf{H}_{I_1} + vec(\mathbf{W}_1\mathbf{H}_1^\dagger + \mathbf{H}_2\mathbf{W}_2^\dagger) \end{aligned} \tag{3.48}$$

$$\begin{aligned} \widetilde{\mathbf{g}_{c2}} &= \mathbf{g}_{c2} - \widetilde{\mathbf{z}_1}\mathbf{S}\mathbf{H}_{I_2} \\ &= \mathbf{z}_2\mathbf{S}\mathbf{H}_{S_2} + (\mathbf{z}_1 - \widetilde{\mathbf{z}_1})\mathbf{S}\mathbf{H}_{I_2} + vec(\mathbf{W}_2\mathbf{H}_2^\dagger - \mathbf{H}_1\mathbf{W}_1^\dagger) \end{aligned} \tag{3.49}$$

The first term in (3.48) and (3.49) is the desired signal part, and the other two are the residual interference and colored noise terms. In this case, the likelihoods of $\widetilde{\mathbf{g}_{c1}}$ and $\widetilde{\mathbf{g}_{c2}}$ follow the multivariate Gaussian distribution as:

$$p\left(\widetilde{\mathbf{g}_{c1}} \mid \mathbf{z}_1, \mathbf{S}\mathbf{H}_{S_1}\right) \sim \mathcal{N}\left(\mathbf{z}_1\mathbf{S}\mathbf{H}_{S_1}, \mathbf{\Sigma}_1\right); \quad p\left(\widetilde{\mathbf{g}_{c2}} \mid \mathbf{z}_2, \mathbf{S}\mathbf{H}_{S_2}\right) \sim \mathcal{N}\left(\mathbf{z}_2\mathbf{S}\mathbf{H}_{S_2}, \mathbf{\Sigma}_2\right)$$

where

$$\mathbf{\Sigma}_1 = \mathbb{E}\left[\left(\widetilde{\mathbf{g}_{c1}} - \mathbf{z}_1\mathbf{S}\mathbf{H}_{S_1}\right)^\dagger \left(\widetilde{\mathbf{g}_{c1}} - \mathbf{z}_1\mathbf{S}\mathbf{H}_{S_1}\right)\right] \tag{3.50}$$

$$\mathbf{\Sigma}_2 = \mathbb{E}\left[\left(\widetilde{\mathbf{g}_{c2}} - \mathbf{z}_2\mathbf{S}\mathbf{H}_{S_2}\right)^\dagger \left(\widetilde{\mathbf{g}_{c2}} - \mathbf{z}_2\mathbf{S}\mathbf{H}_{S_2}\right)\right] \tag{3.51}$$

Let us define:

$$V_1\left(\mathbf{z}_1\right) = \widetilde{\mathbf{g}_{c1}} - \mathbf{z}_1\mathbf{S}\mathbf{H}_{S_1} \tag{3.52}$$

$$V_2\left(\mathbf{z}_2\right) = \widetilde{\mathbf{g}_{c2}} - \mathbf{z}_2\mathbf{S}\mathbf{H}_{S_2} \tag{3.53}$$

After the interference and colored noise covariance matrices $\mathbf{\Sigma}_i$ are computed, the soft-input soft-output (SISO) detector computes the extrinsic probabilities $\xi_i\left(c_j\right)$ that the j^{th} bit of codeword i is equal to 1, as given by the slight modification of (2.23) as:

$$\xi_1(c_\ell) = \frac{\sum_{\mathbf{z}_1' \in \Omega_c(c_\ell=1)} exp\left[-V_1\left(\mathbf{z}'_1\right)\mathbf{\Sigma}_1^{-1}V_1\left(\mathbf{z}_1'\right)^\dagger\right]\prod_{r\neq\ell}\pi_1(c_r)}{\sum_{\mathbf{z}_1\in\Omega_c} exp\left[-V_1(\mathbf{z}_1)\mathbf{\Sigma}_1^{-1}V_1(\mathbf{z}_1)^\dagger\right]\prod_{r\neq\ell}\pi_1(c_r)} \tag{3.54}$$

and

$$\xi_2(c_\ell) = \frac{\sum_{\mathbf{z}_2' \in \Omega_c(c_\ell=1)} exp\left[-V_2\left(\mathbf{z}_2'\right)\mathbf{\Sigma}_2^{-1}V_2\left(\mathbf{z}_2'\right)^\dagger\right]\prod_{r\neq\ell}\pi_2(c_r)}{\sum_{\mathbf{z}_2\in\Omega_c} exp\left[-V_2(\mathbf{z}_2)\mathbf{\Sigma}_2^{-1}V_2(\mathbf{z}_2)^\dagger\right]\prod_{r\neq\ell}\pi_2(c_r)} \tag{3.55}$$

Where $\pi_1(c_r)$ and $\pi_2(c_r)$ are *a priori* probabilities generated by soft-input soft-output (SISO) decoders for the 1^{st} and the 2^{nd} convolutional codes respectively. As shown in Fig. 3.8 below, the extrinsic probabilities are then fed back from the SISO detectors to their respective SISO decoders that use the forward-backward (BCJR) algorithm to give *a posteriori* probabilities of the coded bits. In addition, the decoders give back *a priori* $\pi_1(c_r)$ and $\pi_2(c_r)$ probabilities to their respective SISO detectors as in the classical receiver, and also to the detectors of different indices in order to compute the covariance matrices $\mathbf{\Sigma}_i$ and better remove the interference at each iteration. Unlike the conventional receiver where the extrinsic probabilities generated by the detector are computed once at the first iteration using (2.23), the extrinsic probabilities (3.54) and (3.55) in this case are computed at each iteration as the $\mathbf{\Sigma}_i$ matrices change. However, in most cases, this linear increase in complexity is negligible compared to the exponential increase in complexity introduced by a signal set of higher cardinality. Let us take the following example: suppose we have a conventional ST-BICM with $R_c = 3/4$ and $n_t = 4$ transmit antennas. In order to recover maximal diversity, we need to use a space-time precoder with $s = 4$. This gives a cardinality of the space-time signal vector as $|\Omega| = 2^{mN_t} = 2^{16m}$, over which the exhaustive search to compute the extrinsic information in (2.23) is performed. However, with the matrix-Alamouti scheme, $s = 2$ is sufficient to recover the diversity. This gives $|\Omega_c| = 2^{8m}$, using a higher order M-QAM constellation to compensate $R_p = 1/2$. So even if we need t iterations for the receiver to converge, we still have a drastic complexity reduction, as $2 \times t \times 2^{8m} \ll 2^{16m}$.

In computer simulations presented in the next section, vectors $\mathbf{z}_1$ and $\mathbf{z}_2$ in (3.50) – (3.53) were replaced by their soft estimates. Thus, we have:

$$\mathbf{\Sigma}_1 \backsimeq \frac{1}{N}\sum_{i=1}^{\frac{N}{4}}\left[\left(\widetilde{\mathbf{g}_{c1i}} - \mathbf{z}_{1i}\mathbf{S}\mathbf{H}_{S_1}\right)^\dagger\left(\widetilde{\mathbf{g}_{c1i}} - \mathbf{z}_{1i}\mathbf{S}\mathbf{H}_{S_1}\right)\right] \tag{3.56}$$

$$\mathbf{\Sigma}_2 \backsimeq \frac{1}{N}\sum_{i=1}^{\frac{N}{4}}\left[\left(\widetilde{\mathbf{g}_{c2i}} - \mathbf{z}_{2i}\mathbf{S}\mathbf{H}_{S_2}\right)^\dagger\left(\widetilde{\mathbf{g}_{c2i}} - \mathbf{z}_{2i}\mathbf{S}\mathbf{H}_{S_2}\right)\right] \tag{3.57}$$

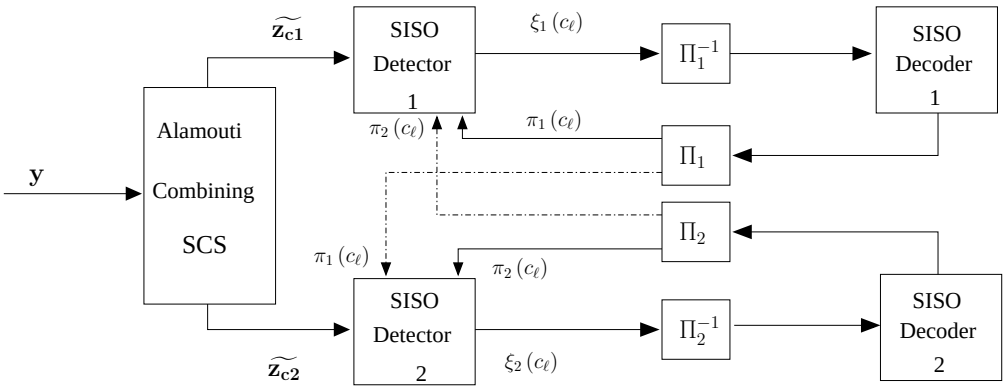

Figure 3.8: Iterative receiver model for matrix-Alamouti encoded ST-BICM

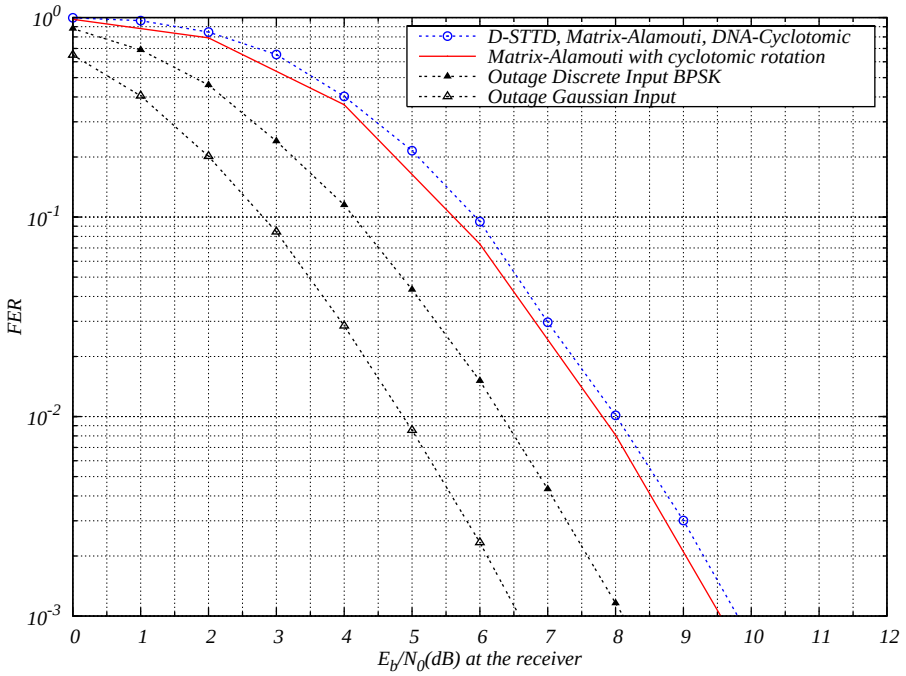

Figure 3.9: Performance for a frame size of 4096 coded bits (2×2048 for matrix-Alamouti), $R_c = 1/2$, $n_t = 4$ and $n_r = 2$ antennas.

3.7.4 Simulation results

In this section, frame error probabilities are illustrated versus signal-to-noise ratios and frame size for $n_t = 4$ and $n_r = 2$. Comparisons are done with respect to discrete input and Gaussian input outage probabilities. The convolutional code is the half-rate 16-state $(23, 35)_8$ non-recursive non-systematic code (NRNSC) and the interleavers are the optimized interleavers from [18]. Fig. 3.9 shows the frame error rate performance for different a frame sizes of 4096 coded bits. The matrix-Alamouti scheme is compared to

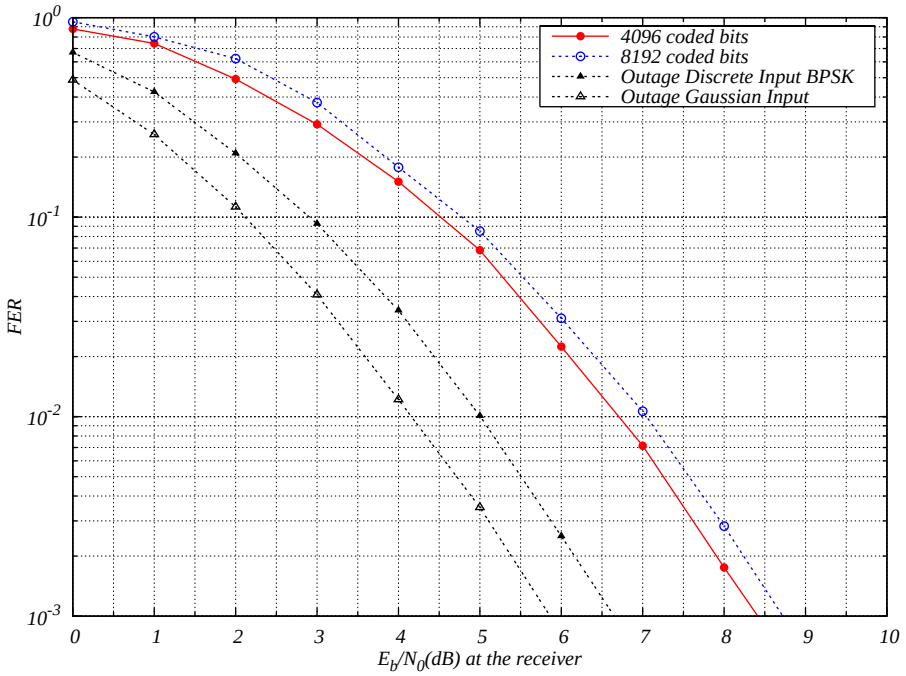

Figure 3.10: Performance for $R_c = 2/3$, BPSK modulation, $n_t = 4$ and $n_r = 2$ antennas.

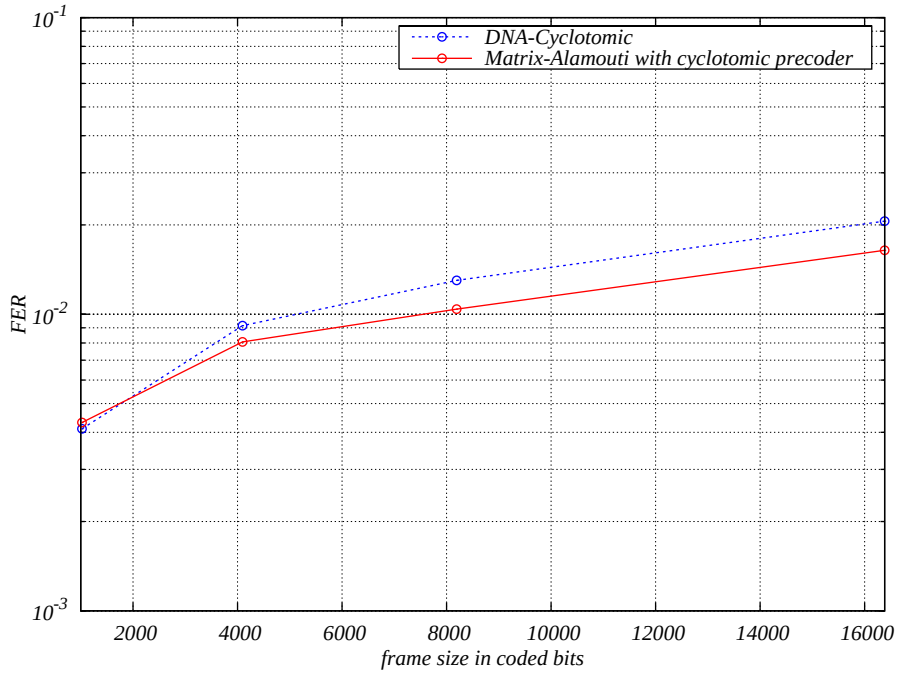

Figure 3.11: Frame error rate versus frame size, $R_c = 1/2$, $E_b/N_0 = 9$ dB, $n_t = 4$ and $n_r = 2$ antennas.

the DNA-cyclotomic rotations and the D-STTD scheme first proposed in [60] and included

in the IEEE802.11n standard, all at a coding rate $R_c = 1/2$. As DNA-cyclotomic rotations are full-rate (i.e. $R_p = 1$), it was simulated with BPSK modulation in order to preserve the same spectral efficiency with the other two schemes that are simulated with QPSK modulations. In fact, with half-rate coding, the matrix $\mathbf{S}$ of matrix-Alamouti scheme does not need to spread the symbol vectors, as diversity can be ensured with $s = 1$. In this case, our scheme performs equally with the two others. However, by setting $\mathbf{S} = \mathbf{S_{Cyclo}}$ from (3.3), we observe a gain with respect to the other schemes. This for sure is at the cost of a slight additional complexity, as $s = 2$ in this case. Fig. 3.10 shows the performance Alamouti scheme with $R_c = 2/3$, that is the half-rate 16-state $(23, 35)_8$ NRNSC code with puncturing, with BPSK modulation. When $\mathbf{S} = \mathbf{S_{Cyclo}}$, the coded modulation achieves full diversity with $s = 2$ as explained in section 3.7.2. With this coding rate, the D-STTD scheme does not ensure maximum diversity, and the standard ST-BICM requires a spreading factor of $s = 4$ as defined in 3.24 to achieve maximum diversity. Finally, Fig. 3.11 compares the performance of the matrix-Alamouti scheme with the DNA-cyclotomic scheme for different frame sizes at a signal-to-noise ratio of 9dB. We can see that our scheme is more robust to an increase in the frame size than the conventional scheme.

3.8 Outage-approaching turbo codes for the multiple-antenna channels

3.8.1 Introduction

As shown in section 3.3, the frame error rate of uncoded space-time signaling is upper-bounded by a quantity that varies as $\log^d(n)$, where d is the diversity order. In order to approach the outage probability limit, the frame error rate of any given coding scheme should be independent of the block length [10, 16]. Therefore, such space-time coding techniques will fail in approaching the outage capacity limit of the quasi-static MIMO channel. Algebraic space-time codes described in section 3.2 and any convolutionally/algebraically coded STBC also fail in approaching the outage limit. Hence, our objectives are

- Design a space-time code based on state multiplexing [53] and turbo encoding [61][62] in order to achieve near outage limit performance.

- Control the detection/decoding complexity and propose relatively low complexity schemes.

- Make the word error probability insensitive to the block length. This is the interleaving gain of turbo codes translated to the field of non-ergodic fading channels as discovered in [16][10].

3.8.2 Code multiplexing over channel states

The physical channel we consider is a quasi-static frequency non-selective MIMO channel with n_t transmit antennas and n_r receive antennas. On a Gaussian channel, the pairwise error probability supposing the zero codeword is emitted by a linear encoder is given by:

$$P(0 \rightarrow c) = Q\left(\sqrt{\frac{2R_cE_b}{N_0}\omega_H(c)}\right) \tag{3.58}$$

where $\omega_H(c)$ is the Hamming weight of the codeword and E_b/N_0 is the signal-to-noise ratio. Now, on a Rayleigh fading channel with D_{st} states, the conditional pairwise error probability becomes:

$$P(0 \rightarrow c) = Q\left(\sqrt{\frac{2R_cE_b}{N_0}\sum_{i=0}^{D_{st}}\omega_i(c)|h_i|^2}\right) \tag{3.59}$$

where $\omega_i(c)$ represents the partial weight of the codeword c undergoing fading h_i, and $\sum_i \omega_i(c) = \omega_H(c)$. After performing a mathematical expectation over the channel states, we can upper-bound the pairwise error probability as:

$$P(0 \rightarrow c) \leq \frac{1}{2}\prod_{i=1}^{D_{st}}\frac{1}{1+\omega_i(c)\frac{RE_b}{N_0}} \tag{3.60}$$

Hence the diversity order $d(c)$ that can be achieved by the code is given by the number of non-zero partial weights $\omega_i(c)$. In addition, for high signal-to-noise ratios, the pairwise error probability behaves like:

$$P(0 \rightarrow c) \propto \frac{1}{\prod_{i=1}^{D_{st}}\omega_i(c)} \times \frac{1}{(E_b/N_0)^{d(c)}} \tag{3.61}$$

So our objectives are to first guarantee that $\forall i,\ \omega_i(c) \neq 0$, to attain maximum diversity, second to maximize the product $\prod_{i=1}^{D_{st}}\omega_i(c)$ and hence the coding gain. For this purpose, the authors in [53] proposed the "code multiplexer" defined as follows:

Definition 2 *The multiplexer is an intelligent switch that distributes turbo coded bits s_i over the D_{st} parallel sub-channels of the BO-channel.*

Actually, the multiplexer should be called "de-multiplexer" or equivalently "channel interleaver". We have chosen the word "multiplexer" in order to avoid any confusion with the interleaver denoted by $\mathbf{\Pi}$ used inside a turbo code. Fig. 3.12 shows two important multiplexing examples from [53] suite for a non-ergodic fading channel with $D_{st} = 2$ states. The two digits 1 and 2 represent the two states of the BO-channel. The symbol X represents a punctured parity bit. Note that in this chapter we will only consider half-rate codes multiplexed over two-state non-ergodic channels, but generalization to any rate codes on non-ergodic channels is straight-forward as long as $R_c \leq 1/D_{st}$.

Horizontal Multiplexer						
$\mathbf{s_1}$	1	1	1	1	1	1
$\mathbf{s_2}$	2	X	2	X	2	X
$\mathbf{s_3}$	X	2	X	2	X	2

H-π-diagonal Multiplexer						
$\mathbf{s_1}$	1	2	1	2	1	2
$\mathbf{s_2}$	2	X	2	X	2	X
$\pi^{-1}(\mathbf{s_3})$	X	1	X	1	X	1

Figure 3.12: Horizontal (top) and h-π-diagonal (bottom) multiplexers for a rate 1/2 parallel turbo code.

Proposition 1 *Let C be a rate 1/2 parallel turbo code transmitted on a 2-state channel and built from $RSC(g_1(x), g_2(x))$. Under horizontal state multiplexing and for any input weight ω, the number η of codewords in C with incomplete state diversity is*

$$\eta(\omega, d_{st} < 2) = 0 \quad \forall \ \ \omega \geq 2$$

Proof 1 *For any non-zero turbo codeword, it is well-known that the Hamming weight of s_1 is $\omega \geq \omega_{min} = 2$ [62]. Also, the Hamming weight of both s_2 and s_3 must be positive despite puncturing. Hence, it is trivial that $d_{st} = 2$ since s_1 is always transmitted on the first channel state and (s_2, s_3) are transmitted on the second channel state.*

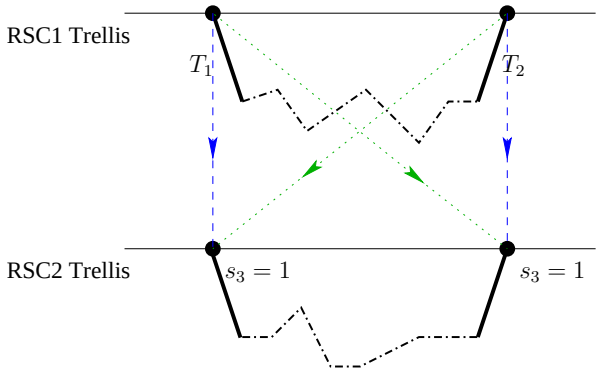

Figure 3.13: Trellis error events for input weight $\omega = 2$. The two interleaving configurations are indicated. Diversity is guaranteed by full-span transitions.

The recursive systematic convolutional constituent has constraint length $\nu + 1$. Its feedback generator polynomial is $g_1(x)$ and its forward generator polynomial is $g_2(x)$.

Definition 3 *A recursive systematic convolutional code is said to be a* full-span *convolutional code if the generators satisfy* $\deg(g_i(x)) = \nu$ *and* $g_i(0) = 1$*, for* $i = 1, 2$.

Trellis transitions outgoing from the 0-state and those incoming to the 0-state will be called *full-span transitions*, i.e. both bits are set to 1 on the transition label.

Proposition 2 *Let* C *be a rate* $1/2$ *parallel turbo code transmitted on a 2-state channel and built from a full-span RSC*$(g_1(x), g_2(x))$*. Under h-*π*-diagonal state multiplexing and for any input weight* ω*, the number* η *of codewords in* C *with incomplete state diversity is*

$$\eta(\omega, d_{st} < 2) = 0 \quad \forall \ \ \omega \geq 2$$

Proof 2 *For* $\omega = 2$ *and* $\omega = 3$*: if a full-span transition is interleaved (via* π*) into a full-span transition, then state diversity is guaranteed. As shown in Fig. (3.13) and (3.15), one of the full-span transitions in RSC1 is converted into a full-span transition in RSC2. For* $\omega \geq 4$*: Consider the case where* $\omega = 4$*. Except for the unique interleaving configuration depicted in Fig. (3.16), all turbo codewords exhibit* $d_{st} = 2$ *due to full-span transitions. Now, let* $\chi_i(s_j) \in \{1, 2\}$ *denote the BO-channel state over which the binary element* s_j *belonging to RSC*$_i$ *is transmitted. We distinguish two cases when a critical configuration is transmitted on the channel.*
Case 1: error event in RSC1 starts at state 1, $\chi_1(s_1) = 1$*. Diversity is guaranteed by RSC1 because* $\chi_1(s_2) = 2$.
Case 2: error event in RSC1 starts at state 2, $\chi_1(s_1) = 2$*. Then, we distinguish two sub-cases:*
Case 2.1: Information bit s_1 *is set to 1 within the error event and hits state 1 yielding* $\chi_1(s_1) = 1$*. Hence, diversity is guaranteed by RSC1 without the help of RSC2.*
Case 2.2: Information bit $s_1 = 1$ *never hits state 1 in the trellis event of RSC1,* $\chi_1(s_1) \neq 1$*. This situation occurs because equality is not satisfied in (2.25) when* $R_c = 1/2$ *and* $D_{st} = 3$*, i.e. it is possible to create RSC1 codewords that never hit state 1. Thanks to the structure of the h-pi-diagonal multiplexer, at least one full-span transition in RSC2 has* $\chi_2(s_3) = 1$ *for* $\chi_1(s_1) = 2$.
The same proof applies for $\omega > 4$.

Example with RSC$(7, 5)_8$
A critical configuration is a configuration (or an event) in which the diversity is not guaranteed by the first RSC alone, thus the receiver relies on the parity bit of RSC 2 to recover the diversity. Let us now give an example of critical configurations for $\omega = 4$ as defined in the proof of prop. 2. When $\chi_1(s_1) = 1$ and $\chi_1(s_2) = 2$, the RSC trellis is represented by the transition matrix

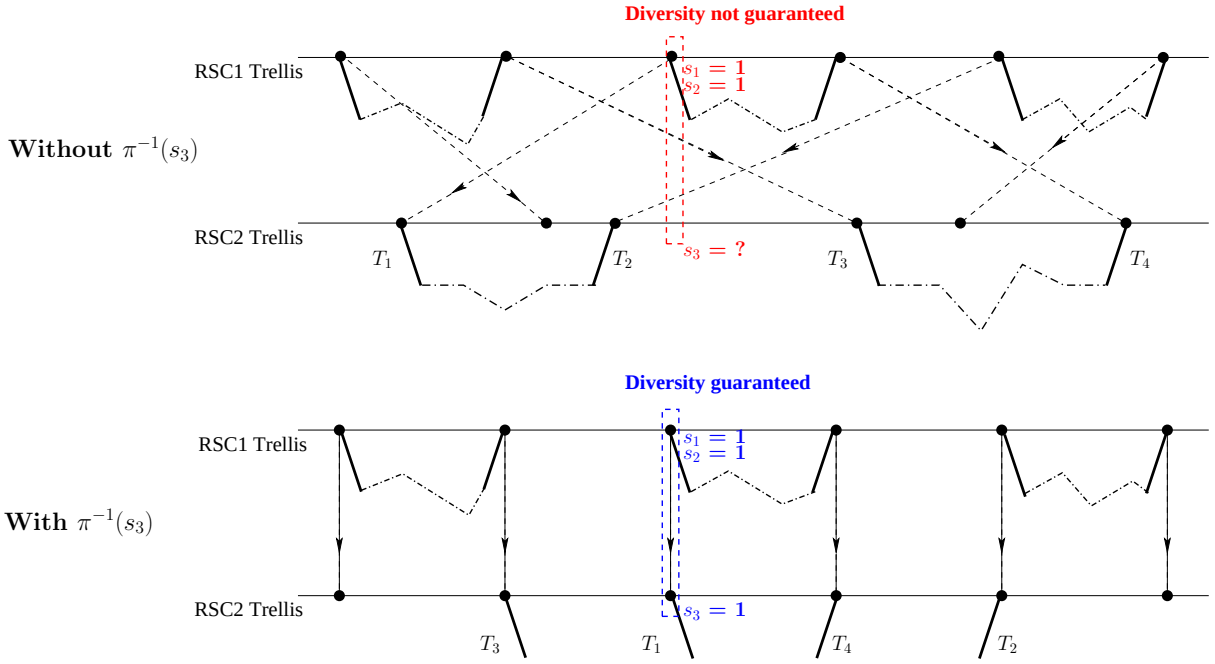

Figure 3.14: Effect of h-π-diagonal multiplexing on trellis events. Illustration for input weight $\omega = 6$ with and without de-interleaving of the second parity bit.

$$A_1 = \begin{bmatrix} 0 & 0 & D_1D_2LW & 0 \\ D_1D_2LW & 0 & L & 0 \\ 0 & D_1LW & 0 & D_2L \\ 0 & D_2L & 0 & D_1LW \end{bmatrix}$$

When $\chi_1(s_1) = 2$ and $\chi_1(s_2) = X$, the transition matrix is

$$A_2 = \begin{bmatrix} 0 & 0 & D_2D_3LW & 0 \\ D_2D_3LW & 0 & L & 0 \\ 0 & D_2LW & 0 & D_3L \\ 0 & D_3L & 0 & D_2LW \end{bmatrix}$$

The complete weight enumerator $T(W, D, L)$ of simple error events is given by the top left entry of the product $A_1A_2A_1A_2\ldots$ or $A_2A_1A_2A_1\ldots$ depending on the position of the outgoing transition. A critical configuration is given by a product of type $A_2(A_1A_2)^\ell$ for an event of length $2\ell + 1$. For $\ell = 1\ldots3$ no critical configurations are found. For $\ell = 4$, we have

$$T(W, D, L) = \ldots + (2D_1D_2^5D_3^4 + D_2^8D_3^2)L^9W^4 + \ldots$$

Therefore, the shortest critical event for $\omega = 4$ has length $L = 9$. It includes 4 information bits with $\chi_1(s_1 = 1) = 2$, 4 parity bits with $\chi_1(s_2 = 1) = 2$, and 2 punctured bits with $\chi_1(s_2 = 1) = X$. In this case, without a de-interleaver at the output of RSC 2, one cannot track the position of the parity bit s_3 at the output, as shown in Fig. 3.14. Therefore, we

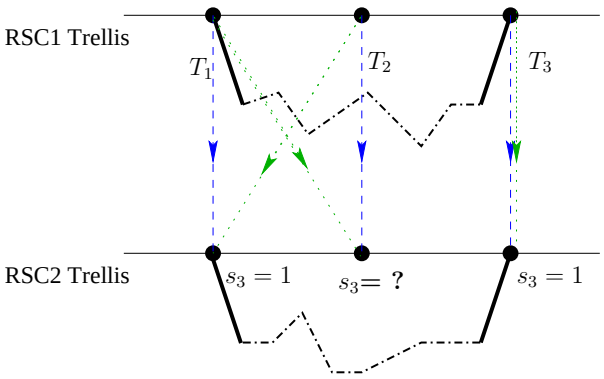

Figure 3.15: Trellis error events for input weight $\omega = 3$. The six interleaving configurations are equivalent to two distinct configurations.

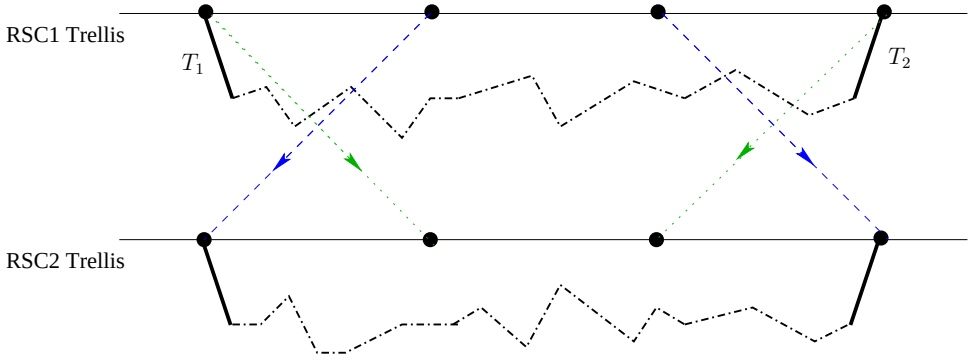

Figure 3.16: A critical configuration for full-span outgoing and incoming transitions. Input weight $\omega = 4$.

cannot make sure that full diversity is attained. However, a de-interleaver at the output of RSC 2 makes the coded bits of the turbo code synchronized within the trellis of the RSC constituents.

At this point, based on the study of η, the reader sees no difference between h-π-diagonal and horizontal multiplexers. Indeed, propositions (1) and (2) state that both multiplexers achieve full state diversity. The error rate performance depends on the achieved diversity and on the so-called *coding gain* or *product distance* defined by the product $\omega_1\omega_2$ of partial Hamming weights. Now, it should be clear that horizontal multiplexing shows a great unbalance between ω_1 and ω_2. As an example, for input weight $\omega = 2$, consider RSC(7,5) error events of length $L = 4{+}3i$ and total Hamming weight $w_H = 6{+}2i$, $i = 0 \ldots (N{-}4)/3$. For horizontal multiplexing, $\omega_1 = 2$ and $\omega_2 = 4 + 2i$. Therefore, its coding gain behaves as $O(N)$. For h-π-diagonal multiplexing, $\omega_1 = \omega_2 = 3 + i$. Hence, the coding gain of h-π-diagonal multiplexing increases as $O(N^2)$. The loss is even more dramatic for $\omega = 3$. The latter is neglected on the Gaussian channel since its contribution to the

error rate performance is $O(1/N)$. On non-ergodic fading channels, when $\omega = 3$, turbo codewords satisfying $w_H(s_2) >> 1$ and $w_H(s_3) >> 1$ will suffer from the unbalance of horizontal multiplexing. A comparison between h-π-diagonal and horizontal multiplexers is illustrated in Fig. 3.18 with 2 transmit antennas and a QPSK modulation.

3.8.3 Word error rate performance with $n_t = 2$

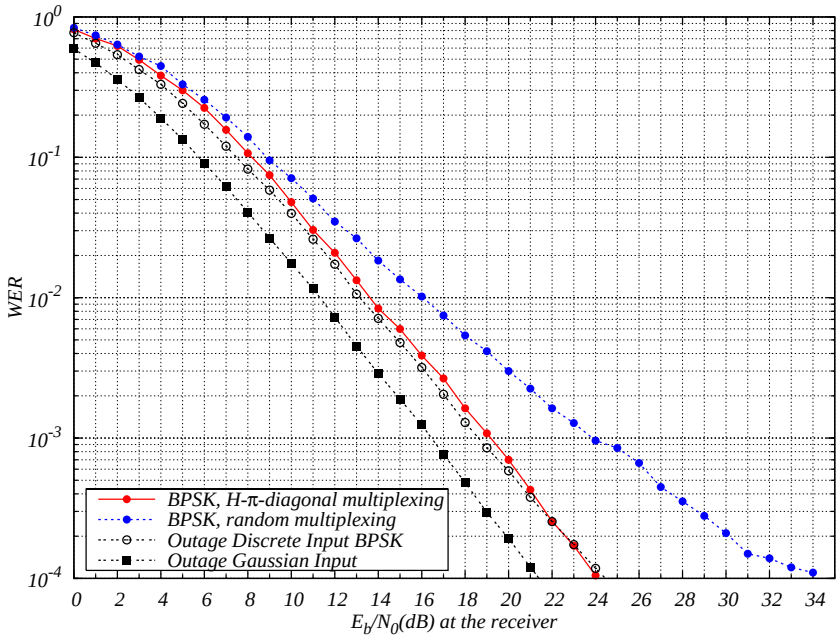

Figure 3.17: BPSK modulation, quasi-static channel, $n_t = 2$, $n_r = 1$, turbo code with $R_c = 1/2$, $(17, 15)_8$, $N = 400$.

In this section, computer simulations are made for $n_t = 2$ and without linear precoding ($s = 1$) on the quasi-static MIMO channel. The rate 1/2 turbo code is built from $\text{RSC}(17, 15)_8$ and a pseudo-random interleaver π of size N. All curves include word error rate versus signal-to-noise ratio per bit. Fig. 3.17 shows the performance of a BPSK modulation with 2 transmit and 1 receive antenna, and $N = 400$. Fig. 3.18 shows a similar situation with a QPSK modulation. The performance with 2 transmit and 2 receive antennas is given in Fig. 3.19. Notice that the word error rate is roughly the same for $N = 400$ and $N = 6400$. Finally, the performance of 8-PSK is illustrated in Fig. 3.20 and compared to both outage limits (discrete and Gaussian inputs).

3.8.4 Linear precoding via DNA rotations with $n_t = 4$

In the case of $n_t = 4$ transmit antennas, we have $D_{st} = 4$. Maximum state diversity in (2.25) cannot be attained with $R_c = 1/2$ if $D_{st} = 4$. Therefore, we add a linear precoder

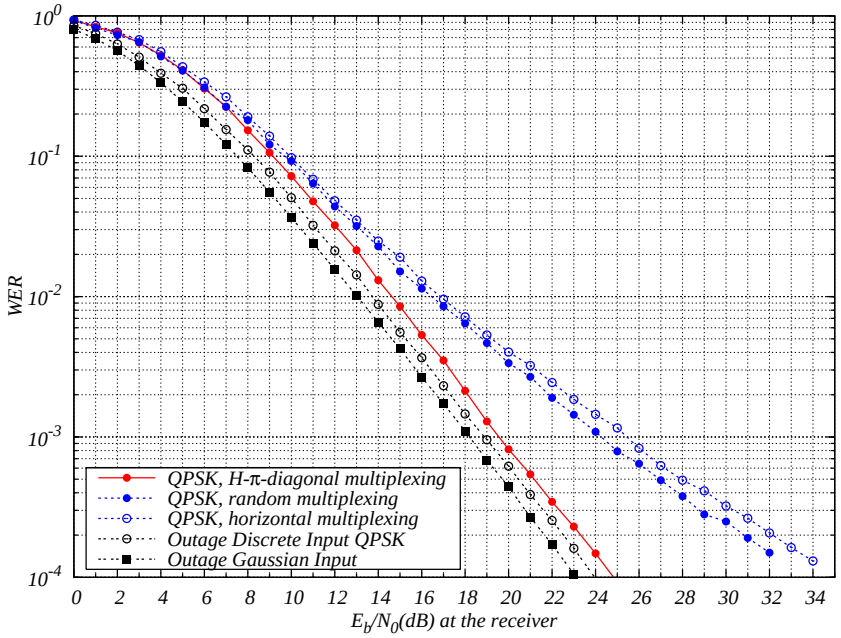

Figure 3.18: QPSK modulation, quasi-static channel, $n_t = 2$, $n_r = 1$, turbo code with $R_c = 1/2$, $(17, 15)_8$, $N = 400$.

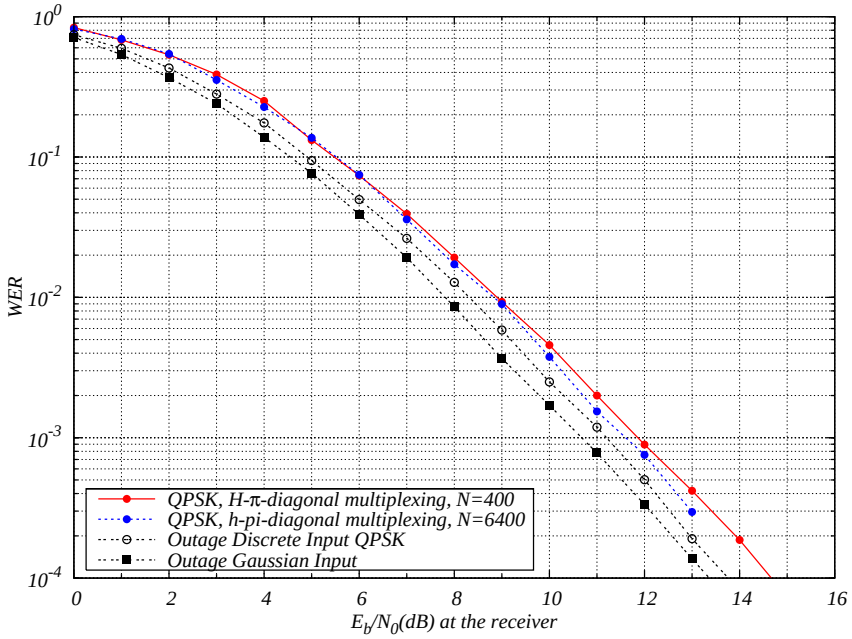

Figure 3.19: QPSK modulation, quasi-static channel, $n_t = 2$, $n_r = 2$, turbo code with $R_c = 1/2$, $(17, 15)_8$, $N = 400/6400$.

in order to downgrade D_{st} from 4 to 2. This does not affect the physical channel diversity D_{ch}. If the rotation has $s = 4$, i.e. a full spreading unitary precoder as usually studied

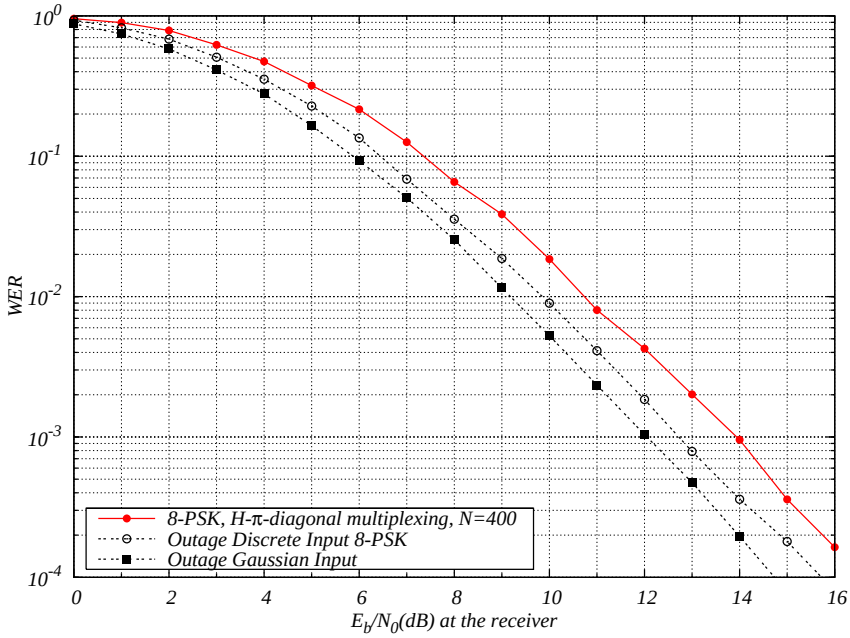

Figure 3.20: 8-PSK modulation, quasi-static channel, $n_t = 2$, $n_r = 2$, turbo code with $R_c = 1/2$, $(17, 15)_8$, $N = 1600$.

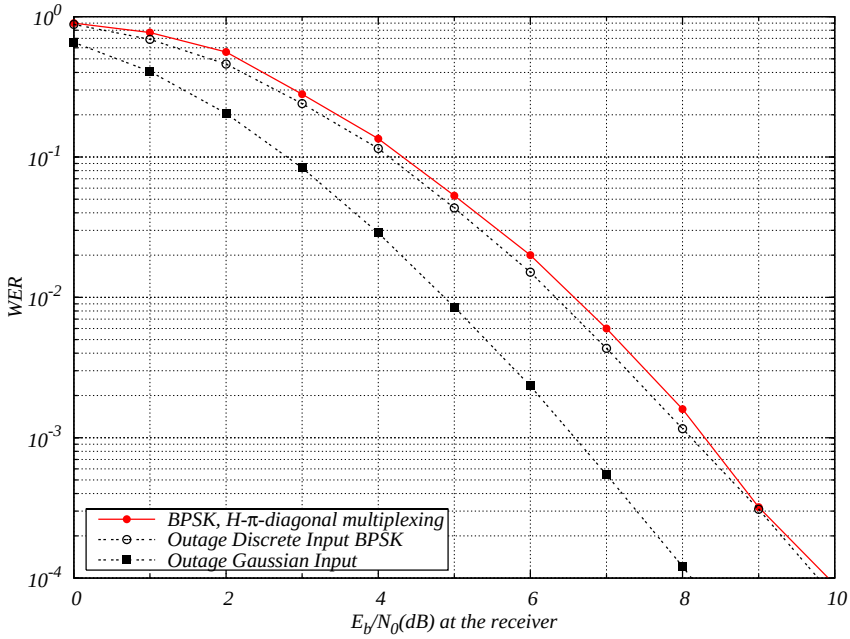

Figure 3.21: BPSK modulation, quasi-static channel, $n_t = 4$, $n_r = 2$, turbo code with $R_c = 1/2$, $(17, 15)_8$, $N = 1600$. Linear precoding via a cyclotomic DNA rotation

in the literature, then D_{st} will reduce to 1. Also, MIMO detection complexity increases exponentially with s. The solution to maintain $D_{st} = 2$ is given by Dispersive Nucleo

Algebraic (DNA) precoders discussed in section 3.6 for $s \leq n_t$. Now, let us observe the MIMO channel with $\mathbf{S_{DNA}}$ as in (3.30). The QAM vector $z = (z_1, z_2, \ldots, z_8)$ goes through the precoder before $\mathbf{H}$. Consider the lattice point $\mathbf{zSH}$ without adding Gaussian noise. One would notice that z_i is transmitted via the 1st and 2nd transmit antennas if i is odd, and via the 3rd and 4th transmit antennas if i is even. Consequently, the DNA precoder converts the $4 \times n_r$ MIMO channel onto two $2 \times n_r$ MIMO channels. Binary elements mapped to z_i when i is odd (resp. i is even) will be sent through the first BO-sub-channel (resp. the second BO-sub-channel). As a final illustration, Fig. 3.21 shows the error rate of BPSK modulation with 4 transmit and 2 receive antennas.

3.9 Conclusions

In this chapter, we proposed space-time bit-interleaved coded modulations for the multiple-antenna channel that perform close to outage limit. In [18], it was shown that cyclotomic rotations satisfying genie/DNA conditions are the best choice for precoding in space-time bit-interleaved coded modulations, due to their enhanced performance and their flexibility. These rotations are optimal in both algebraic and information theoretical senses. They exist for any set of MIMO channel parameters, mainly the number of transmit antennas and the precoder time-spreading factor. However, the families of IOM linear precoders we presented in this chapter correct the failure of cyclotomic rotations to lead the system to reasonable performance since the first iteration in an iterative receiver when the system has delay constraints. They also exist whatever the MIMO system configuration is, with the difference in that their design requires Monte Carlo simulations. They can be designed by relaxing the genie constraints or by maintaining one constraint depending on the decoding technique we want to employ.

In addition, we proposed a low-complexity space-time coding scheme for $n_t = 4$ based on the Alamouti scheme. This low-complexity scheme ensures state diversity $D_{st} = 1$, which means it can be used with all coding rates $R_c \in [0, 1]$ while maintaining maximal channel diversity $d_{ch} = 4 \times n_r$. In addition to exponentially reducing the detection complexity, this scheme showed a slight degradation of the frame error rate over a quasi-static fading channel, that is more robust than classical ST-BICM. As configurations with $n_t = 4$ are particularly of interest in recent wireless communication systems (such as IEEE.802a/b/g standards), the low-complexity solution together with the high performance provided by this scheme are valuable.

Finally, we studied turbo-coded modulations for the MIMO channel based on the works in [53] on "code multiplexers". When the coding rate of the turbo-code satisfies $R_c \leq 1/D_{st}$, the use of multiplexers at the output of the encoder ensures low detection complexity and near-outage limit performance. Surprisingly enough, the frame error rate performance of turbo-coded modulations is insensitive to block length. This is probably due to the interleaving gain of the turbo-code on AWGN channels translated to non-ergodic fading

channels, whereas the number of neighbors of a turbo-codeword increases linearly with the interleaver size [63]. Note that it was recently shown in [64] that LDPC codes have almost the same behavior over block-fading channels. However, the coding gain with regular turbo codes on block-fading channels is slightly better than that of regular LDPC codes.
To summarize, we can follow these strategies for low-complexity decoding of coded modulations over the MIMO channel:

- If $R_c \leq 1/D_{st}$ and an iterative receiver can be used, use turbo-codes with multiplexers for $n_t = 2$ antennas and turbo-codes with multiplexers along with DNA rotation for $n_t = 4$ as proposed in section 3.8.
- If $n_t = 4$ and an iterative receiver can be employed, use the Matrix-Alamouti scheme presented in section 3.7 whatever the channel coding rate is.
- Else, if $R_c > 1/D_{st}$, use cyclotomic rotations [18] with an iterative receiver.
- If no iterations are allowed at the receiver, use IOM rotations presented in section 3.6 with all channel configurations.

Chapter 4

Coded modulations for the amplify-and-forward cooperative channel

4.1 Introduction

As discussed in the previous chapter, multiple-antenna systems can provide reliable communication (through large diversity orders) and high data rates in block-fading environments. The advantages of such systems is widely recognized and they are proposed in many standards. However, due to size (and sometimes cost) limitations, the implementation of many antennas on a single terminal is unfeasible. This is the case of the uplink transmission in a cellular link for instance.

Since the early 1970s, the idea of the relay channel in information theory was proposed [65]. In [66], the authors proved the gain in capacity the relay channel has and sketched the rate regions for this channel under different hypothesis. Inspired by these works, the authors in [67, 68] proposed the concept of "user cooperation diversity", whereas user's terminals help each other to convey their signals to a destination. This allows for the signals to attain high spatial diversity orders by using the antennas of other terminals and thus by forming a virtual antenna array. Note that this is not a simple relaying problem, as users are responsible for the "partner's" signals as well as their own signals.

One main application is the cooperation of in-cell users in a cellular system. Reliable communication can be achieved through diversity and by relaying signals from terminals that are far from the base station. The drawback is the fact that the inter-user channel is noisy, thus imposing various cooperation protocols we will discuss later in this report.

Another potential application is in wireless *ad hoc* networks, such as mesh networks for instance. A wireless *ad hoc* network does not depend on a central control unit, and it does not have a fixed infrastructure. The nodes communicate by forming a network based on channel conditions and mobile locations.

The main problems in non-cooperative networks is their rigid infrastructure, whose blocking probability increases with the number of terminals that are sharing the network. Many

service providers have experience dealing with temporary elevations in network traffic. COSMOTE, the Greek telecommunications company responsible for providing service to the 2004 Olympic games, had to deploy additional resources in the area surrounding the Olympic complex. This extra equipment allowed this system to successfully deliver over 100 million text messages during the 17 day duration of the games. Similarly, sporting events and large public gatherings in the United States regularly take advantage of the so-called Cell-on-Wheels (COW) services in order to account for location-dependent traffic spikes. With cooperative communications, networks will not experience such problems anymore, as the more users there are in a network, the more reliably one can communicate. In addition, the hardware implementation of multiple antennas on the same terminal that is difficult to realize is traded for protocol algorithms shared among terminals through the network, which is easily updatable and gains in flexibility.
In this chapter, we will start by recalling the communication protocols for the cooperative fading channel. We will then establish the system model for coded modulations over the amplify-and-forward protocol. Then we will discuss bounds on diversity for this type of protocol, that are followed by coding strategies and simulation results. The last part of this chapter discusses channel multiplexing issues for turbo-coded modulations over such protocols.

4.2 Cooperative communications protocols

After the authors in [67, 68] introduced the concept of cooperative diversity, many papers proposed cooperation protocols that define the way the cooperation between users is performed. These protocols can be classified into two major categories, that are amplify-and-forward (AF) and decode-and-forward (DF). Note that the large majority of the existing designs we will recall in the sequel are based on the so-called "Diversity-Multiplexing Tradeoff" (DMT) of the channel [69]. The DMT is a piece-wise linear function that represents, at very high signal-to-noise ratios, the tradeoff between the maximum achievable rate (as a function of the signal-to-noise ratio) and the maximal achievable diversity order over the wireless channel. Although the DMT bound gives an insight on the superiority of a given protocol (or a given antenna configuration for MIMO systems) and allows for the design of optimal space-time precoders for uncoded systems, its relevance as a design tool for coded modulations with iterative decoding is arguable.

4.2.1 Amplify-and-forward protocols

In these protocols, the relays scale the signals received from the source (or by other relays) and forward them to the destination (or to other relays) without other treatment. These protocols are easy to implement in practical communication systems, as the computational complexity they introduce at the relay is limited to the scaling operation. The orthogonal amplify-and-forward (OAF) protocol was first introduced in [70] for the single-relay case.

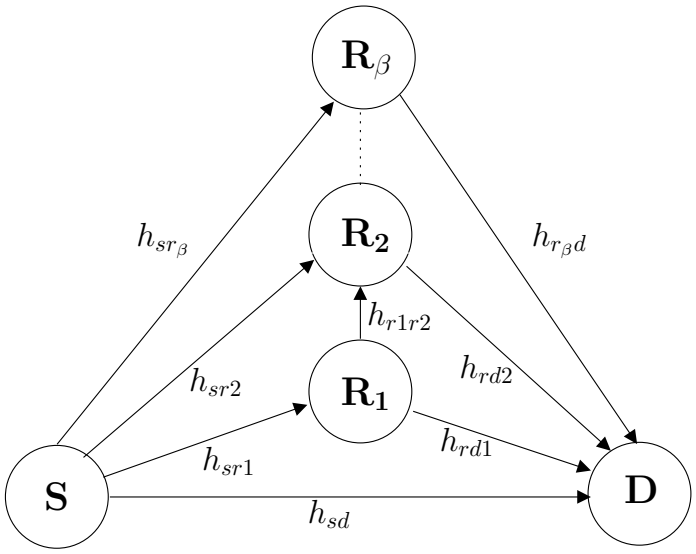

Figure 4.1: Cooperative fading channel.

By orthogonal we mean that the source and the relay do not send data simultaneously. The second major work concerning this family of protocols is the framework established in [71] for the single-relay case. The authors proposed three amplify-and-forward protocols that are:

- Protocol I: the source broadcasts a signal to both the relay and the destination in the first phase. In the second phase, the relay scales the signal and forwards it to the destination, while the source transmits another message to the destination. This protocol is also known as the non-orthogonal amplify-and-forward (NAF) protocol [72].

- Protocol II: the source broadcasts a signal to both the relay and the destination in the first phase like in Protocol I. In the second phase, only the relay scales the signal it received in the previous phase and forwards it to the destination. This protocol is the OAF protocol introduced in [70].

- Protocol III: the source sends a signal only to the relay in the first phase. The second phase is similar to the second phase in Protocol I.

In addition to introducing these protocols, the authors discussed and analyzed some information theoretical aspects of cooperative protocols that brought insight to the behavior of such systems. From these three protocol, Protocol I caught the attention of the researchers in the community as it allows for high data rates (the source always transmits). Indeed, in [72], it is shown that the NAF protocol outperforms the AF protocol for high data rates. However, for the case of more than one relay, the NAF protocol suffers from a

limitation , as half of the symbols in the cooperation frame are protected. For this reason, the authors in [73] proposed the slotted amplify-and-forward (SAF) scheme; by allowing inter-relay communication (see Fig. 4.1), on can protect β out of $\beta + 1$ symbols. For this reason, the SAF scheme largely outperforms the β-relay NAF scheme for high data rates. Many space-time code design for uncoded fading channels for the AF protocols were proposed, among them [74] [75] [76, 77], but optimal space-time codes for uncoded systems can be found in [73] [78].

4.2.2 Decode-and-forward protocols

This class groups the protocols in which the relays operate on the signal they receive from the source (or from other relays) before forwarding it. The first protocol, the selection decode-and-forward, was introduced in [70] for the single-relay cooperative channel. In this protocol, the relay estimates the channel coefficient between the source and the relay, say h_{sr}, and it computes $|h_{sr}|^2$. If this value falls below a threshold, the relay remains idle. If not, the relay decodes the message and forwards it to the destination. This scheme was generalized to multiple relays in [79]. In [72], the authors introduced the dynamic decode-and-forward protocol wherein the time for which the relays listen to the source depends on the source-relay channel gain. In [80], the authors treated the compress-and-forward protocol and proved it to be optimal for the single-relay channel. Note that unlike the decode-and-forward protocol where the relays have to know the source-relay channel, the relays in the compress-and-forward protocol have to know all the channel coefficients of the incoming paths. In [81], the authors proposed an intuitive distributed turbo code that achieves high performance; it consists of broadcasting a convolutional codeword to both the relay and the destination, the relay decodes the codeword, interleaves it, and encodes it prior to forwarding to the destination that performs iterative decoding between the two codes. Similar constructions can be found in [82] for distributed turbo codes and in [83] for LDPC codes.

4.3 Space-time bit-interleaved coded modulations for the amplify-and-forward cooperative channel

As discussed in section 4.2.1, many distributed space-time codes for uncoded systems have been proposed in the literature. However, the optimal codes in [73] [78] that achieve the DMT frontier of the channel introduce delay in the cooperation frame of the NAF/SAF protocol, which means that the source broadcasts for several time slots before the co-operation at the relay starts. Indeed, as these codes were initially designed for MIMO systems, the spreading factor $s = n_t$ for such systems is translated into a delay $d = s - 1$ for the NAF/SAF protocols. This delay actually results in an exponential growth of the detection complexity at the receiver.

Nevertheless, in the presence of an error correcting code, it was shown in chapter 3 that one can trade diversity from the channel detector to the channel decoder over block-fading channels by using space-time rotations. In addition, for the SAF channel, unlike for the MIMO channel, the maximal diversity order $\beta+1$ of the channel can be achieved using a rotation that does not lead additional complexity. This is a key point for our design framework in the rest of this chapter.
To our knowledge, no work has yet treated channel coding issues for AF cooperative protocols in general. In this chapter, we consider the problem of coding for the half-duplex non-orthogonal slotted amplify-and-forward (NAF/SAF) cooperative channel. We only consider a network with single-antenna nodes. We derive bounds on the diversity order of this protocol that are achieved by a distributed space-time bit-interleaved coded modulation (D-ST-BICM) scheme under iterative APP detection and decoding. These bounds lead to the design of space-time precoders that ensure maximum diversity and high coding gains.

4.4 System model and parameters

We consider the amplify-and-forward fading relay channel. We impose the half-duplex constraint, whereas terminals cannot transmit and receive signals simultaneously. We consider the TDMA-based Protocol I from [71] that is also known as the non-orthogonal amplify-and-forward (NAF) protocol. For the case of more than one relay, we use the "naive" slotted amplify-and-forward (SAF) cooperative protocol proposed in [84], where inter-relay communication is allowed; the source transmits in all time slots, and starting from the second slot, only one relay scales and transmits the message received in the previous time slot. By protecting β symbols out of $\beta+1$, this protocol can achieve a diversity order of β with a length-$\beta+1$ vector, whereas the classical β-relay NAF scheme achieves the same diversity order with a length-2β vector. The main reason we use this protocol is because it induces low detection complexity. The "naive" SAF protocol gives the following signal model:

$$y_{d_i} = \sqrt{\mathcal{E}_i}h_{sd}x_i + \sqrt{1-\mathcal{E}_i}h_{r_id}\gamma_{i-1}y_{r_{i-1}} + w_{d_i} \quad (4.1)$$

$$y_{r_i} = \sqrt{g_{sr_i}\mathcal{E}_i}h_{sr_i}x_i + \sqrt{g_{r_{i-1}r_i}(1-\mathcal{E}_i)}h_{r_{i-1}r_i}\gamma_{i-1}y_{r_{i-1}} + w_{r_i} \quad (4.2)$$

with $i=1,...,\beta+1$. Subscripts s, d, and r_i correspond to *source*, *destination*, and i^{th} *relay*. The unit variance complex symbol x_i is transmitted in the i^{th} slot, the received signal at the destination in the i^{th} time slot is y_{d_i}, while y_{r_i} is the signal received by the i^{th} relay. The coefficients $\mathcal{E}_i$ represent the energy transmitted by the source in the i^{th} slot. The geometric gain $g_{j\ell}$ is defined as $\mathbb{E}|h_{j\ell}|^2/\mathbb{E}|h_{s\ell}|^2$ [73]. The h_{kl} are the complex Gaussian fading coefficients that are constant for the duration of a codeword and w_{d_i} and w_{r_i} are AWGN noise components. The γ_i are the energy normalization coefficients at the i^{th} relay, subject to $\mathbb{E}|\gamma_i y_{r_{i-1}}|^2 \leq 1$, and $\gamma_0 = 0$. In matrix form, we can write for a system

with β relays:

$$\mathbf{y}_d = \mathbf{xH} + \mathbf{w}_c = \mathbf{zSH} + \mathbf{w}_c \tag{4.3}$$

where $\mathbf{y}_d$ is the length-$(\beta+1)$ vector of received signals and $\mathbf{z}$ is the length-$(\beta+1)$ vector of M-QAM symbols. S is a $(\beta+1)\times(\beta+1)$ precoding matrix, and $\mathbf{H}$ is given by:

$$\mathbf{H} = \begin{bmatrix} h_{11} & h_{12} & h_{13} & \cdots \\ 0 & h_{22} & h_{23} & \cdots \\ 0 & 0 & h_{33} & \cdots \\ \vdots & \vdots & \vdots & \ddots \end{bmatrix} \tag{4.4}$$

where

$$\begin{aligned} h_{ii} &= \sqrt{\mathcal{E}_i} h_{sd} \\ h_{12} &= \sqrt{g_{sr_1}\mathcal{E}_1(1-\mathcal{E}_2)}\gamma_1 h_{sr_1} h_{r_1 d} \\ h_{13} &= \sqrt{g_{sr_1} g_{r_1 r_2}\mathcal{E}_1(1-\mathcal{E}_2)(1-\mathcal{E}_3)}\gamma_1\gamma_2 h_{sr_1} h_{r_1 r_2} h_{r_2 d} \\ h_{23} &= \sqrt{g_{sr_2}\mathcal{E}_2(1-\mathcal{E}_3)}\gamma_2 h_{sr_2} h_{r_2 d} \end{aligned}$$

Finally, the vector $\mathbf{w}_c$ is a length-$(\beta+1)$ colored Gaussian noise vector whose entries are given by:

$$\begin{aligned} w_1 &= w_{d,1} \\ w_2 &= \sqrt{(1-\mathcal{E}_2)}\gamma_1 h_{r1d} w_{r,1} + w_{d,2} \\ w_3 &= \sqrt{(1-\mathcal{E}_2)(1-\mathcal{E}_3)}\gamma_1\gamma_2 h_{r1r2} h_{r2d} w_{r,1} + \sqrt{(1-\mathcal{E}_3)}\gamma_2 h_{r2d} w_{r,2} + w_{d,3} \end{aligned}$$

an so on. We set:

$$\mathbf{\Gamma} = \mathbf{E}\left[\mathbf{w}_c^\dagger \mathbf{w}_c\right] = 2N_0\mathbf{\Theta} \tag{4.5}$$

Where the † operator denotes transpose conjugate. By performing a Cholesky decomposition on $\mathbf{\Theta}$, we get:

$$\mathbf{\Theta} = \mathbf{\Psi}^\dagger \mathbf{\Psi} \tag{4.6}$$

Thus the equivalent channel model would become:

$$\mathbf{y}_d \mathbf{\Psi}^{-1} = \mathbf{zSH}\mathbf{\Psi}^{-1} + \mathbf{w} \tag{4.7}$$

where $\mathbf{w}$ is a white Gaussian noise vector.

4.5 The diversity of coded modulations over precoded SAF channels

The maximum diversity inherent to the SAF channel is $d_{max} = \beta + 1$, and it can be collected by an APP detector (at the destination) if linear precoding is used at the transmitter. In general, it is sufficient to use a linear precoder that mixes the $\beta+1$ constellation

symbols being transmitted on the channel to achieve the full diversity with uncoded systems and without increasing the decoder complexity. However, using larger precoders can further improve the performance. From an algebraic point of view, a linear precoder of size $(\beta+1)^2 \times (\beta+1)^2$ is the minimal configuration to achieve the best coding gains (without channel coding) at the price of an increase in detection complexity (The complexity of an APP detector grows exponentially with the number of dimensions) [85].
On the other hand, for coded systems transmitted on block-fading channels, the channel decoder is capable of collecting a certain amount of diversity that is however limited by the Singleton bound [35]. As shown in [86], the lowest complexity solution is to first recover the channel code diversity and then collect the remaining diversity through linear precoding. For this purpose we derive hereafter an upper bound on the diversity order of a coded transmission through a precoded SAF channel, and deduce the precoding strategy to achieve the full diversity.

First, we will introduce a new model of block-fading channel that will be used in the following to compute the bounds on the diversity order of coded SAF channels.

4.5.1 Matryoshka block-fading channels

In this section we consider a block-fading channel model where the set of random variables of a higher diversity block always include the set of random variables of a lower diversity one, like Matryoshka dolls:

Definition 4 *Let us consider λ independent Rayleigh fading distributions. Let $\mathcal{M}(\mathcal{D}, \mathcal{L})$ be a channel built from the concatenation of $|\mathcal{D}|$ blocks, where $\mathcal{D}$ and $\mathcal{L}$ are the sets of diversity order and lengths of each block, respectively. The integer $|\mathcal{D}|$ is the cardinality of $\mathcal{D}$. The i-th diversity block is defined by a linear combination of a subset $\mathcal{S}(i)$ of $\mathcal{D}(i) \leq \lambda$ Rayleigh distributions, such that $\mathcal{S}(i+1) \subset \mathcal{S}(i)$, i.e., the blocks are sorted such that $\forall i < j, \mathcal{D}(i) \geq \mathcal{D}(j)$ and we assume that $\mathcal{D}(1) = \lambda$ has the highest diversity order.*

Fig. 4.2 shows the representation of the Matryoshka block-fading channel. Notice that $n_{\mathcal{D}} = \lambda$ for the non-precoded channel.

$\mathcal{D}(1)$	$\mathcal{D}(2)$	$\cdots$	$\mathcal{D}(n_{\mathcal{D}})$
$\mathcal{S}(1) = \{\alpha_1, \cdots, \alpha_\lambda\}$	$\mathcal{S}(2) \subset \mathcal{S}(1)$		$\mathcal{S}(n_{\mathcal{D}}) \subset \mathcal{S}(n_{\mathcal{D}} - 1)$
$\leftarrow \quad \mathcal{L}(1)$ bits $\quad \rightarrow$	$\leftarrow \mathcal{L}(2)$ bits $\rightarrow$		$\leftarrow \quad \mathcal{L}(n_{\mathcal{D}})$ bits $\quad \rightarrow$

Figure 4.2: Matryoshka block-fading channel model.

Let us now transmit a BPSK-modulated and interleaved codeword of a rate-R_c code on the channel $\mathcal{M}(\mathcal{D}, \mathcal{L})$. First, let us focus on the pairwise error probability (PEP) of

two given binary codewords c and c'. Due to the channel model, the diversity order of this PEP is equal to the diversity order of the lowest index block seeing a non null bit of $c - c'$. The performance of the coded modulation has a diversity order upper bounded by δ_{max} defined as follows:

Proposition 3 *The diversity observed after decoding a rate-R_c code transmitted over a $\mathcal{M}(\mathcal{D}, \mathcal{L})$ channel is maximized by δ_{max} :*

$$\delta_{max} = \mathcal{D}(i) \text{ where } \sum_{k=1}^{i-1} \mathcal{L}(k) < R_c \sum_{k=1}^{|\mathcal{D}|} \mathcal{L}(k) \leq \sum_{k=1}^{i} \mathcal{L}(k) \tag{4.8}$$

and is achievable for any linear code.

Proof: This proof is inspired from the Singleton bound's one. The code has parameters (N, K), where $N = \sum_{k=1}^{|\mathcal{D}|} \mathcal{L}(k)$ and $K = R_c N$.

If $K > \sum_{k=1}^{i-1} \mathcal{L}(k)$, whatever the code, a puncturing of the last $\sum_{k=i}^{|\mathcal{D}|} \mathcal{L}(k)$ bits leads to a null minimal Hamming distance code. This means that there exists two codewords c and c' such that the first $\sum_{k=i}^{|\mathcal{D}|} \mathcal{L}(k)$ bits of $c - c'$ are null, and involves that $\delta_{max} \leq \mathcal{D}(i)$.

If the code is linear, there exists an interleaver that makes the code systematic. If the information bits are transmitted on the blocks of higher diversity order and $K \leq \sum_{k=1}^{i} \mathcal{L}(k)$, the Hamming distance after puncturing the last $\sum_{k=i+1}^{|\mathcal{D}|} \mathcal{L}(k)$ bits remains strictly positive and induces that $\delta_{max} \geq \mathcal{D}(i)$.□

As a remark, whatever the QAM modulation is, the log-likelihood ratio expression of the channel model at the output of the APP detector always takes equivalent BPSK modulations at its input. The bound on the diversity order applies then to any discrete modulation.

4.5.2 Precoded SAF channel models and associated bounds

Non-precoded SAF channels

The time periods of the SAF channel can be sorted into $\beta + 1$ blocks, the j-th block corresponding to the transmission through $0 \leq j - 1 \leq \beta$ relays. We will assume that the interleaver of the BICM is ideal, i.e., that for any pair of codewords (c, c'), the w non-null bits of $c - c'$ are transmitted in different blocks of $\beta + 1$ time periods. The interleaving, modulation and transmission through the channel transform the coded words c and c' into the points $\mathcal{C}$ and $\mathcal{C}'$ in an Euclidean space. For a fixed channel, the performance is directly linked to the Euclidean square distance $|\mathcal{C} - \mathcal{C}'|^2$, which can be rewritten as a sum of w square Euclidean distances associated to the non-null bits of $c - c'$.

The performance of a BPSK modulation transmitted through $j-1$ relays during j time periods of a quasi-static SAF channel has a diversity order j. The square distance $|\mathcal{C}-\mathcal{C}'|^2$ is a function of the fading coefficients of the equivalent channel. It can be factorized as follows: $\sum_{k=1}^{\beta+1} d_k^2$ where d_k is the total Euclidean distance seen by the k-th block. Finally, the diversity order of a given pairwise error probability is equal to the maximal index k such that d_k is non-null. At very high SNR, the performance is lead by the worse pairwise error probability, the diversity order of the BICM is then the lower bound of all pairwise error probabilities diversity orders.

At the output of the APP detector, an equivalent block-fading channel is observed and the constituent blocks do not have the same intrinsic diversity order: A soft output belonging to the $\beta+2-j$-th block carries the attenuation coefficients $\{h_{sd}; h_{sr_1}h_{r_1d}; \ldots; h_{sr_1}h_{r_1r_2}\cdots h_{r_{j-2}r_{j-1}}h_{r_{j-1}d}\}$. As a remark, blocks are sorted such that the j-th block carries a diversity order $\beta+2-j$. Under perfect interleaving, the equivalent SAF channel at the output of the APP detector is a matryoshka $\mathcal{M}([\beta+1,\beta,\ldots,1],[N/(\beta+1),\ldots,N/(\beta+1)])$ channel, where N is the number of coded bits per codeword. With this observation, we can conclude that the upper bound on the diversity order of a non-precoded SAF channel is

$$\delta_{max,1}(\beta,R_c) = 1 + \lfloor (1-R_c)\,(\beta+1) \rfloor \tag{4.9}$$

which is equal to the classical Singleton bound on the diversity order of block-fading channels [16].

Precoded SAF channels

Let us now introduce a linear precoder that rotates symbols of s different diversity order blocks together. First of all, let us focus on two different scenarios:

- The linear precoder size is lower than (or equal to) $\beta+1$. In this case, the dimension of the received vector $\mathbf{y}_d$ remains unchanged, thus there is no increase in detection complexity, and no delay is introduced to the protocol.
- The linear precoder size is lower than (or equal to) $(d+1)(\beta+1)\times(d+1)(\beta+1)$, where d is the delay (i.e. the source broadcasts for $d+1$ time slots before the relays start to cooperate). In this case, the complexity of the detector increases exponentially with d. As mentioned previously, these precoders are mandatory to achieve optimal performance for uncoded systems. However, in the presence of channel coding, they can be avoided.

We will now present two precoding strategies and compute the bound (4.8) for these two particular cases.

First strategy: a single precoder First, let us assume that s diversity blocks of size $N/(\beta+1)$ are linearly precoded together, then the diversity order of the new $sN/(\beta+1)$-length block is the maximum diversity order of the precoded blocks. As the other blocks keep their own diversity, it seems natural to maximize their diversity orders in a way to increase the coding gain at the output of the decoder (The best performance is achieved for a block-fading channel with diversity orders as equal as possible.). The length of the precoder input vector is $\beta+1$. We propose to precode the first block with the $s-1$ last blocks, i.e., the highest diversity order with the $s-1$ lowest ones. At the output of the APP detector, the channel model is a matryoshka $\mathcal{M}(\mathcal{D},\mathcal{L})$ where $\mathcal{D}=[\beta+1,\beta,\ldots,s]$ and $\mathcal{L}=[sN/(\beta+1),N/(\beta+1),\ldots,N/(\beta+1)]$, which leads to the following upper bound on the diversity order:

$$\delta_{max,2}(\beta,R_c,s)=\min(s+\lfloor(1-R_c)(\beta+1)\rfloor,\beta+1) \tag{4.10}$$

Indeed, by replacing $\mathcal{D}=[\beta+1,\beta,\ldots,s]$ and $\mathcal{L}=[sN/(\beta+1),N/(\beta+1),\ldots,N/(\beta+1)]$ in (4.8), we observe that if $R_c\leq s/(\beta+1)$ then $R_c(\beta+1)\leq s+i-1<R_c(\beta+1)+1$, else we have that $i=1$ and $\delta_{max,2}(\beta,R_c,s)=\mathcal{D}(1)$. It is then easy to show that the upper bound on the diversity is given by (4.10). Note that, in the representation of Fig. 4.2, we have that $n_{\mathcal{D}}=\lambda-s+1$ with precoding.

If $s=1$, then $\delta_{max,2}(s)$ is equal to the Singleton bound on the diversity order of an uncorrelated block fading channel with equal per-block diversity. If $s\geq 1$, $\delta_{max,2}(s)$ is greater than the upper bound on the diversity order for block fading channels. For example, the full diversity order cannot be achieved for the transmission of a $s=2$-precoded BICM with rate 2/3 on a block fading with diversity order 3 (the diversity is upper bounded by 2). For the SAF channel, the full diversity order can be achieved in that case, as shown in Fig. 4.3.

As a remark, in order to achieve the upper bound on the diversity of a block fading channel, at least one non null bit of any word $c-c'$ should be placed in as many independent blocks as given by the singleton bound. For precoded SAF channels, the bound is achieved as soon as one non null bit of any word $c-c'$ is placed in a block of diversity higher than $\delta_{max,1}(s)$. The last problem has less constraint than the first one. Tables 4.1 and 4.2 show the values of $\delta_{max,2}(\beta,R_c,s)$ for different coding rates with respect to the number of relays and the value of s. We can notice that full diversity is obtained with $s\geq(\beta+1)R_c$ in all configurations.

Second strategy: $(\beta+1)/s$ precoders Let us assume that s divides $\beta+1$, we can then use $(\beta+1)/s$ precoders: The first precodes the highest diversity order block with the $s-1$ lowest ones. The second, if any, precodes the second highest diversity order block with the $s-1$ lowest non-precoded ones, and so on. By using this precoding strategy that includes several independent precoders, we further increase the diversity of the extrinsic probabilities at the input of the decoder, and consequently the diversity

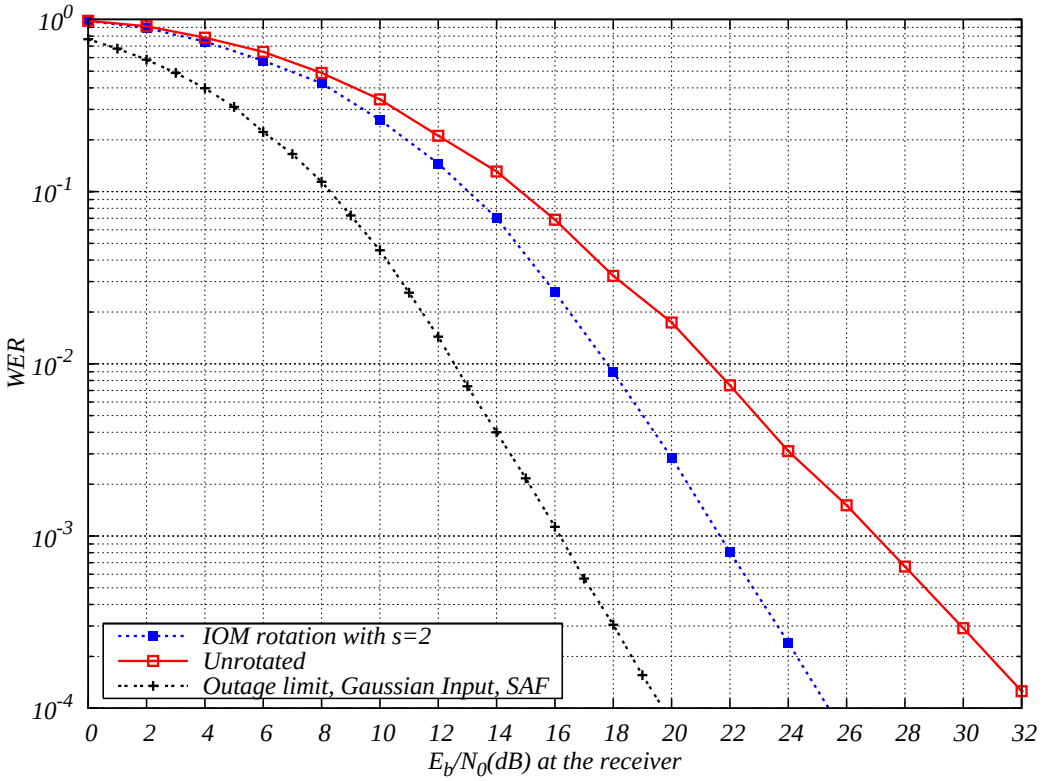

Figure 4.3: Two-relay SAF cooperative channel, R_c=2/3 RSC $(25,37,35)_8$ code, BPSK modulation, 1440 coded bits.

Table 4.1: $\delta_{max,2}(\beta, R_c, s)$ for $R_c = 1/2$

$\beta \setminus$ s	**1**	**2**	**3**	**4**	**5**
1	2	2			
2	2	3	3		
3	3	4	4	4	
4	3	4	5	5	5
5	4	5	6	6	6
6	4	5	6	7	7
7	5	6	7	8	8
8	5	6	7	8	9

at the output of the decoder. Indeed, the equivalent $\mathcal{M}(\mathcal{D}, \mathcal{L})$ channel has parameters $\mathcal{D} = [\beta+1, \beta, \ldots, \beta+2-(\beta+1)/s]$ and $\mathcal{L} = [sN/(\beta+1), \ldots, sN/(\beta+1)]$, which leads to the following upper bound on the diversity order:

$$\delta_{max,3}(\beta, R_c, s) = min\left(\frac{(\beta+1)(s-1)}{s} + 1 + \left\lfloor \frac{(1-R_c)(\beta+1)}{s} \right\rfloor, \beta+1\right) \tag{4.11}$$

Table 4.2: $\delta_{max,2}(\beta, R_c, s)$ for $R_c = 3/4$

$\beta \setminus \mathbf{s}$	**1**	**2**	**3**	**4**	**5**	**6**
1	1	2				
2	1	2	3			
3	2	3	4			
4	2	3	4	5		
5	2	3	4	5	6	
6	2	3	4	5	6	7
7	3	4	5	6	7	8

It can be easily shown that

$$\delta_{max,2}(\beta, R_c, s) \leq \delta_{max,3}(\beta, R_c, s) \tag{4.12}$$

However, the maximum diversity order $\delta_{max,2}(\beta, R_c, s) = \delta_{max,3}(\beta, R_c, s) = \beta + 1$ is achieved for the same $s \geq (\beta+1)R_c$. The advantage of $\delta_{max,3}(\beta, R_c, s)$ over $\delta_{max,2}(\beta, R_c, s)$ is for non-full diversity schemes. In addition, it is important to note that the bounds in (4.10) and (4.11) have straight-forward applications to systems employing delay precoders.

4.6 Coding strategies

Based on the bounds on the diversity order derived in the previous section, one can choose a good coding strategy given the system parameters (i.e. number of relays, coding rate...). As for the coding gain, it is tedious to analytically compute the pairwise error probability for the NAF and SAF protocols, as it involves integrations over the product of two or more complex Gaussian variables representing the different channel gains $h_{j\ell}$. Now consider $\Delta^2 = \| \left(\mathbf{x} - \mathbf{x}'\right)\mathbf{SH} \|^2$ with $\mathbf{x} - \mathbf{x}' = \sum_{k=1}^{\beta+1} d_k^2$. Next, we look at the distribution of Δ^2 as an empirical tool that helps us in choosing the best coding strategy. Fig. 4.4 shows the distribution of Δ^2 for the single-relay NAF protocol. From the bounds on diversity of (4.10) and (4.11), we notice that if $R_c \leq 1/(\beta + 1)$, we do not need to precode for diversity purpose, as the channel decoder recovers the entire diversity of order $\beta + 1$. However, we can see that for unrotated QPSK input, there is a high number of small squared distances, thus we can eliminate the small values of Δ^2 by rotating the QPSK vector. When the vector $\mathbf{z}$ has relatively small cardinality, it is useful to rotate the transmitted signal constellation with $s = s_{max} = \beta+1$ in a way to combine all the symbols together. A rotation plays the role of "smoothing" the distribution of the input vector $\mathbf{x}$, making it tend to the Gaussian distribution. However, unlike for MIMO systems (see Fig. 3.2), the rotation in this case keeps the length of the transmitted vector unchanged.

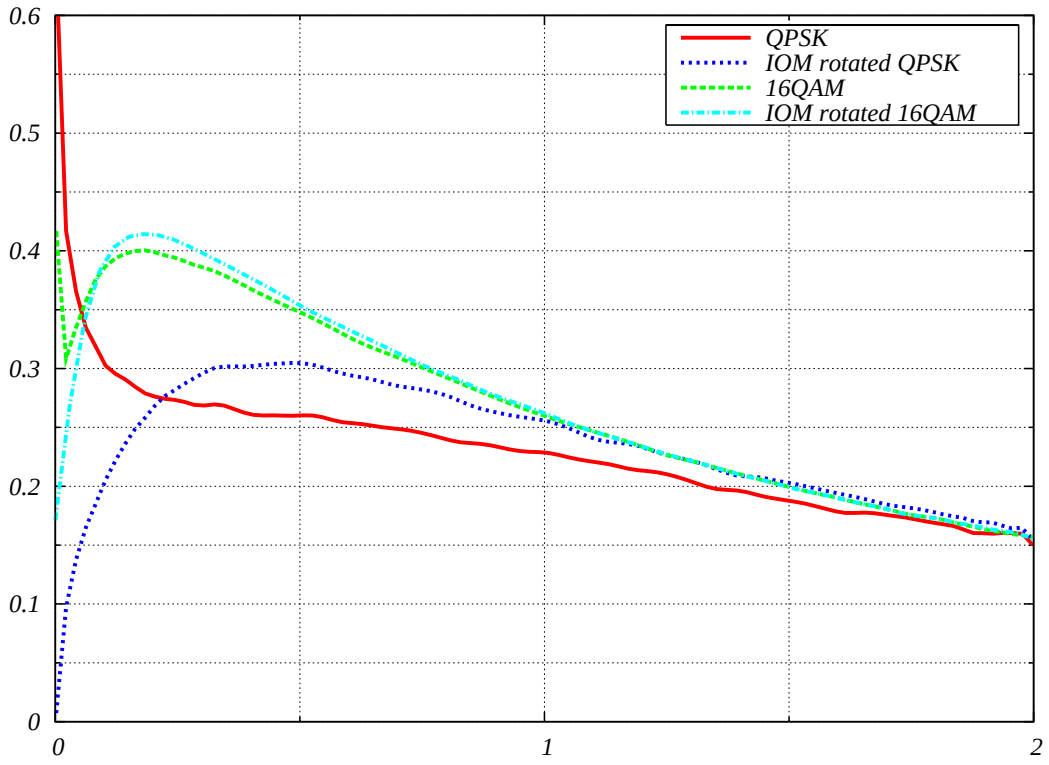

Figure 4.4: Distribution of Δ^2 for the single-relay NAF protocol.

With an increase in the constellation size, a rotation with s_{max} generates a dense vector space, making the extrinsics at the output of the detector suffer from interference between symbols. In this case, as the unrotated constellation generates a reasonable Δ^2 distribution with a small number of small distances, an optimized interleaver [18] that approaches the ideal interleaving condition is sufficient to provide high coding gains and maximum diversity. Now if $R_c > 1/(\beta+1)$, rotations are mandatory to ensure full diversity at the receiver. For the same reasons as when $R_c \leq 1/(\beta+1)$, we use rotations with s_{max} for small size constellations. With large size constellations, it is judicious to minimize the inter-symbol interference and choose a rotation with the minimum s that satisfies the bounds $\delta_{max,2}(\beta, R_c, s)$ or $\delta_{max,3}(\beta, R_c, s)$. We can then ensure full diversity and at the same time deliver better quality extrinsics (than with s_{max}) to the channel decoder. Note that if no iterations are possible at the receiver, the s_{min} that allows for maximal diversity leads the optimal performance of the D-ST-BICM.
The threshold at which we can change the coding strategy (i.e. the value of s) cannot be computed analytically, but simulations showed that a rotation with s_{max} gives better performance with BPSK and QPSK modulations, while degrading the coding gain with 16-QAM constellations or higher. To conclude as to which strategy to follow in order to achieve high coding gains, we can say that:
I) With BPSK and QPSK modulations, always use precoders with s_{max} whatever the coding rate R_c is.

II) With 16-QAM modulations and higher:
1) If $R_c \leq 1/(\beta+1)$, do not precode, use optimized interleavers from [18].
2) If $R_c \geq 1/(\beta+1)$, precode with s_{min} that satisfies $\delta_{max,2}(\beta, R_c, s)$ or $\delta_{max,3}(\beta, R_c, s)$.
III) If no iterations are possible, precode with s_{min} that satisfies $\delta_{max,2}(\beta, R_c, s)$ or $\delta_{max,3}(\beta, R_c, s)$ whatever the coding rate R_c is.
These strategies will be illustrated in the next section. Finally, note that whatever the value of s is, there is no increase in the APP detection complexity.

4.6.1 Simulation results

In this section, word error rate performances are compared to information outage probability for different system configurations to illustrate the results presented in the previous sections. We consider the half-duplex SAF cooperative channels with different coding rates and constellation sizes. We set the values of $\mathcal{E}_1 = 1$, and $\mathcal{E}_2 = \mathcal{E}_3 = \mathcal{E}_1/2$ so that the received energy is invariant from slot to slot. The geometric gain coefficients g_{ij} are all set to 0 dB in this section. The space-time precoders are (IOM) as presented in section 3.6. They are selected from the ensemble of random rotations as:

$$P_{out}(\mathbf{S}) = P\left(\mathcal{I}_{SH} < (\beta+1).m.R_c\right) \tag{4.13}$$

As an example, the 3×3 rotation $S_{IOM,s=2}$ that satisfies $\delta_{max,2}(\beta, R_c, s)$ obtained for the SAF protocol with two relays, 16-QAM input, and half-rate channel coding is given by:

$$\mathbf{S_{NAF-IOM,s=2}} = \begin{bmatrix} 0.69e^{-2.84} & 0 & 0.72e^{-0.12} \\ 0 & 1 & 0 \\ 0.72e^{-1.11} & 0 & 0.69e^{-1.29} \end{bmatrix} \tag{4.14}$$

Fig. 4.5 shows the outage probability for QPSK input, rotated QPSK input with an IOM rotation, and Gaussian input of the single-relay NAF protocol. Without rotation, the discrete input curve is about 2dB away from the Gaussian input. With IOM rotation, the curve roughly achieves the lower bound without any increase in detection complexity.

In Fig. 4.6, we consider a 16-QAM modulation coded with half-rate codes over the two-relay SAF channel. Without rotation, the decoder is not capable of recovering the diversity as shown in (4.10). Adding a rotation with s_{max} ensures the diversity, but mixes three 16-QAM symbols which results in a dense signal space. We can achieve slightly better performance using a precoder with $s = 2$ as it creates less interference between signals, while ensuring maximum diversity. Note that this gain appears since the first iteration.

Finally, Fig. 4.7 shows the performance of QPSK constellation on a three-relay SAF cooperative channel using $R_c = 1/2$ and $R_c = 3/4$ codes. Diversity is provided in several ways; for $R_c = 3/4$ codes, a rotation with $s = 3$ is sufficient to provide diversity, while two $s = 2$ rotations are used for $R_c = 1/2$. However, to achieve optimal coding gains, a rotation with s_{max} has to be used.

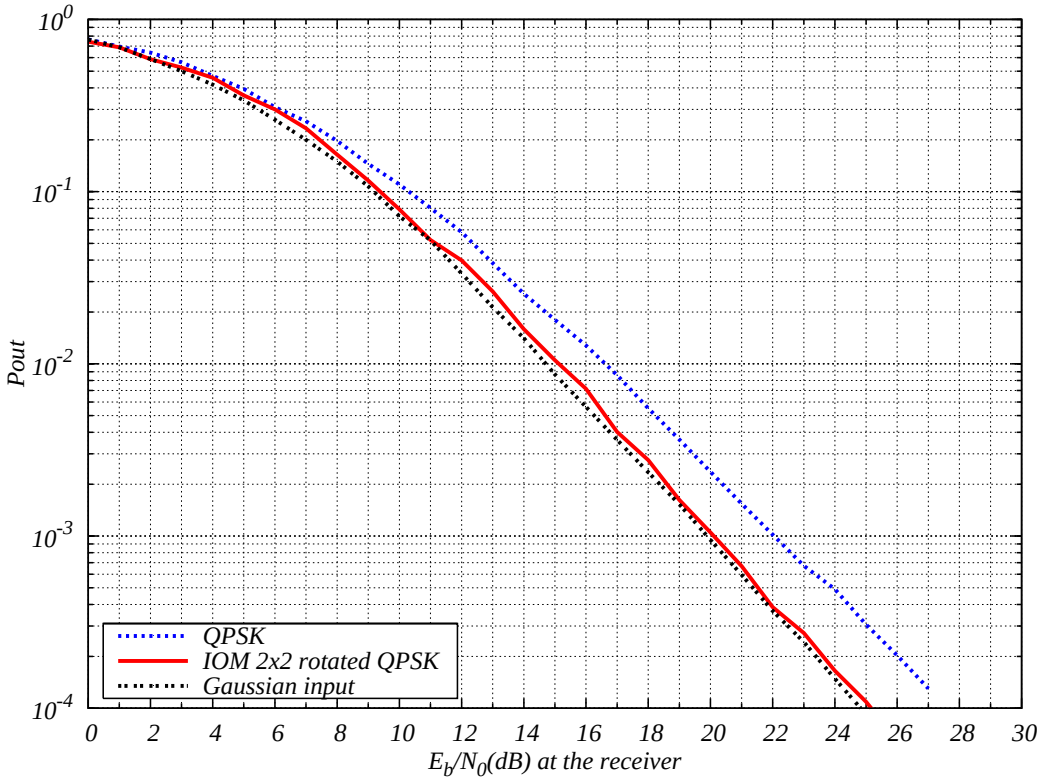

Figure 4.5: Outage probability comparison for the single-relay NAF protocol: QPSK input, rotated QPSK input with 2×2 IOM rotation, and Gaussian input.

For all these configurations, performance less than 2dB away from outage probability is achieved for codeword sizes in the range of 1000-1500 coded bits.

4.7 Code multiplexing over channel states for the half-duplex NAF cooperative channel

As discussed in section 3.8, channel multiplexers can ensure maximal diversity orders and optimal coding gains for turbo codes on block-fading channels provided the rate of the code respects $R_c \leq 1/D_{st}$, where D_{st} is number of states of the BO channel. For both the cases of single-input single-output block-fading channel with D_{st} blocks [53] and the MIMO channel with D_{st} channel states (see section 3.8), both the horizontal multiplexer and the h-π-diagonal multiplexer ensured maximal diversity for turbo codes. However, the h-π-diagonal multiplexer showed better coding gain as it helped to equalize the partial Hamming weights in (3.59). It is of great benefit to see what is the optimal channel multiplexer for turbo codes in the NAF protocol, as it was discussed in section 4.6 that for high spectral efficiencies a rotation degrades the performance of the code. In the sequel, we will only discuss the case of half-rate turbo codes over the single-relay half-duplex NAF cooperative channel. The generalization to the β-relay case is straight-forward as long as

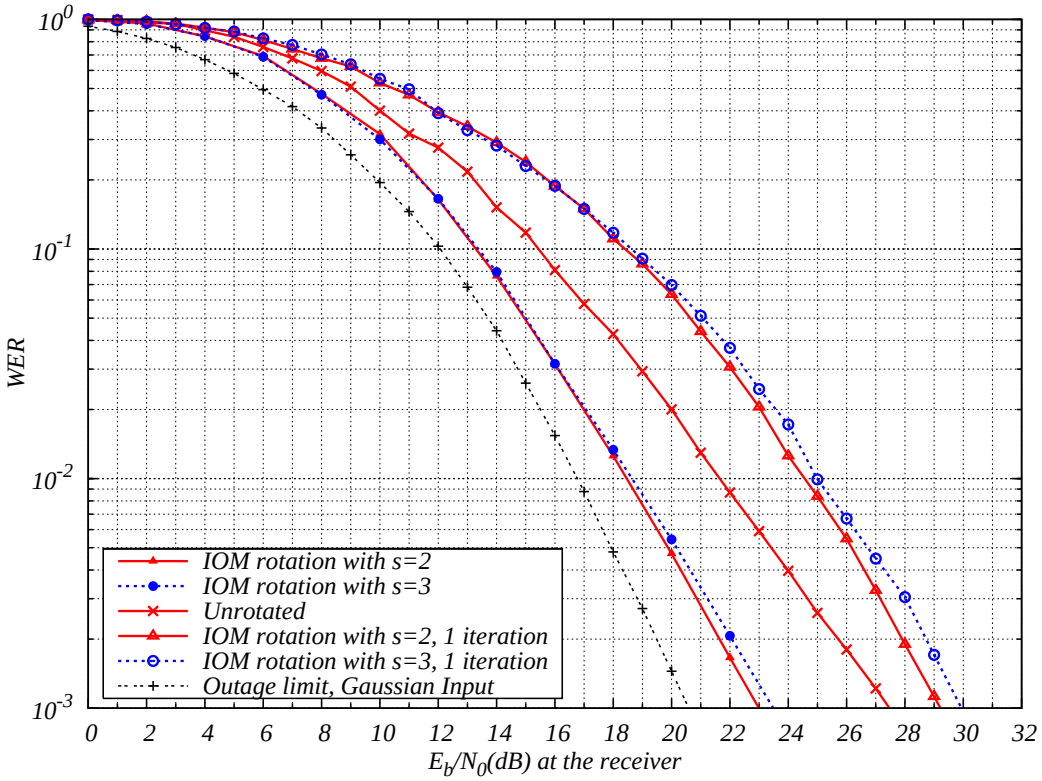

Figure 4.6: Two-relay SAF cooperative channel, R_c=1/2 NRNSC $(23,35)_8$ code, 16-QAM modulation, 1440 coded bits.

$R_c \leq 1/(\beta+1)$. We show in Fig. 4.8 the channel multiplexers for half-rate turbo codes over the NAF channel. Note that when the two channel states of the BO-channel are separated by a commas, this means that the binary element s_i is sent in the first time slot of the cooperation frame, and consequently it sees all the states of the matryoshka channel. The two multiplexers of Fig. 4.8 ensure maximal state diversity at the receiver over a two-state BO-channel as shown for MIMO channel with $n_t = 2$ (see section 3.8). The difference is that with horizontal multiplexing, diversity is always guaranteed by the first RSC code, as all the information bits see the two states of the BO-channel. With h-π-diagonal multiplexing, diversity is ensured through the two constituent codes as for the MIMO channel. However, the coding gains provided by the two multiplexers for the NAF protocol are different from that of the MIMO channel. To illustrate this issue, let us consider the product $\omega_1\omega_2$ of the partial Hamming weight in (3.59). Suppose that the constituent RSC codes are two half-rate $(7,5)_8$ codes, and that the input weight is $\omega = 2$. Consider now error events of length $L = 4+3j$ and total Hamming weight $w_H = 6+2j$, $i = 0\ldots(N-4)/3$. For horizontal multiplexing, $\omega_1 = 6+2j$ and $\omega_2 = 2$. For h-π-diagonal multiplexing, $\omega_1 = 6+2j$ and $\omega_2 = 3+j$. Let ω_{1i}, ω_{2i}, ω_{1p}, and ω_{2p} be the partial weights of information and parity bits. For horizontal multiplexing, $\omega_{1i} = \omega_{2i} = 2$, $\omega_{1p} = 6+2j$, while $\omega_{2p} = 0$. For h-π-diagonal multiplexing, $\omega_{1i} = 2$, $\omega_{2i} = 2$ if j is odd, $\omega_{2i} = 1$ otherwise. $\omega_{1p} = 4+2j$, $\omega_{2p} = 1+j$ if j is odd, $\omega_{2p} = 2+j$ otherwise. Unlike

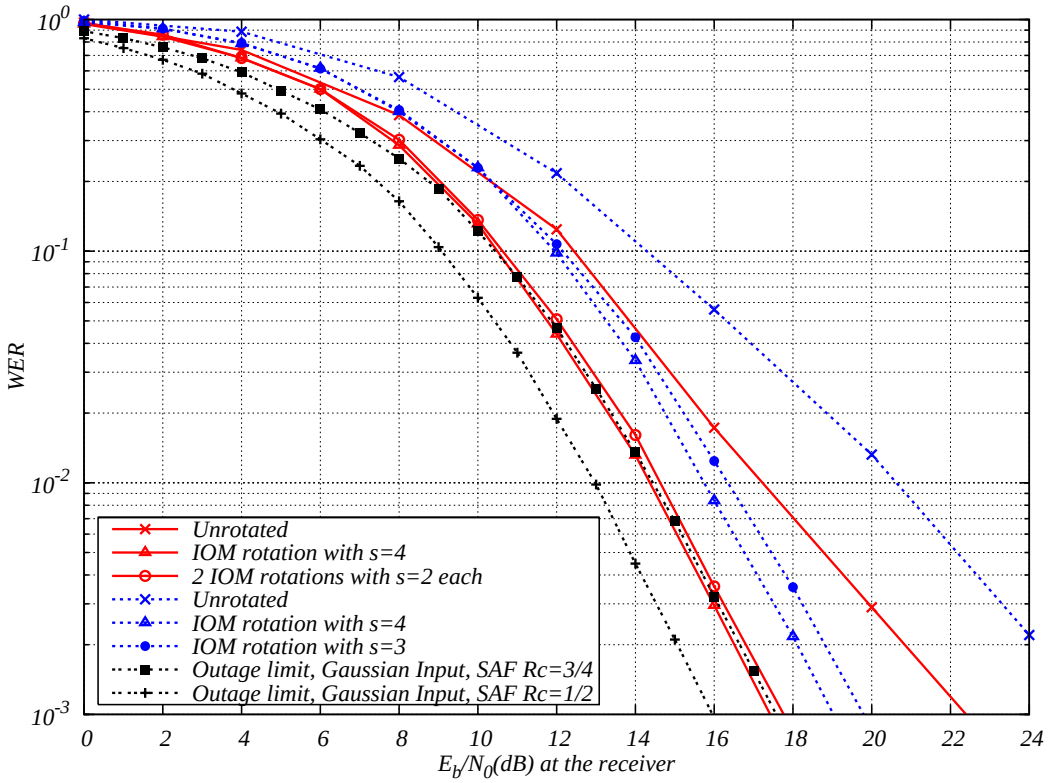

Figure 4.7: Three-relay SAF cooperative channel, R_c=1/2 $(23,35)_8$ (continuous red lines) and 3/4 $(13,25,61,47)_8$ (dashed blue lines) NRNSC codes, QPSK modulation, 1024 coded bits.

Horizontal Multiplexer						
$\mathbf{s_1}$	1 , 2	1 , 2	1 , 2	1 , 2	1 , 2	1 , 2
$\mathbf{s_2}$	1	X	1	X	1	X
$\mathbf{s_3}$	X	1	X	1	X	1

H-π-diagonal Multiplexer						
$\mathbf{s_1}$	1 , 2	1	1 , 2	1	1 , 2	1
$\mathbf{s_2}$	1	X	1	X	1	X
$\pi^{-1}(\mathbf{s_3})$	X	1 , 2	X	1 , 2	X	1 , 2

Figure 4.8: Single-relay NAF channel: Horizontal (top) and h-π-diagonal (bottom) multiplexers for a rate 1/2 parallel turbo code.

the case of two-state BO-channel where information bits have diversity 1 with horizontal multiplexing, the horizontal multiplexer better protects the information bits than the h-π-diagonal multiplexer over the single-relay NAF channel. In fact, this interpretation

joins the results on the bound on the diversity of Matryoshka block-fading channels under ideal interleaving derived in section 4.5, whereas an optimized interleaver makes the code systematic and places the information bits on the block carrying the maximal diversity order.

4.7.1 Simulation results

Fig. 4.9 and 4.10 shows the performance of half-rate turbo codes with different channel multiplexers and with 2×2 IOM rotations over the single-relay NAF protocol. As shown in section 4.6, IOM rotations are best performing for QPSK constellations, allowing the code to approach the outage probability by less than a dB. On the opposite, it is impossible for the code to manage the interference between QAM symbols created by IOM rotations for large constellations. In addition, horizontal multiplexing slightly outperforms the h-π-diagonal multiplexing in Fig. 4.9 for large constellations, as it better protects information symbols. The gain of horizontal multiplexing is even higher in Fig. 4.10 when the geometric gain g_{sr} between the source and the relay is considerable. Note that, like for MIMO systems, word error rate performance of turbo-coded modulations over the NAF protocol is insensitive to interleaver size.

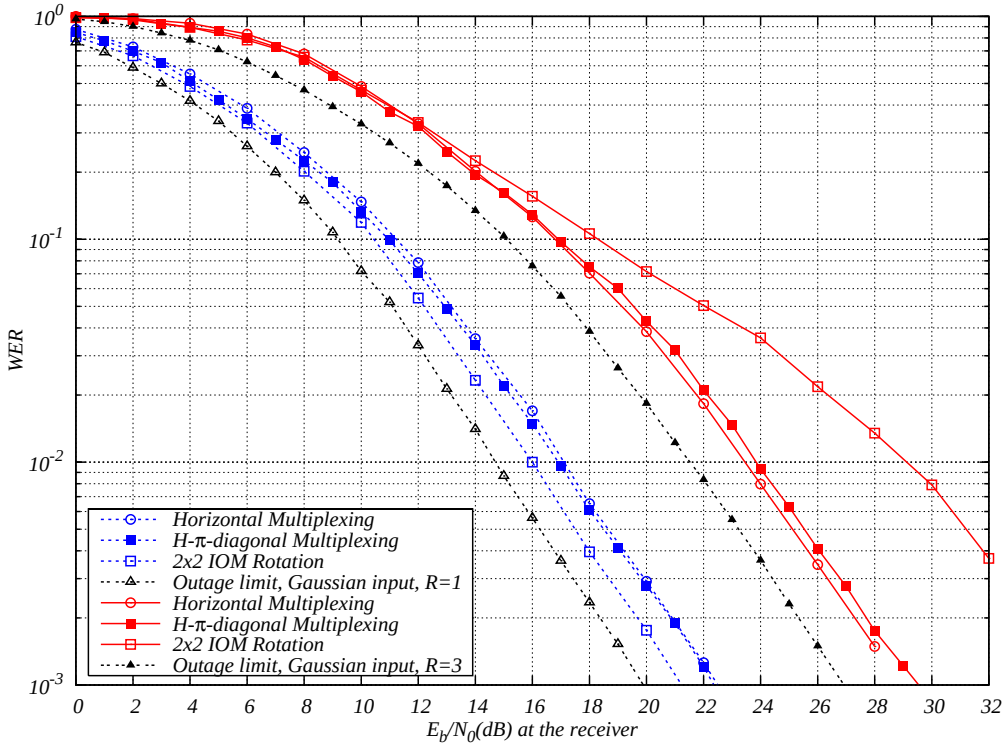

Figure 4.9: Single-relay NAF channel: Frame error rate comparison for QPSK (dashed blue lines) and 64-QAM (continuous red lines) modulations, turbo code with $R_c = 1/2$, $(17, 15)_8$. $g_{sr} = 0$ dB.

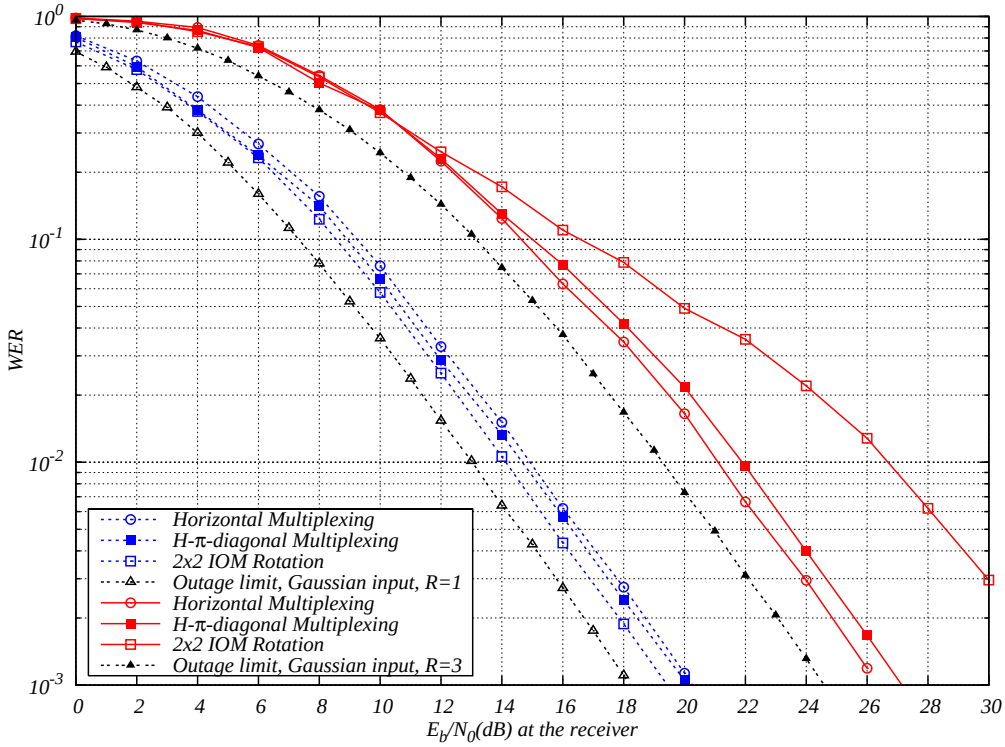

Figure 4.10: Single-relay NAF channel: Frame error rate comparison for QPSK (dashed blue lines) and 64-QAM (continuous red lines) modulations, turbo code with $R_c = 1/2$, $(17, 15)_8$. $g_{sr} = 20$ dB.

4.8 Conclusions

In this chapter, a framework for channel coding over the amplify-and-forward cooperative protocol with iterattive decoding was established. Bounds on the diversity orders for coded systems for the case where all terminal have a single antenna. It was shown that precoding without introducing time delay to the cooperation frame can lead the D-ST-BICM to achieve maximal diversity. The absence of delay is even more important in that it does not increase the detection complexity at the destination. It was also discussed that precoding all the symbols together, which might look as a reliable maximum diversity solution, is in fact harmful for the overall coding gain for large constellations. These coding strategies also hold when no iterations are possible at the receiver. We also presented channel multiplexing issues for turbo codes over the AF protocol, and showed that we can closely approach the outage probability limit even for large constellations.

Chapter 5

Design of irregular turbo codes for block-fading channels

5.1 Introduction

In section 3.8 and 4.7, we showed that turbo-coded modulations using conventional turbo codes are capable of approaching the outage limit of two types of block-fading channels, that are the MIMO channel and the NAF cooperative channel. Fig. 5.1 shows the outage boundaries for a two-state block-fading channel. The fading coefficients α_1 and α_2 belong to $\{0, +\infty\}$. It was discussed in [52] and [64] that, in order to approach the outage limit over block-fading channels, two conditions have to be met:

- Reducing the gap on the ergodic line: this is done by using a code that has a low decoding threshold.

- Reducing the gap at infinity: this is done by using a block-wise maximum distance separable (MDS) code, i.e. a code that achieves the Singleton bound of (2.25) [87].

In this chapter, in a goal to outperform conventional turbo codes on the block-fading channel, we design irregular turbo codes with excellent decoding thresholds over the AWGN channel, which meets with the first condition. We then propose a slight modification of the h-π-diagonal multiplexer [53] that suits the irregular turbo code, in a way to ensure full diversity and meet with the second condition. Our design is limited to half-rate irregular turbo codes over two-state block-fading channels. Generalization to higher state diversity channels is straight-forward as long as $Rc \leq 1/D_{st}$. We will start by introducing turbo codes in general, which allows us to present the structure suitable for the design of irregular turbo codes. We will then present the Density Evolution (DE) and Gaussian Approximation (GA) methods that allow us to design our codes. We will conclude by showing finite-length results for the AWGN channel and DE results for the block-fading channel.

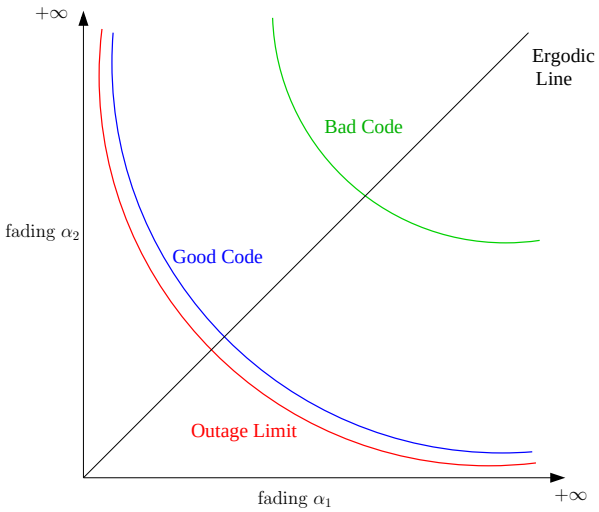

Figure 5.1: Outage boundaries for 2-state block-fading channel.

5.2 Turbo codes

In 1993, Berrou *et al.* [88] astonished the coding community by introducing a new class of "turbo codes" that could achieve near-Shannon-limit performance with relatively low decoding complexity. In this chapter, we will consider the concept of turbo coding to design irregular turbo codes for different channel types.
The encoder of a parallel turbo code is shown in Fig. 5.2 below. An information sequence **b** is encoded by a recursive systematic convolutional (RSC) code to generate a first parity bit sequence; the same sequence is then scrambled by an interleaver Π and encoded by a second RSC code to generate a second parity bit sequence. If the turbo encoder transmits all the three sequences, the overall rate would be 1/3. In order to obtain a half-rate turbo encoder, we usually puncture half of the parity bits of the first parity sequence, and alternatively half of the bits of the second parity sequence. The use of recursive convolutional encoders and a random interleaver is essential to make the turbo code "random-like". Indeed, the work of Battail in [38] on random codes was the motivation behind the turbo codes.

The iterative probabilistic decoder for the above turbo encoder is shown in Fig. 5.3. Decoders SISO 1 and SISO 2 are soft-input soft-output [89] decoders using the forward-backward algorithm [89] for RSC code 1 and RSC code 2. Each decoder reads the observations on information bits and the observations on its own parity bits. The interleaver Π permutes the observations of the first decoder to give them to the second one. A decoder generates extrinsic probabilities on information bits that are fed to the other decoder as *a priori* probabilities on information bits.

At the first iteration, all *a priori* probabilities are set to 1/2. With the iterative process, only extrinsic information evolves through the iterative process, not the channel

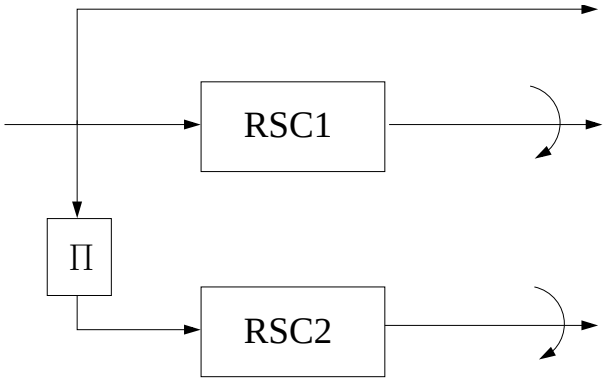

Figure 5.2: Parallel turbo encoder.

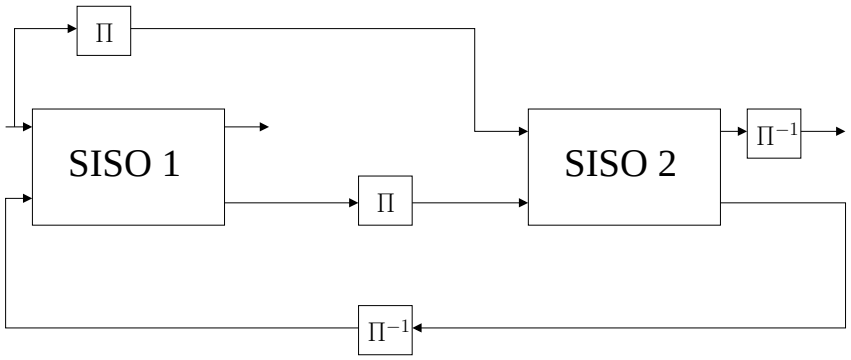

Figure 5.3: Parallel turbo decoder.

observations. At the last iteration, decisions are made on the *a posteriori* probabilities on information bits. We can see that turbo codes are actually turbo decoded not turbo encoded, as the iterative feedback of extrinsic information recalls the feedback of exhaust gases in a turbo-charged engine.
Fig. 5.4 shows the performance of a half-rate parallel turbo code with two RSC $(37, 21)_8$ constituent codes on an AWGN channel for different interleaver sizes.

The curve has two main regions; the waterfall region, that is due to the fact that the use of a length-N interleaver effectively reduces the number of low-weight codewords by a factor of N [62] [63]; and the error floor region, that is due to the relatively poor minimum distance. Indeed, it was shown in [90] that the minimum distance of turbo codes is upper-bounded by a quantity that grows only logarithmically with the interleaver size, and the authors in [91] proposed an interleaver design that always ensures this bound.
In most cases, the two constituent RSC encoders in Fig. 5.2 are identical (i.e. same constraint length and generator polynomials). This is equivalent to the fact of merging the two constituent encoders into a single one, and doubling the size of the interleaver. To do so, a 2-fold repeater has to be added before interleaving. Fig. 5.5 below gives the

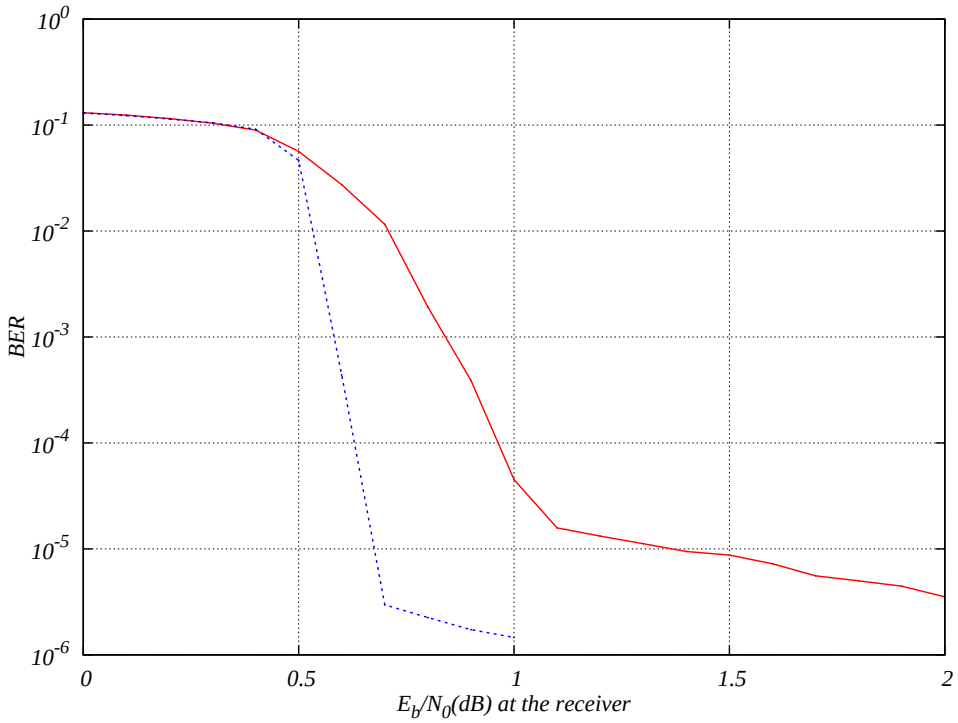

Figure 5.4: Performance of half-rate parallel turbo code with two RSC $(37, 21)_8$ constituent codes, $N = 4096$ (continuous red curves) and $N = 65536$ (dashed blue curves).

representation of the equivalent encoder, that we will call "self-concatenated" turbo code:

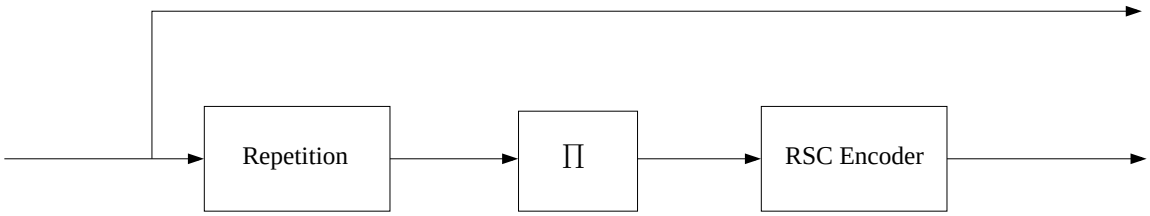

Figure 5.5: Equivalent "self-concatenated" turbo encoder.

It looks actually as a repeat-accumulate (RA) code in which the information sequence is transmitted as well. The decoder for such a turbo encoder is different from the classical turbo encoder, as there is only one SISO decoding block (see Fig. 5.6). In this case, extrinsic information is generated by the "extrinsic computing" (EC) block by simply setting the *a priori* probability on an information bit equal to the extrinsic probability of the other bit in the repeated pair.

In this new representation, each information bit is connected to the code trellis via two edges in the propagation tree. We hence say that the *degree* of the information bits is

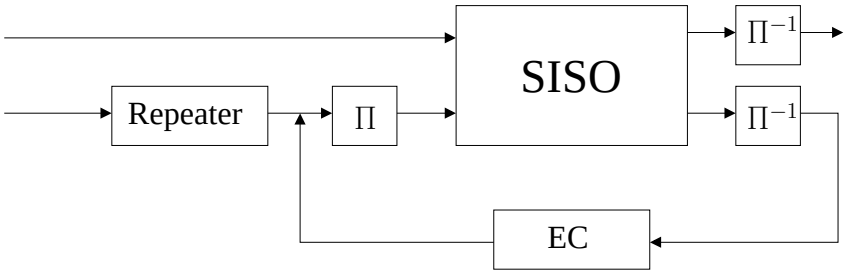

Figure 5.6: Equivalent turbo decoder.

$d = 2$, and that the turbo code is regular. Using this structure, one can create irregularity by repeating a certain fraction f_i of the bits i times, providing bits that are more protected than in the regular case. Like for low-density parity check (LDPC) codes [1] [92], irregularity can boost the performance of turbo codes for large block lengths. The first work that introduced irregularity to turbo codes in order to achieve better performance is [93]. Results as close as 0.3dB from capacity at bit error rate of 10^{-4} were obtained by repeating a fraction of the coded bits (i.e. both the information and parity bits) more than twice. In [94], in a slightly different design, a fraction of the information bits is repeated d times with $d > 2$, while the parity bits remained of degree 1. In order not to alter the coding rate, a fraction f_p of the parity bits is punctured, which lead to even better results.

The encoder of an irregular turbo code is similar to that of Fig. 5.5, with the difference that an information sequence $\mathbf{b}$ is fed to a non-uniform repeater that divides the information bits into d classes with $d = 2, ..., d_{max}$, where d_{max} is the maximum bit-node degree. The number of bits in a class d is a fraction f_d of the total number of information bits at the turbo encoder input, knowing that bits in class d are repeated d times. Finally, the output of the non-uniform repeater is interleaved and fed to the RSC constituent code, of which $(1 - f_p)\%$ of the parity bits are transmitted. The decoder is also similar to that of Fig. 5.6, with the difference in that the extrinsic probabilities in the EC block are computed as:

$$\xi(b_{dj}) = \prod_{\ell=0,\ell\neq j}^{d_b-1} \xi(b_{d\ell}) \tag{5.1}$$

The normalization of these extrinsic probabilities is not necessary as far as we operate with log-likelihood ratios (LLR). However, this normalization is performed for finite length simulations in section 5.6. Now let K denote the length of the information sequence, N the interleaver size, ρ the rate of the RSC constituent code, and R_c the rate of the turbo code. We can write the following:

$$\sum_{d=2}^{d_{max}} f_d = 1 \tag{5.2}$$

$$\sum_{d=2}^{d_{max}} d.f_d = \overline{d} \tag{5.3}$$

$$N = K \sum_{d=2}^{d_{max}} d.f_d = K.\overline{d} \tag{5.4}$$

$$R_c = \frac{K}{K + \frac{N}{\rho} - N} = \frac{1}{1 + \left(\frac{1}{\rho} - 1\right)\overline{d}} \tag{5.5}$$

$$\rho = \frac{1}{1 + (1 - f_p)\left(\frac{1}{\rho_0} - 1\right)} \tag{5.6}$$

where $\rho_0 = k/n$ is the initial rate of the constituent RSC code before puncturing. In the next sections we will introduce methods that allow to evaluate the convergence behavior of codes defined on graphs in general, that will be used to design irregular turbo codes in the sequel.

5.3 Density evolution for irregular turbo codes

In this section, we consider rate-R_c irregular turbo codes built from a rate-ρ RSC constituent code and degree profile $\{f_d\}_{d=1,...,d_{max}}$. We assume that the all-zero codeword is modulated into $x = -1, -1, ..., -1$ and transmitted over an AWGN channel with variance N_0. At the output of the channel, each received BPSK symbol can be written as $y = x + n = -1 + n$, so the conditional probability density function (PDF) is given by:

$$p(y|x = -1) = \frac{1}{\sqrt{2\pi N_0}} e^{-(y+1)^2/2N_0} \tag{5.7}$$

The LLR of the channel observation y is thus:

$$LLR_0 = \log \frac{p(y|x = -1)}{p(y|x = +1)} = \frac{2}{N_0} y = \frac{2}{N_0}(-1 + n) \tag{5.8}$$

This gives a Gaussian random variable that follows the distribution $p_0(x) \sim \mathcal{N}(m_0, v_0)$ with:

$$m_0 = -\frac{2}{N_0}, \quad v_0 = \frac{4}{N_0} \tag{5.9}$$

The propagation tree for irregular turbo codes is shown in Fig. 5.7. A bit-node of degree d with probability $\mu_d = d.f_d/\overline{d}$ has $d - 1$ incoming extrinsic probabilities and one outgoing *a priori* probability also called partial APP. The APP of an information bit is obtained by the sum of the incoming extrinsics and the outgoing partial APP associated to the same edge of the graph. We assume that the infinite-size interleaver has no cycles, assumption that gives a perfect tree graph representation.
For every bit b_d of degree d, we compute the forward-backward algorithm [89] over a

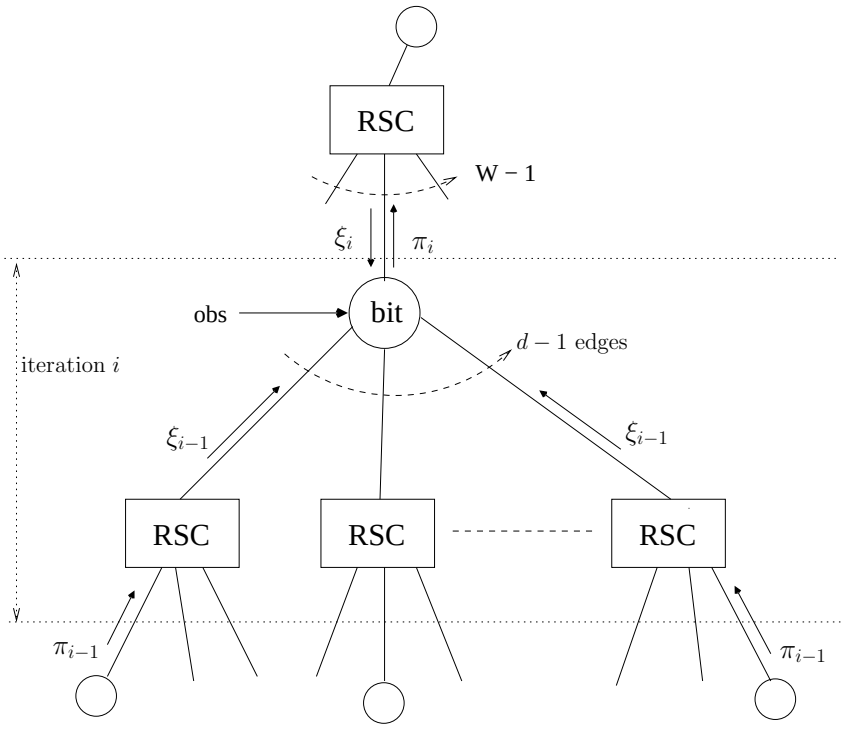

Figure 5.7: Propagation tree of an irregular turbo code.

window W around the bit, whose size should be large enough to guarantee a correct APP evaluation. The algorithm computes extrinsic information on b_d whose distribution is computed. In [95], it was shown that for convolutional codes, when the channel observation and the *a priori* probabilities at the input of the code are independent and identically distributed (i.i.d), the *a posteriori* probability density is independent of the bit position. Consequently, the extrinsics are independent from *a priori* probabilities, thus only one histogram is sufficient to evaluate the extrinsic probability distribution of all the information bits $b_d, d = 1, ..., d_{max}$. Throughout the iterative process, the *a priori* probability of a bit of degree d is computed as the sum of $d-1$ extrinsics given by the distribution of the extrinsics.
The log-ratio of the extrinsic information at iteration i is defined as:

$$LLR_i = \frac{\log(\xi_i(b_d = 1)}{\log(\xi_i(b_d = 0)} \tag{5.10}$$

A signal-to-noise ratio is said to be *admissible* if the error probability vanishes after a finite number i_{max} of iterations of the APP decoder. The smallest admissible signal-to-noise ratio is called *threshold*. We describe hereafter the Density Evolution (DE) method:

- Initialize the channel noise variance $N_0 = N_0(E_b/N_0)$.
- Initialize the extrinsic probability density function $p_{LLR_i}(x)$ by a Dirac impulse.

- For each iteration $i = 1, ..., i_{max}$
  - Given the density $p_{LLR_{i-1}}(x)$ of LLR_{i-1}, compute the new density $p_{LLR_i}(x)$ of the outgoing extrinsic information LLR_i.
  - Compute the error probability $P_b(i)$ on information bits.
  - Stop the density evolution if $P_b(i)$ is vanishing (i.e. $< 10^{-5}$).
- if $i = i_{max}$ and $P_b(i) > 10^{-5}$, choose a greater value for E_b/N_0 and restart, else choose a smaller value and restart.

The total bit error probability at iteration i is given by:

$$P_b(i) = \sum_{d=2}^{d_{max}} f_d P_b(d, i) \tag{5.11}$$

Where $P_b(d, i)$ is the bit error probability of class d given by the area under the tail of the probability density function $p_{d,i}(x)$ of the APP inside class d written as:

$$p_{d,i}(x) = \mathcal{F}^{-1}\left[\mathcal{F}\left[p_0(x)\right]\mathcal{F}^d\left[p_{LLR_i}(x)\right]\right] \tag{5.12}$$

Where $p_0(x) \sim \mathcal{N}(-2/N_0, 4/N_0)$ is the probability density function of the channel likelihood. Density evolution gives a very accurate limit on the convergence behavior of capacity-approaching codes, and it was used to find optimal degree profiles for LDPC codes in [1] [96]. However, finding a good degree profile using density evolution requires intensive computations and a long search, since the optimization problem is not convex [97]. Furthermore, it does not provide any insight to the design process, as one has to perform an exhaustive search over a wide range of profiles to find the best ones. In the next section, a less-accurate - but much faster - method for studying the convergence behavior of iterative decoding will be studied.

5.4 Gaussian approximation for irregular turbo codes

In [98], an approach for finding convergence behavior of iterative decoders using extrinsic information transfer (EXIT) charts was proposed. Although this method is not as accurate as density evolution, its low computational complexity makes it very attractive. EXIT charts provide one-dimensional analysis that can reduce the problem of optimizing the degree profile of an irregular code to a linear program. This way the optimization algorithm becomes much faster and gives a qualitative insight to the convergence behavior of the decoder.
There have been many approaches based on one-dimensional analysis of graph codes, and they assume that the PDF of the decoder's log-ratio is approximately Gaussian. All GA are more or less equivalent, differences stand in the Gaussian parameters estimation and

in the chart parameters (mutual information, signal-to-noise ratio, error probability...). The problem with GA methods with LDPC codes is that approximation is accurate only for messages sent from bit-nodes, as the convolution of the extrinsic distribution with the PDF of the channel likelihood (that is Gaussian) in (5.12) gives a "somehow" Gaussian distribution. On the opposite, the extrinsics distribution from check-nodes is far from being Gaussian, as the checks are connected to a small number of bit-nodes in a LDPC code propagation tree. With convolutional codes however, as the check constitues the whole window over which the decoding algorithm is computed, the distribution of the extrinsic probabilities at the output of the decoder is closer to a Gaussian distribution. In the density evolution method, we need the output density $p_{LLR_{i-1}}(x)$ of the previous iteration in order to compute the input density of the next iteration. The advantage of GA on this issue is that it allows to start the analysis from any stage of the decoding process. To analyze one iteration, consider the tree of Fig. 5.7. We want to track the behavior of the iterative decoder through the value of the output error probability P_{out} at the bit-node as a function of the input error probability P_{in} at the check-nodes. The values of the input error probabilities are picked from the range $[0, Pe_0]$, where Pe_0 corresponds to the error probability given the channel signal-to-noise ratio per receive symbol E_s/N_0. The different values of P_{in} are then mapped onto Gaussian distributions that are fed to check-node input. After a "one-step" density evolution (as explained in section 5.3), the distribution obtained at the output of the bit node is approximated by a Gaussian distribution, from which P_{out} is finally computed. There exist several metrics to approximate the distribution of the output of the bit-node with a Gaussian one, the most accurate being the matching of the symmetric Gaussian density to the true density based on a mutual information measure as in [99].
In [100], the author proposed a function $J(\sigma)$ that maps standard deviation σ of a symmetric Gaussian density to its mutual information, with:

$$J(\sigma) = 1 - \int_{-\infty}^{+\infty} \frac{e^{-(t-\sigma^2/2)^2/2\sigma^2}}{\sqrt{2\pi}\sigma} \; . \; \log(1+e^{-t})dt \tag{5.13}$$

With irregular turbo codes, the channel observation is available at the parity bits of the RSC constituent code, thus P_{out} is computed by approximating the distribution of the extrinsics at the output of the check-node by a Gaussian distribution using (5.13) without an additional convolution with the channel observation.

5.5 Irregular turbo code design

Designing irregular turbo codes for the AWGN channel was done in [93] [94]. In this section, we propose a new method for designing irregular turbo codes based on both GA from [99] and DE methods.
First, we compute the EXIT chart for different values of f_d as in [99]. This chart gives us

the value of $P_{out,d}$ for degree d as a function of P_{in} as:

$$P_{out,d} = f_d(p_{in}) \tag{5.14}$$

Next, by imposing the constraints:

- $f_d \geq 0 \ \ \forall\ d$
- $\sum_{d\geq 2}^{d_{max}} f_d = 1$

We compute:

$$\sum_{d\geq 2}^{d_{max}} \frac{d.f_d}{\overline{d}} \ .\ f_d(p_{in}) < p_{in} \ \ \forall p_{in} \ \in \ \ (0, p_0] \tag{5.15}$$

using the method described in section 5.4. The above equation gives us a range of values of f_d such that the tunnel in the EXIT chart is open, which means that the iterative decoding converges. The final step is then to perform density evolution over the range of values of the f_d, and choose the degree profile that has the lowest threshold. Note that in order to get $R_c = 1/2$ or $R_c = 1/3$ codes for instance, strict constraints are imposed on f_p. For this reason, the linear programming method used to optimize the degree profile of LDPC codes in [99] was not considered for irregular turbo codes. In fact, this method consists of maximizing the rate of the code by maximizing a function that depends on $\overline{d}$, giving no insight on the puncturing rate f_p. In order to optimize the degree profile at a fixed rate, one should disregard this method. Indeed, our design gives the following expression for the rate of the irregular turbo code:

$$R = \frac{K}{K + \lfloor K\overline{d}\,(1 - f_p)\rfloor + n\lceil \frac{L-1}{k}\rceil} \tag{5.16}$$

This means that $\lim_{K\to\infty} R = 1/2$. Optimization results have shown that one can obtain good performance codes by only selecting a small number of non-zero degrees, thus lowering the number of density evolution simulations to be performed. As an example, suppose we want to design a half-rate irregular turbo code with only two non-zero fractions, say f_2 and f_{12}. The capacity limit for $R_c = 1/2$ and BPSK modulation is around 0.18dB. We set the signal-to-noise ratio per receive symbol to -2.8dB, such that by introducing a half-rate code (i.e. by loosing 3dB) we fall slightly above the capacity limit. We next draw the EXIT chart as shown in Fig. 5.5; as there is one constituent RSC code in a self-concatenated turbo code, we can judge if the iterative receiver converges for a certain degree if the transfer fucntion of (5.14) falls below the bisectrix of the $[P_{in}, P_{out}]$ plane. We then select the degree profile pair $\{f_2, f_{12}\}$ that allow for the tunnel to be open, and we finally get the results of Tab. 5.1 by DE simulation. Similarly, the degree pair $\{f_2, f_{10}\}$ gives the results of Tab. 5.2. In Fig. 5.5, we can see that the number of iterations needed for the DE method to converge increases while approaching the decoding threshold of the code. Thus at 0.27dB, the decoder needs about 278 iterations to converge.

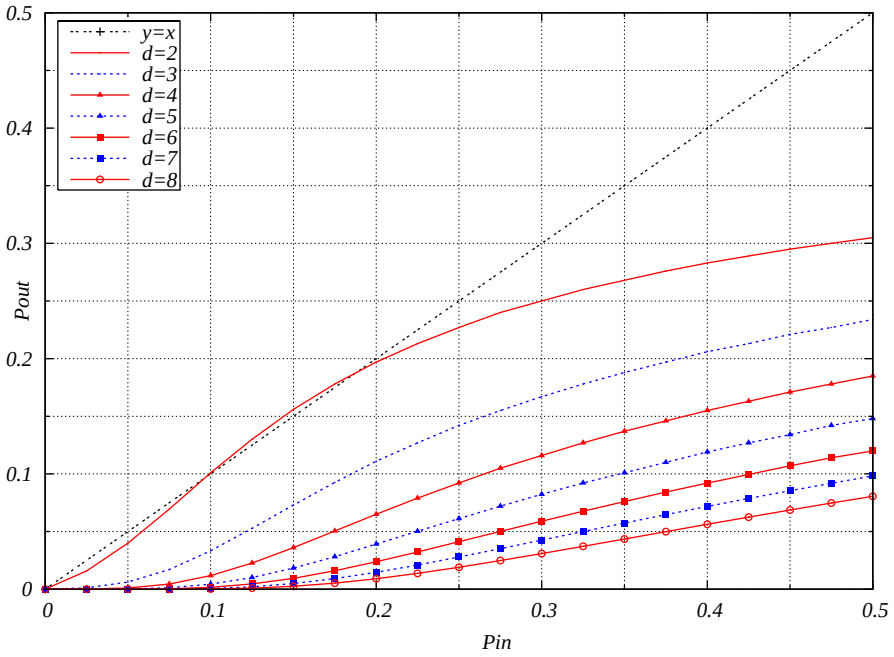

Figure 5.8: EXIT charts, single Gaussian distribution, $E_s/N_0 = -2.80$dB.

Table 5.1: Convergence for half-rate irregular turbo codes, AWGN channel, degree profile $\{f_2, f_{12}\}$.

f_2	f_{12}	$(E_b/N_0)_{min}$	$\overline{d}$	f_p
0.89	0.11	>1.00	3.10	0.354839
0.90	0.10	0.32	3.00	0.333333
0.91	0.09	0.34	2.90	0.310345
0.92	0.08	0.27	2.80	0.285714
0.93	0.07	0.32	2.70	0.259259
0.94	0.06	0.35	2.60	0.230769
0.95	0.05	0.40	2.50	0.200000
0.96	0.04	0.41	2.40	0.166667
0.97	0.03	0.45	2.30	0.130435
0.98	0.02	0.47	2.20	0.090909
0.99	0.01	0.51	2.10	0.047619
1.00	0.00	0.55	2.00	0.000000

5.6 Simulation results

5.6.1 Finite-length performance over the AWGN channel

Fig. 5.10 shows the performance of the rate-1/2 irregular turbo code designed in section 5.5 with (25,37,35) RSC code constituent against irregular LDPC code from [1]. The

Table 5.2: Convergence for half-rate irregular turbo codes, AWGN channel, degree profile $\{f_2, f_{10}\}$.

f_2	f_{10}	$(E_b/N_0)_{min}$	$\overline{d}$	f_p
0.87	0.13	>1.00	3.04	0.342105
0.88	0.12	0.42	2.96	0.324324
0.89	0.11	0.44	2.88	0.305556
0.90	0.10	0.38	2.80	0.285714
0.91	0.09	0.32	2.72	0.264706
0.92	0.08	0.41	2.64	0.242424
0.93	0.07	0.40	2.56	0.218750
0.94	0.06	0.41	2.48	0.193548
0.95	0.05	0.42	2.40	0.166667
0.96	0.04	0.44	2.32	0.137931
0.97	0.03	0.47	2.24	0.107143
0.98	0.02	0.50	2.16	0.074074
0.99	0.01	0.53	2.08	0.038462
1.00	0.00	0.55	2.00	0.000000

irregular turbo code clearly outperforms the irregular LDPC code for a codeword size of 10^5, while the gain is smaller for 10^6. It is important to mention that the number of iterations needed for the decoder to converge is logarithmically proportional to the interleaver size N of the code [101]. Now as irregular codes are by definition asymptotically good, it is better to use regular turbo codes for smaller interleaver sizes. The structure of the self-concatenated turbo code presented in this chapter allows to easily switch between irregular and regular configurations, by only making the repeater uniform and sending all the parity bit sequence (i.e. no puncturing).

5.6.2 Density evolution over block-fading channels

In this section we show the word error rate performance of half-rate irregular turbo codes over a two-state block-fading channel via density evolution. As in section 5.3, we assume that the all-zero codeword is modulated into $x = -1, -1, ..., -1$ and transmitted over a block-fading channel with n_c states ($n_c = 2$ in our case). The received signal y can be written as:

$$y = hx + w \tag{5.17}$$

where w is the AWGN component with zero mean and variance N_0, and h is the real fading coefficient that belongs to the set:

$$\Psi = \{\alpha_1, \alpha_2, \cdots, \alpha_{n_c}\} \tag{5.18}$$

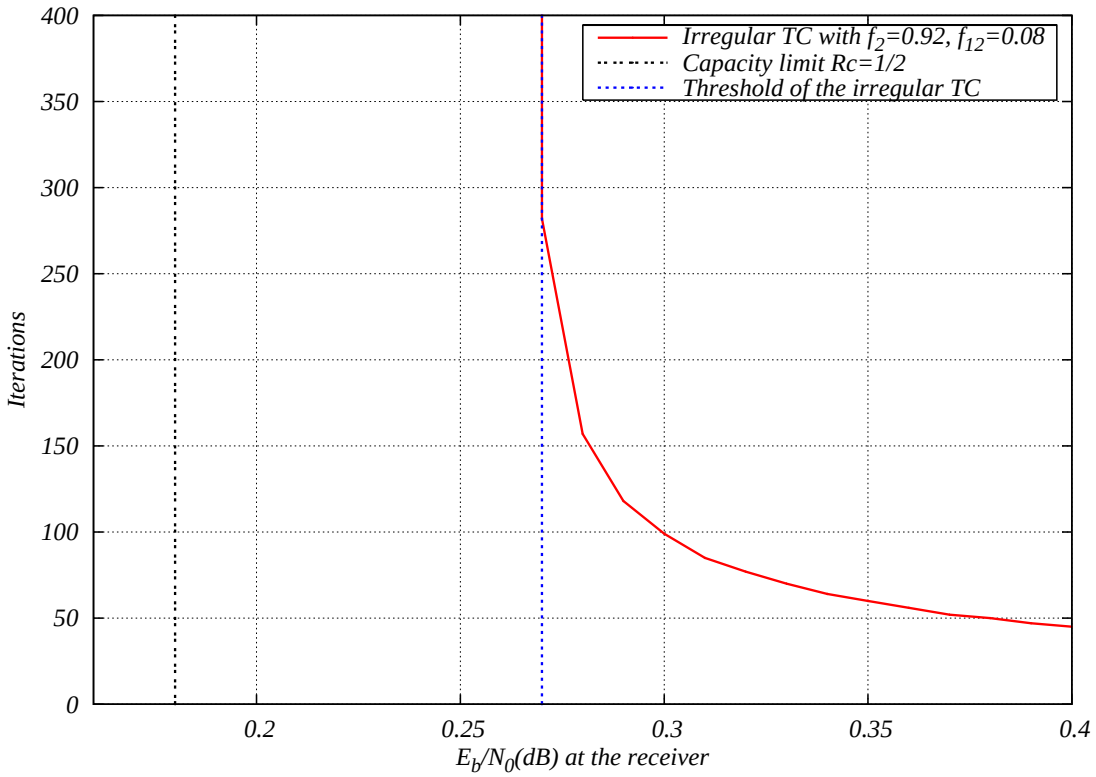

Figure 5.9: Convergence behavior of half-rate irregular turbo codes with degree profile $f_2 = 0.92$ and $f_{12} = 0.08$.

In [52], it was shown that the frame error rate performance of turbo codes under iterative decoding can be written as:

$$P_{ef} = \int_{\Psi \in D_0(c)} p(\Psi) d\Psi \tag{5.19}$$

where

$$D_0(c) = \left\{ \Psi \in \mathbb{R}_+^{n_c} \mid \lim_{i \to \infty} \lim_{N \to \infty} P_{ew}^i(N) = 1 \right\} \tag{5.20}$$

is the outage region of the turbo code and i is the number of iterations of the decoder. This region contains the values of the fading coefficients that lead the decoder not to converge. This means that the error probability of large interleaver sizes is given by the distribution of the decoding threshold as a function of the fading. As in [52], we decided to run the DE algorithm only when there is no outage, and when $\alpha_{min} \frac{E_b}{N_0} > \frac{E_b}{N_0} \mid_{th}$, where α_{min} is the lowest fading value within the set Ψ, and $\frac{E_b}{N_0} \mid_{th}$ is the code threshold over the AWGN channel. To attain the best possible performance over the two-state block-fading channel, we consider the half-rate irregular turbo code with degree profile $f_2 = 0.92$ and $f_{12} = 0.08$ that exhibits a threshold of $\frac{E_b}{N_0} \mid_{th}$= 0.27dB over the AWGN channel that is the best among all other profiles. Note that as this code is self-concatenated, the h-π-diagonal multiplexer does not apply as it is. Now for this code to attain the maximal diversity $D_{st} = 2$ with optimal coding gain, we propose the modification of the h-π-diagonal multiplexer as shown

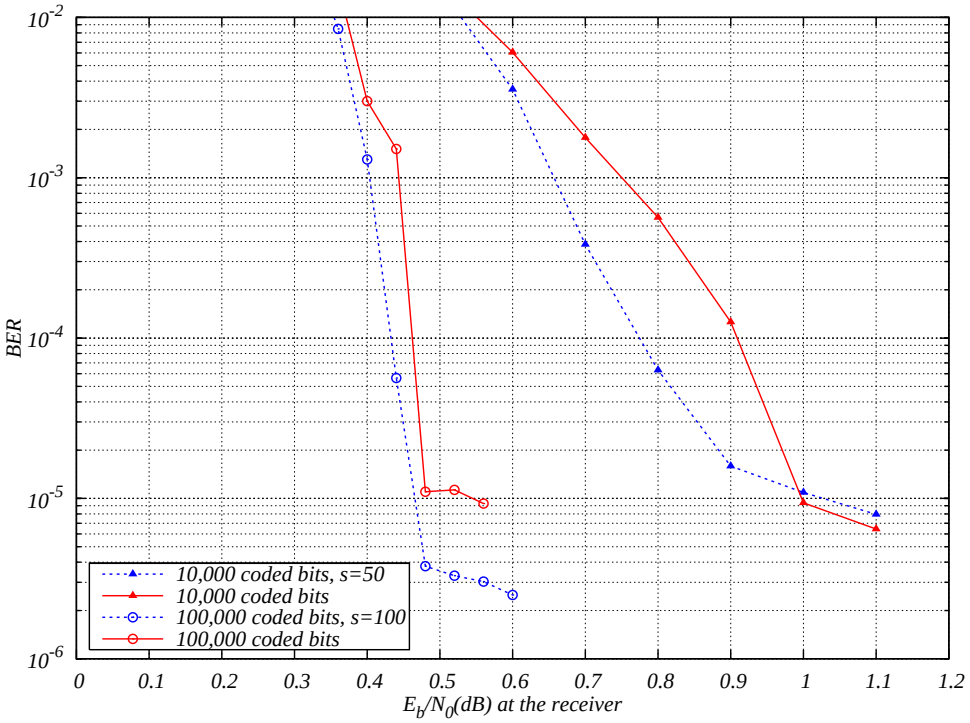

Figure 5.10: Irregular turbo code with Rc=1/2, (25,37,35) RSC code constituent, $f_2 = 0.92$, $f_{12} = 0.08$, $f_p = 0.28$, s-random interleaving (dashed blue curves), versus half-rate irregular LDPC [1] code (continuous red curves), AWGN channel.

in Fig. 5.11. where s_1 represents the information bits and s_2 the parity bits of the RSC

H-π-diagonal Multiplexer						
$\mathbf{s_1}$	1	2	1	2	1	2
$\pi^{-1}(\mathbf{s_2})$	2/X	1/X	2/X	1/X	2/X	1/X

Figure 5.11: H-π-diagonal multiplexer for a rate 1/2 irregular turbo code.

code, among which a fraction f_p is punctured (represented by the X). In Fig. 5.12, we show the word error rate performance of the half-rate irregular turbo code with (25,37,35) RSC code constituent, degree profile $f_2 = 0.92$ and $f_{12} = 0.08$, is compared to that of a regular turbo code with two (13,15) RSC code constituents whom half parity bits are punctured over the two-state block-fading channel, BPSK input. The regular turbo code with h-π-diagonal multiplexing is about 1dB away from outage probability, while the irregular turbo code with the modified h-π-diagonal multiplexer roughly coincides with the BPSK input outage probability.

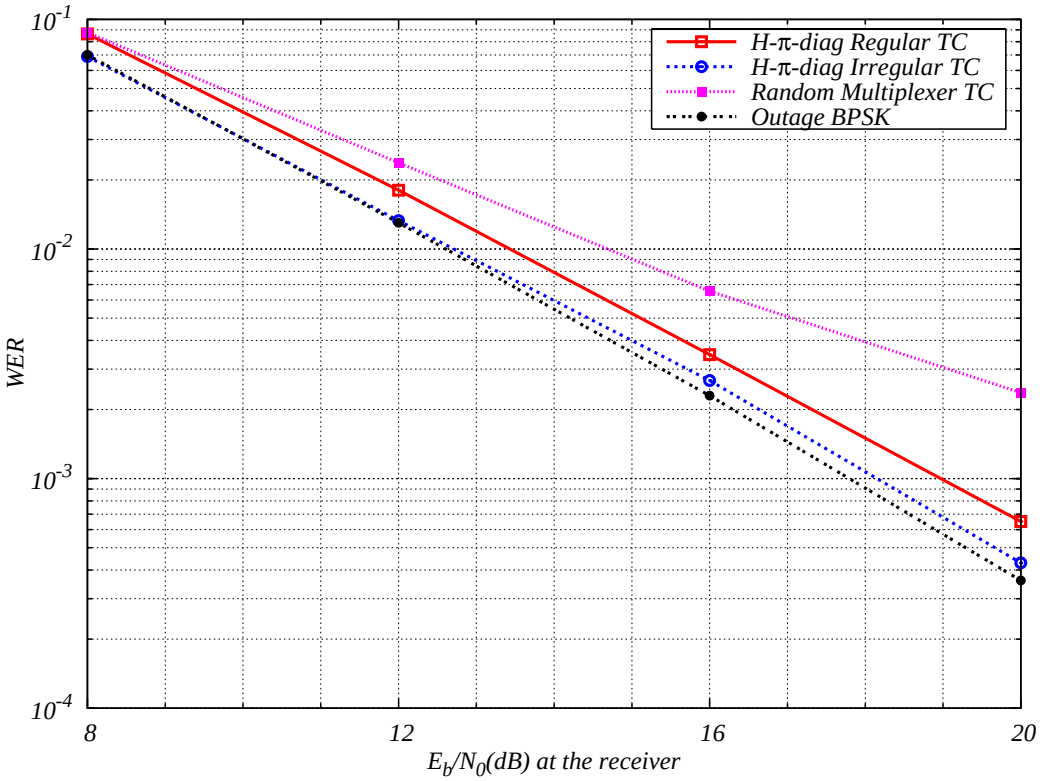

Figure 5.12: Word error rate computed with the DE algorithm for $R_c = 1/2$ turbo codes over the 2-state block-fading channel, BPSK modulation.

5.7 Conclusions

In this chapter, we presented the design of irregular turbo codes that are capable of achieving the outage probability of the block-fading channel. By satisfying the two conditions that are 1) a low decoding threshold over the AWGN channel and 2) full diversity through channel multiplexing, irregular turbo codes outperform all other existing codes for sufficiently large block length. Following the definitions in [16], irregular turbo codes are *good* codes, i.e. they exhibit a vanishing gap with the outage limit for $N \to \infty$, while regular turbo codes are *weakly good* codes, as they achieve a constant gap from outage probability for any interleaver size.

Chapter 6

Conclusions

This manuscript presented space-time bit-interleaved coded modulations for both the multiple-antenna block-fading channel and the amplify-and-forward cooperative fading channel with single-antenna nodes. What these schemes have in common is that they were capable of achieving the maximal diversity orders the block-fading channels -they were designed for- allowed and they provided high coding gains with relatively low decoding complexity at the receiver.

For the multiple-antenna channel, we proposed the following:

- *Information Outage Minimizing* (IOM) space-time precoders: these precoders allow for optimal performance of the ST-BICM if no iterations are possible at the receiver. They can also be adapted so that they become optimal for both "one-shot" decoding and iterative decoding

- Matrix-Alamouti space-time precoder: application of the Alamouti scheme with two transmit antennas to four transmit antennas. With proper signal decoupling and iterative interference cancellation/decoding, frame error rate robust with respect to the frame size was achieved.

- Turbo-code design for multiple-antenna systems: these systems achieved optimal word error rate performance insensitive to the interleaver size by using a special multiplexer that places the binary elements at the output of the code "intelligently" on the channel states. This performance is achieved at no additional cost in complexity.

For the amplify-and-forward cooperative fading channel, the following results were carried out:

- Bounds on the diversity order of coded systems over the Matryoshka block-fading channel representing the slotted amplify-and-forward protocol were derived. These bounds can be achieved by judicious precoding without affecting the decoding complexity.

- Coding strategies based on the bounds on diversity that allow to achieve high coding gains depending on the coding rate, modulation size, and number of relays.

- Turbo-code design for the amplify-and-forward cooperative fading channel: the code multiplexer that suits the Matryoshka block-fading channel model proved to be optimal. Again, word error rate performance insensitive to block size at no increase in complexity is achieved.

Finally, we proposed irregular turbo codes that exhibit a vanishing gap with the outage probability for large block lengths over the single-input single-output block-fading channel. This is done through an adapted channel multiplexer that suits the self-concatenated structure of the code. This result can be applied to any block-fading channel type. The material elaborated in this report opens the way for the following perspectives:

- Study of sub-optimal receivers for the SAF protocol: indeed, the upper-triangular structure of the channel matrix can allow for the implementation of sub-optimal detectors such as the Successive Interference Cancellation (SIC) or the SISO-Minimum Mean-Square Error (MMSE) detectors that can provide a drastic complexity reduction with respect to the exhaustive APP detector.

- Derive bounds on the diversity order of the MIMO-SAF channel: investigate on what diversity orders a D-ST-BICM can achieve in the case where the nodes have multiple antennas.

- Study of Decode-and-Forward protocols from the D-ST-BICM point-of-view.

- Study of the schemes proposed in this manuscript for Multi-Carrier (MC)-CDMA systems and OFDM systems.

Bibliography

[1] T.J. Richardson, M.A. Shokrollahi, and R.L. Urbanke, "Design of capacity-approaching irregular low-density parity-check codes," *IEEE Transactions on Information Theory*, vol. 47, no. 2, pp. 619–637, 2001.

[2] J. G. Proakis, *Digital communications*, McGraw-Hill New York, 1989.

[3] L.H. Ozarow, S. Shamai, and A.D. Wyner, "Information theoretic considerations for cellular mobile radio," *IEEE Transactions on Vehicular Technologies*, vol. 43, no. 2, pp. 359–378, May 1994.

[4] C.E. Shannon, "The Mathematical Theory of Communication," *Bell System Technical J*, vol. 27, pp. 379–423, 1948.

[5] I.E. Telatar, "Capacity of Multi-Antenna Gaussian Channels," *European Transactions on Telecommunications*, vol. 10, no. 6, November 1999.

[6] G.J. Foschini and M.J. Gans, "On Limits of Wireless Communications in a Fading Environment when Using Multiple Antennas," *Wireless Personnal Communications*, vol. 6, no. 3, pp. 311–335, March 1998.

[7] S. Verdu and Te Sun Han, "A general formula for channel capacity," *IEEE Transactions on Information Theory*, vol. 40, no. 4, pp. 1147–1157, July 1994.

[8] E. Biglieri, J. Proakis, and S. Shamai, "Fading channels: information-theoretic and communications aspects," *IEEE Transactions on Information Theory*, vol. 44, no. 6, pp. 2619–2692, October 1998.

[9] G. Caire, G. Taricco, and E. Biglieri, "Optimum power control over fading channels," *IEEE Transactions on Information Theory*, vol. 45, no. 5, pp. 1468–1489, July 1999.

[10] A. Guillén i Fàbregas, *Concatenated Codes for Block-Fading Channels*, Ph.D. thesis, EPFL, Lausanne, 2004.

[11] Z. Wang and G.B. Giannakis, "Outage mutual information of space-time MIMO channels," *IEEE Transactions on Information Theory*, vol. 50, no. 4, pp. 657–662, April 2004.

[12] T.M. Cover and J.A. Thomas, *Elements of Information Theory*, Wiley New York, 1991.

[13] G. Ungerboeck, "Channel coding with multilevel/phase signals," *IEEE Transactions on Information Theory*, vol. 28, no. 1, pp. 55–67, 1982.

[14] E. Zehavi, "8-PSK trellis codes for a Rayleigh channel," *IEEE Transactions on Communications*, vol. 40, no. 5, pp. 873–884, 1992.

[15] G. Caire, G. Taricco, and E. Biglieri, "Bit-interleaved coded modulation," *IEEE Transactions on Information Theory*, vol. 44, no. 3, pp. 927–946, May 1998.

[16] A. Guillén i Fàbregas and G. Caire, "Coded modulation in the block-fading channel: coding theorems and code construction," *IEEE Transactions on Information Theory*, vol. 52, no. 1, pp. 91–114, Jan. 2006.

[17] J.J. Boutros, N. Gresset, and L. Brunel, "Turbo coding and decoding for multiple antenna channels," *International Symposium on Turbo Codes & Related Topics*, 2003.

[18] N. Gresset, *New space-time coding techniques with bit-interleaved coded modulations*, Ph.D. thesis, ENST, Paris, 2004.

[19] D.J. Costello Jr and G.D. Forney Jr, "Channel Coding: The Road to Channel Capacity," *Arxiv preprint cs.IT/0611112*, 2006.

[20] P. Elias, "Coding for noisy channels," *IRE Conv. Rec*, vol. 4, no. S 37, pp. 47, 1955.

[21] P. Elias, "Error-free Coding," *IEEE Transactions on Information Theory*, vol. 4, no. 4, pp. 29–37, 1954.

[22] G.D. Forney Jr, *Concatenated codes*, Cambridge MA, MIT Press, 1966.

[23] R. Gallager, "Low-density parity-check codes," *IEEE Transactions on Information Theory*, vol. 8, no. 1, pp. 21–28, 1962.

[24] D. Divsalar and F. Pollara, "Turbo codes for PCS applications," *IEEE International Conference on Communications, 1995*, vol. 1, 1995.

[25] S. M. Alamouti, "A simple transmit diversity technique for wireless communications," *IEEE Journal on Selected Areas in Communications*, vol. 16, no. 8, pp. 1451–1458, October 1998.

[26] V. Tarokh, N. Seshadri, and A.R. Calderbank, "Space-Time Codes for High Data Rate Wireless Communication: Performance Criterion and Code Construction," *IEEE Transactions on Information Theory*, vol. 44, no. 2, March 1998.

[27] J.J Boutros, N. Gresset, L. Brunel, and M. Fossorier, "Soft-input soft-output lattice sphere decoder for linear channels," *IEEE Global Telecommunications Conference*, vol. 3, 2003.

[28] H. V. Poor, "Iterative Multiuser Detection," *IEEE Signal Processing Magazine*, pp. 81–88, January 2004.

[29] M. Sudan, "Decoding of Reed-Solomon codes beyond the error-correction bound," *Journal of Complexity*, vol. 13, no. 1, pp. 180–193, 1997.

[30] R. Koetter and A. Vardy, "Algebraic soft-decision decoding of Reed-Solomon codes," *IEEE Transactions on Information Theory*, vol. 49, no. 11, pp. 2809–2825, 2003.

[31] A. Viterbi, "Error bounds for convolutional codes and an asymptotically optimum decoding algorithm," *IEEE Transactions on Information Theory*, vol. 13, no. 2, pp. 260–269, 1967.

[32] R. Silverman and M. Balser, "Coding for constant-data-rate systems," *IEEE Transactions on Information Theory*, vol. 4, no. 4, pp. 50–63, 1954.

[33] G. Battail, "Pondération des symboles décodés par l'algorithme de Viterbi," *Annales des télécommunications*, vol. 42, no. 1-2, pp. 31–38, January-February 1987.

[34] E. Malkamaki and H. Leib, "Evaluating the performance of convolutional codes over block fading channels," *IEEE Transactions on Information Theory*, vol. 45, no. 5, pp. 1643–1646, July 1999.

[35] R. Knopp and P.A. Humblet, "On coding for block fading channels," *IEEE Transactions on Information Theory*, vol. 46, no. 1, pp. 189–205, Jan. 2000.

[36] G.J. Foschini, "Layered space-time architecture for wireless communication in a fading environment when using multielement antennas," *Bell Labs Technical Journal*, pp. 41–49, October 1996.

[37] J.-C. Guey, M.P. Fitz, M.R. Bell, and W.-Y. Kuo, "Signal design for transmitter diversity wireless communication systems over Rayleigh fading channels," *IEEE Vehicular Technology Conference*, 1996.

[38] G. Battail, "Rotating a redundant constellation in signal space against channel fluctuations," *International Conference on Communications Technology, Beijing, China, July. Also ENST, Paris, France, internal report*, 1989 (postponed until 1990).

[39] K. Boulle and J.-C. Belfiore, "Modulation scheme designed for the Rayleigh fading channel," *Conference on Information Sciences and Systems (CISS 1992), Princeton University, March 1992.*, pp. 288–293, 1992.

[40] V. M. DaSilva and E.S. Sousa, "Fading-resistant modulation using several transmitter antennas," *IEEE Transactions on Communications*, vol. 45, no. 10, pp. 1236–1244, Oct. 1997.

[41] J.J. Boutros and E. Viterbo, "Signal space diversity: a power-and bandwidth-efficient diversitytechnique for the Rayleigh fading channel," *IEEE Transactions on Information Theory*, vol. 44, no. 4, pp. 1453–1467, July 1998.

[42] D. Rainish, "Diversity Transform for Fading Channels," *IEEE Transactions on Information Theory*, vol. 44, no. 12, pp. 1653–1661, December 1996.

[43] C. Lamy and J. Boutros, "On Random Rotations Diversity and Minimum MSE Decoding of Lattices," *IEEE Transactions on Information Theory*, vol. 46, pp. 1584–1589, July 2000.

[44] H. El Gamal and M. O. Damen, "Universal space-time coding," *IEEE Transactions on Information Theory*, vol. 49, no. 5, pp. 1097–1119, May 2003.

[45] B.A. Sethuraman, B.S. Rajan, and V. Shashidhar, "Full-diversity, high-rate space-time block codes from division algebras," *IEEE Transactions on Information Theory*, vol. 49, no. 10, pp. 2596–2616, October 2003.

[46] M.O. Damen, A. Tewfik, and J.-C. Belfiore, "A construction of a space-time code based on number theory," *IEEE Transactions on Information Theory*, vol. 48, no. 3, pp. 753–760, March 2002.

[47] J.-C. Belfiore, G. Rekaya, and E. Viterbo, "The Golden code: a 2×2 full-rate space-time code with nonvanishing determinants," *IEEE Transactions on Information Theory*, vol. 51, no. 4, pp. 1432–1436, April 2005.

[48] P. Dayal and M. K. Varanasi, "An Optimal Two-Transmit Antenna Space-Time Code and its Stacked Extensions," *IEEE Transactions on Information Theory*, vol. 51, no. 12, pp. 4348–4355, Dec. 2005.

[49] Yao and G.W. Wornell, "Achieving the full MIMO diversity-multiplexing frontier with rotation-based space-time codes," *41st Allerton Conf. Commun., Control and Computing, Monticello, IL.*

[50] F. Oggier, G. Rekaya, J.-C. Belfiore, and E. Viterbo, "Perfect Space-Time Block Codes," *IEEE Transactions on Information Theory*, vol. 52, no. 9, pp. 3885–3902, April 2005.

[51] B. Hassibi and B.M. Hochwald, "High-rate codes that are linear in space and time," *IEEE Transactions on Information Theory*, vol. 48, no. 7, pp. 1804–1824, July 2002.

[52] J.J. Boutros, E. Calvanese Strinati, and A. Guillén i Fàbregas, "Analysis of coding on non-ergodic block-fading channels," *43nd Allerton Conference on Communications, Control and Computing, Monticello, IL*, September 2005.

[53] J.J. Boutros, E. Calvanese Strinati, and A. Guillén i Fàbregas, "Turbo code design for block fading channels," *42nd Allerton Conference on Communications, Control and Computing, Monticello, IL*, September 2004.

[54] J.J. Boutros, F. Boixadera, and C. Lamy, "Bit-interleaved coded modulations for multiple-input multiple-output channels," *IEEE International Symposium on Spread Spectrum Techniques and Applications*, 2000.

[55] E. Biglieri, *Coding for Wireless Channels*, Springer, 2005.

[56] N. Gresset, J.J. Boutros, and L. Brunel, "Optimal linear precoding for BICM over MIMO channels," *IEEE International Symposium on Information Theory*, 2004.

[57] P.J. Smith and M. Shafi, "On a Gaussian approximation to the capacity of wireless MIMO systems," *IEEE International Conference on Communications*, 2002.

[58] O. Tirkkonen, A. Boariu, and A. Hottinen, "Minimal non-orthogonality rate 1 space-time block code for 3+ Tx antennas," *IEEE Sixth International Symposium on Spread Spectrum Techniques and Applications*, vol. 2, 2000.

[59] J. J. Boutros and G. Caire, "Iterative multiuser joint decoding: unified framework and asymptotic analysis," *IEEE Transactions on Information Theory*, vol. 48, pp. 1772–1793, July 2002.

[60] "Double-STTD scheme for HSDPA systems with four transmit antennas: Link Level Simulation Results," *TSGR1-20(01)-0458, TSG-RAN Working Group 1 meeting no. 20*, May 21-25, 2001, Busan, Korea.

[61] C. Berrou and A. Glavieux, "Near Shannon limit error-correcting coding and decoding: Turbo-codes.," *IEEE Transactions on Information Theory*, vol. 44, no. 6, pp. 2619–2692, October 1996.

[62] S. Benedetto and G. Montorsi, "Unveiling turbo codes: some results on parallel concatenated coding schemes," *IEEE Transactions on Information Theory*, vol. 42, no. 2, pp. 409–428, March 1996.

[63] L.C. Perez, J. Seghers, and D.J. Costello Jr, "A distance spectrum interpretation of turbo codes," *IEEE Transactions on Information Theory*, vol. 42, no. 6 Part 1, pp. 1698–1709, 1996.

[64] J.J. Boutros, A. Guillén i Fàbregas, E. Biglieri, and G. Zemor, "Design and analysis of low-density parity-check codes for block-fading channels," *Information Theory and Applications Workshop, UCSD, California.*

[65] E.C. van der Meulen, "Three-terminal communication channels," *Adv. Appl. Prob*, vol. 3, pp. 120–154, 1971.

[66] T. Cover and A. El Gamal, "Capacity theorems for the relay channel," *IEEE Transactions on Information Theory*, vol. 25, no. 5, pp. 572–584, 1979.

[67] A. Sendonaris, E. Erkip, and B. Aazhang, "User cooperation diversity. Part I. System description," *IEEE Transactions on Communications*, vol. 51, no. 11, pp. 1927–1938, November 2003.

[68] A. Sendonaris, E. Erkip, and B. Aazhang, "User cooperation diversity. Part II. Implementation aspects and performance analysis," *IEEE Transactions on Communications*, vol. 51, no. 11, pp. 1939–1948, November 2003.

[69] L. Zheng and D.N.C. Tse, "Diversity and multiplexing: a fundamental tradeoff in multiple-antenna channels," *IEEE Transactions on Information Theory*, vol. 49, no. 5, pp. 1073–1096, 2003.

[70] J.N. Laneman, D.N. Tse, and G.W. Wornell, "Cooperative diversity in wireless networks: Efficient protocols and outage behavior," *IEEE Transactions on Information Theory*, vol. 50, no. 12, pp. 3062–3080, December 2004.

[71] R.U. Nabar, H. Bolcskei, and F.W. Kneubuhler, "Fading relay channels: performance limits and space-time signal design," *IEEE Journal on Selected Areas in Communications*, vol. 22, no. 6, pp. 1099–1109, August 2004.

[72] K. Azarian, H. El Gamal, and P. Schniter, "On the achievable diversity-multiplexing tradeoff in half-duplex cooperative channels," *IEEE Transactions on Information Theory*, vol. 51, no. 12, pp. 4152–4172, December 2005.

[73] S. Yang and J.-C. Belfiore, "Towards the Optimal Amplify-and-Forward Cooperative Diversity Scheme," *Arxiv preprint cs.IT/0603123*, 2006.

[74] Y. Jing and B. Hassibi, "Distributed space-time coding in wireless relay networks-Part I: basic diversity results," *IEEE Transactions Wireless Communications*, 2005.

[75] Y. Ding, J.-K. Zhang, and K. M. Wong, "The amplify-and-forward half-duplex cooperative system: pairwise error probability and precoder design," *IEEE Transactions on Signal Processing*, vol. 55, no. 2, pp. 605–617, Feb. 2007.

[76] G.S. Rajan and B.S. Rajan, "A Non-orthogonal distributed space-time protocol, Part-I: Signal model and design criteria," *IEEE International Workshop on Information Theory, Chengdu, China*, pp. 22–26, October 2006.

[77] G.S. Rajan and B.S. Rajan, "A Non-orthogonal distributed space-time protocol, Part-II: Code construction and DM-G Tradeoff," *IEEE International Workshop in Information Theory, Chengdu, China*, pp. 488–492, October 2006.

[78] S. Yang and J.-C. Belfiore, "Optimal space-time codes for the MIMO amplify-and-forward cooperative channel," *Arxiv preprint cs.IT/0509006*, 2005.

[79] J.N. Laneman and G.W. Wornell, "Distributed space-time-coded protocols for exploiting cooperative diversity in wireless networks," *IEEE Transactions on Information Theory*, vol. 49, no. 10, pp. 2415–2425, October 2003.

[80] M. Yuksel and E. Erkip, "Cooperative Wireless Systems: A Diversity-Multiplexing Tradeoff Perspective," *Arxiv preprint cs.IT/0609122*, 2006.

[81] B. Zhao and M.C. Valenti, "Cooperative diversity using distributed turbo codes," *Virginia Tech Symposium on Wireless Personal Communications, Blacksburg, VA*, June 2003.

[82] Z. Zhang and T.M. Duman, "Capacity-approaching turbo coding and iterative decoding for relay channels," *IEEE Transactions on Communications*, vol. 53, no. 11, pp. 1895–1905, 2005.

[83] A. Chakrabarti, E. Erkip, A. Sabharwal, and B. Aazhang, "Code Designs for Cooperative Communication," .

[84] S. Yang and J.-C. Belfiore, "On Slotted Amplify-and-Forward Cooperative Diversity Schemes," *IEEE International Symposium on Information Theory, Seattle, WA*.

[85] S. Yang and J.-C. Belfiore, "Optimal Space-Time Codes for the Amplify-and-Forward Cooperative Channel," *43rd Allerton Conf. Commun., Control and Computing, Monticello, IL*.

[86] N. Gresset, J.J. Boutros, and L. Brunel, "Linear precoding under iterative processing for multiple antenna channels," *IEEE International Symposium on Control, Communications and Signal Processing*, 2004.

[87] A. Guillén i Fàbregas, "Coding in the Block-Erasure Channel," *IEEE Transactions on Information Theory*, vol. 52, no. 11, pp. 5116–5121, 2006.

[88] C. Berrou, A. Glavieux, and P. Thitimajshima, "Near Shannon limit error-correcting coding and decoding: Turbo-codes.," *IEEE International Conference on Communications, 1993, Geneva*, vol. May, 1993.

[89] F. Jelinek J. Raviv L. Bahl, J. Cocke, "Optimal decoding of linear codes for minimizing symbol error rate," *IEEE Transactions on Information Theory*, vol. 20, no. 2, pp. 284–287, March 1974.

[90] M. Breiling, "A logarithmic upper bound on the minimum distance of turbo codes," *IEEE Transactions on Information Theory*, vol. 50, no. 8, pp. 1692–1710, August 2004.

[91] J.J. Boutros and G. Zemor, "On Quasi-Cyclic Interleavers for Parallel Turbo Codes," *IEEE Transactions on Information Theory*, vol. 52, no. 4, pp. 1732–1739, April 2006.

[92] M.G. Luby, M. Mitzenmacher, M.A. Shokrollahi, and D.A. Spielman, "Improved low-density parity-check codes using irregular graphs," *IEEE Transactions on Information Theory*, vol. 47, no. 2, pp. 585–598, 2001.

[93] B. Frey and D. MacKay, "Irregular Turbo Codes," *International Symposium on Turbo Codes & Related Topics*, September 2000.

[94] J.J. Boutros, G. Caire, E. Viterbo, H. Sawaya, and S. Vialle, "Turbo code at 0.03 dB from capacity limit," *IEEE International Symposium on Information Theory ISIT, 2002*, p. 56.

[95] S. Vialle, *Construction et analyse de nouvelles structures de codage de canal adaptées au traitement itératif*, Ph.D. thesis, ENST, Paris.

[96] S.Y. Chung, G.D. Forney Jr, T.J. Richardson, and R. Urbanke, "On the design of low-density parity-check codes within 0.0045 dB ofthe Shannon limit," *IEEE Communications Letters*, vol. 5, no. 2, pp. 58–60, 2001.

[97] T.J. Richardson and R.L. Urbanke, "The capacity of low-density parity-check codes under message-passing decoding," *IEEE Transactions on Information Theory*, vol. 47, no. 2, pp. 599–618, 2001.

[98] S. ten Brink, "Convergence behavior of iteratively decoded parallel concatenated-codes," *IEEE Transactions on Communications*, vol. 49, no. 10, pp. 1727–1737, 2001.

[99] M. Ardakani and F.R. Kschischang, "A more accurate one-dimensional analysis and design of irregular LDPC codes," *IEEE Transactions on Communications*, vol. 52, no. 12, pp. 2106–2114, December 2004.

[100] S. ten Brink, "Iterative decoding trajectories of parallel concatenated codes," *Proc. 3rd IEEE/ITG Conference on Source and Channel Coding*, pp. 75–80, 2000.

[101] J.J. Boutros and O. Pothier, "Convergence analysis of turbo decoding," *Canadian Workshop on Information Theory, Toronto*, June 1997.